

Copyright

By

Lewis Samuel Agnew, Jr.

2007

**Evaluation of the Fatigue Behavior of Bridge Decks with
Precast Panels at Expansion Joints**

by

Lewis Samuel Agnew, Jr., B.S.

Thesis

Presented to the Faculty of the Graduate School of

The University of Texas at Austin

In Partial Fulfillment

Of the Requirements

For the Degree of

Master of Science in Engineering

**The University of Texas at Austin
May 2007**

**Evaluation of the Fatigue Behavior of Bridge Decks with
Precast Panels at Expansion Joints**

**Approved by
Supervising Committee:**

Sharon L. Wood, Supervisor

James O. Jirsa

Dedication

To my loving family for supporting me and allowing me to spend 7 years in college

To Katie for patiently encouraging me throughout my time in Austin

ad gloria patri

Acknowledgements

I would like to thank the Texas Department of Transportation and the Center for Transportation Research for providing the funding that made graduate school possible for me. My time spent at UT has been an amazing learning experience for which I am truly thankful.

I would like to thank Blake Stasney, Dennis Phillip, and Greg Harris for their assistance in building and testing the specimens for this research project. Also, I would like to thank all of my classmates that have offered a helping hand with the concrete pours.

And lastly, I'd like to thank Sharon Wood for her knowledge, patience and continued guidance throughout the course of this research project. I have learned a great deal from her over the last two years, and I am grateful for the opportunity to have studied and worked for her.

May 4, 2007

Abstract

Evaluation of the Fatigue Behavior of Bridge Decks with Precast Panels at Expansion Joints

Lewis Samuel Agnew, Jr., M.S.E

The University of Texas at Austin, 2007

Supervisor: Sharon L. Wood

In a previous Texas Department of Transportation (TxDOT) research project (0-4418), a new construction detail was developed for bridge decks at expansion joints. This new detail used precast, prestressed concrete (PC) panels as stay-in-place formwork for a 4-in. thick topping slab. The new detail forms an 8-in. composite slab that eliminates thickened end slab diaphragms at expansion joints.

The primary objective of this project was to evaluate the fatigue behavior of this new detail. Four full-scale specimens were designed and constructed and then subjected to various load histories. First, the specimens were subjected to service-level and design-level fatigue loads, and then a static overload test after 2 million cycles. After the static

overload, the fatigue testing was continued to 5 million cycles, and the specimens were then tested to failure.

The research team concluded that the new PC panel for 0° skew bridge decks exhibited satisfactory fatigue response. No delamination was observed at the interface of the PC panel and CIP slab, and the measured response of the specimens did not deteriorate with increasing fatigue cycles.

Table of Contents

Chapter 1 : Objectives and Scope.....	1
1.1 Background.....	1
1.2 Research Objectives and Project Scope.....	6
1.3 Site Visits.....	6
1.4 Outline of Thesis.....	7
Chapter 2 : Literature Review.....	8
2.1 Research Prior to 1990.....	8
2.1.1 Buth, Furr, and Jones (1972).....	8
2.1.2 Kluge and Sawyer (1975).....	9
2.1.3 Fagundo, Tabatabai, Soongswang, Richardson, and Callis (1985) ..	10
2.2 Recent Research: 1990-Present.....	11
2.2.1 Dolan and Frank (1994).....	11
2.2.2 Graddy, Kim, Burns, Whitt, and Klingner (2002).....	12
2.2.3 TxDOT Project 0-4418, Specimen 1 (Ryan 2003).....	13
2.2.4 TxDOT Project 0-4418, Specimen 2 (Griffith 2003).....	20
2.2.5 TxDOT Project 0-4418, Specimen 3 (Coselli 2004).....	23
2.3 Summary.....	25
Chapter 3 : Design of Test Specimens.....	27
3.1 Preliminary Design.....	27
3.1.1 Number of Spans in Transverse Direction.....	28
3.1.2 Length of Test Specimens in the Longitudinal Direction.....	31
3.1.2.1 Computational Models.....	32
3.1.2.2 Applied Loads.....	35
3.1.2.3 Calculated Response.....	37
3.2 Final Design of Test Specimens.....	41
3.2.1 Precast Concrete Support Blocks.....	43
3.2.2 Precast Support Beams.....	44
3.2.3 Bearing Pads.....	47
3.2.4 Bedding Strips.....	47

3.2.5	Precast Prestressed Concrete Panels	49
3.2.6	Steel Reinforcement.....	49
3.2.7	Sealed Expansion Joint (SEJ)	50
3.2.8	Concrete Mixture	51
3.3	Load History	51
3.3.1	Fatigue Loading	52
3.3.2	Periodic Static Loads	53
3.3.3	Load to Failure.....	54
3.4	Reaction Frame	54
Chapter 4 : Experimental Program		58
4.1	Construction of Test Specimens	58
4.1.1	Specimens POP1 and POP2.....	58
4.1.2	Specimens NOP1 and NOP2	65
4.2	Reaction Frame	69
4.2.1	Load Application During Fatigue Tests.....	69
4.2.2	Load Application During Static Tests to Failure	71
4.2.3	Load Plates.....	71
4.3	Material Properties.....	72
4.3.1	Concrete	72
4.3.2	Steel.....	73
4.3.3	Prestressed Concrete Panels.....	73
4.4	Instrumentation	74
4.4.1	Deflection Measurements	74
4.4.2	Strain Measurement	75
4.4.2.1	Positive Moment Specimens.....	76
4.4.2.2	Negative Moment Specimens	78
4.4.3	Load Measurement.....	80
4.4.4	Data Acquisition System.....	80
4.5	Test Procedure	80
4.5.1	Load Control Program	81
4.5.1.1	Control Limits.....	82

4.5.1.2	Specimen POP1	82
4.5.1.3	Specimen POP2	84
4.5.1.4	Specimen NOP1.....	85
4.5.1.5	Specimen NOP2.....	86
Chapter 5	: Measured Response of Test Specimens	87
5.1	Specimen POP1	87
5.1.1	Initial Static Test.....	88
5.1.2	Periodic Static Tests.....	90
5.1.3	Static Overload Test.....	90
5.1.4	Additional Periodic Tests.....	93
5.1.5	Test to Failure	95
5.2	Specimen POP2	100
5.2.1	Initial Static Test.....	100
5.2.2	Periodic Static Tests.....	102
5.2.3	Static Overload Test.....	102
5.2.4	Additional Periodic Tests.....	105
5.2.5	Test to Failure	107
5.3	Specimen NOP1.....	112
5.3.1	Initial Static Test.....	113
5.3.2	Periodic Static Tests.....	116
5.3.3	Test to Failure	118
5.4	Specimen NOP2.....	121
5.4.1	Initial Static Test.....	122
5.4.2	Periodic Static Tests.....	124
5.4.3	Test to Failure	127
Chapter 6	: Discussion of Results	131
6.1	Comparison of Positive Moment Specimens.....	131
6.2	Comparison of Negative Moment Specimens	134
6.3	Comparison between Positive and Negative Moment Specimens.....	138
Chapter 7	: Summary, Conclusions, and Recommendations	139
7.1	Summary	139

7.2	Conclusions.....	140
7.3	Recommendations for Future Research.....	142
	Appendix A.....	143
	References.....	150
	Vita.....	152

List of Figures

Figure 1.1: Typical Prestressed Concrete Bridge Construction Prior to Placing Bridge Deck	2
Figure 1.2: Typical Prestressed Concrete Bridge Construction during Placement of PC Panels	3
Figure 1.3: PC Panels and Reinforcing Steel Prior to Casting Topping Slab.....	3
Figure 1.4: Cross Section of IBTS Detail	4
Figure 1.5: View from Underneath Bridge of Formwork for IBTS Detail.....	4
Figure 1.6: Construction of Expansion Joint with Skewed Angle Orientation.....	5
Figure 1.7: IBTS Detail Prior to Casting Topping Slab.....	7
Figure 2.1: Full-scale Bridge Deck Specimen (Buth, et al. 1972).....	9
Figure 2.2: Sealed Expansion Joint (SEJ-A) Detail (TxDOT)	11
Figure 2.3: Cross Section of TxDOT Armor Joint Rail (TxDOT)	12
Figure 2.4: Plan View of IBTS Detail at Expansion Joints (TxDOT).....	15
Figure 2.5: Cross Section Views of IBTS Detail (TxDOT).....	16
Figure 2.6: Simple Cross Section View of the IBTS Detail at Expansion Joints	17
Figure 2.7: Cross Section of UTSE Detail.....	17
Figure 2.8: Plan View of 0° Skew Bridge Deck Specimen (Ryan 2003).....	18
Figure 2.9: HL-93 Design Truck and Design Tandem (AASHTO)	19
Figure 2.10: Design Vehicle Axle Width (AASHTO).....	19
Figure 2.11: Plan View of 45° Skew Specimen	21
Figure 2.12: Placement of Load Plates in Relation to Skew Angles (Griffith 2003)	21
Figure 2.13: Second Specimen Loading Configurations (Griffith 2003)	22
Figure 2.14: Plan View of PC Panel Detail	23
Figure 2.15: Cross Section view of Proposed PC Panel Detail	24
Figure 2.16: Plan View of PC specimen (Coselli 2004).....	24
Figure 3.1: Transverse Cross Section of Typical Bridge Deck	29
Figure 3.2: Locations of the Axle Loads Used in SAP Analysis.....	30
Figure 3.3: Cross Section Idealization of Proposed Positive Moment Specimen.....	30
Figure 3.4: Idealization of Proposed Negative Moment Specimen	31
Figure 3.5: Slab Moment versus Longitudinal Distance (Ryan 2003)	32

Figure 3.6: Cross Section and Plan Views of 3-D Model of Bridge Deck	33
Figure 3.7: Cross Section and Plan Views of 3-D Model of Positive Moment Specimen	34
Figure 3.8: Cross Section and Plan Views of 3-D Model of Negative Moment Specimen	34
Figure 3.9: 3-D Model for Maximum Positive Moment with HL-93 Design Truck.....	35
Figure 3.10: 3-D Model for Maximum Negative Moment with HL-93 Design Truck ...	35
Figure 3.11: 3-D Model for Maximum Positive Moment with HL-93 Design Tandem .	36
Figure 3.12: 3-D Model for Maximum Negative Moment with HL-93 Design Tandem	36
Figure 3.13: Plots of Maximum Principal Stresses in Full-Width Model	38
Figure 3.14: Plots of Maximum Principal Stresses in Positive Moment Specimen	40
Figure 3.15: Cross Section of Positive Moment Specimens (Not to Scale)	42
Figure 3.16: Plan View of Positive Moment Specimens (Not to Scale).....	42
Figure 3.17: Cross Section View of Negative Moment Specimens (Not to Scale).....	43
Figure 3.18: Plan View of Negative Moment Specimens (Not to Scale)	43
Figure 3.19: Concrete Support Block and Bearing Pad.....	44
Figure 3.20: Typical Placement of PC Panels on Edge of PC Girders	45
Figure 3.21: Cross Section of Typical PC Girder Dimensions (TxDOT).....	45
Figure 3.22: Cross Section of Precast Support Beams	46
Figure 3.23: Cross Section and Limits of Bedding Strip Detail (TxDOT).....	48
Figure 3.24: Test Specimen Bedding Strip and PC Panel Cross Section	49
Figure 3.25: Steel Reinforcement for Positive Moment Specimen	50
Figure 3.26: SEJ-A Steel Studs Prior to Casting	51
Figure 3.27: Histogram of Weigh-In-Motion Data (Wood, et al. 2007).....	52
Figure 3.28: Elevation of Positive Moment Specimen Reaction Frame.....	55
Figure 3.29: Section A-A Positive Moment Specimen Reaction Frame	55
Figure 3.30: Plan View of Positive Moment Test Specimen Reaction Frame	56
Figure 3.31: Elevation of Negative Moment Specimen Reaction Frame (Section B-B).	56
Figure 3.32: Longitudinal Elevation of Negative Moment Specimen Reaction Frame ..	57
Figure 3.33: Plan View of Negative Moment Specimen Reaction Frame.....	57
Figure 4.1: Construction of Positive Moment Specimens (Plan View).....	59
Figure 4.2: Construction of Positive Moment Specimens (Plan View).....	60

Figure 4.3: Specimen POP1 After Placing PC Panel.....	61
Figure 4.4: SEJ and Reinforcing Steel Prior to Casting Topping Slab	62
Figure 4.5: Specimen POP1 Prior to Casting	62
Figure 4.6: Slump Test for specimen POP1.....	63
Figure 4.7: Placing Topping Slab for Specimen POP1.....	63
Figure 4.8: Specimen POP1 Before Testing.....	64
Figure 4.9: Specimen POP2 Curing While Testing Specimen POP1	64
Figure 4.10: Construction Sequence for Negative Moment Specimens (Plan View).....	66
Figure 4.11: Construction Sequence for Negative Moment Specimens (Plan View).....	67
Figure 4.12: Placing Topping Slab on Specimen NOP1	68
Figure 4.13: Construction of Specimen NOP2	68
Figure 4.14: Assembling the Reaction Frame for Specimen NOP1	69
Figure 4.15: MTS Actuator and Load Plate for Positive Moment Specimens	70
Figure 4.16: Actuator and Spreader Beam for Negative Moment Specimens.....	70
Figure 4.17: Hydraulic Ram Setup Used to Test Specimen NOP2 to Failure.....	71
Figure 4.18: Load Plate.....	72
Figure 4.19: Compressive Strength of Concrete Used for Topping Slabs.....	73
Figure 4.20: Locations of Linear Potentiometer for Positive Moment Specimens.....	74
Figure 4.21: Locations of Linear Potentiometers for Negative Moment Specimens	75
Figure 4.22: Photograph of Instrumentation of Specimen POP1	75
Figure 4.23: Strain Gage Locations for Specimen POP1 Plan View.....	76
Figure 4.24: Locations of Strain Gages on SEJ for Specimen POP1	77
Figure 4.25: Strain Gage Locations for Specimen POP2	77
Figure 4.26: Locations of Strain Gages on SEJ for Specimen POP2	78
Figure 4.27: Layout of Strain Gages for Specimen NOP1	79
Figure 4.28: Layout and Nomenclature for Strain Gages in Specimen NOP2.....	79
Figure 4.29: Input and Feedback Signals for Specimen POP1	83
Figure 4.30: Input and Feedback Signals for Specimen POP2.....	84
Figure 4.31: Input and Feedback Signals for Specimen NOP1	85
Figure 4.32: Input and Feedback Signals for Specimen NOP2	86
Figure 5.1: Measured Response of Specimen POP1 during Initial Static Test	89

Figure 5.2: Measured Response of Specimen P0P1 during First Four Static Test	91
Figure 5.3: Measured Response of Specimen P0P1 during Static Overload Test	92
Figure 5.4: Cracks Observed during Static Overload Test for Specimen P0P1	93
Figure 5.5: Measured Response of Specimen P0P1 during Periodic Static Tests after Overload Test.....	94
Figure 5.6: Measured Response of Specimen P0P1 during Static Test to Failure	96
Figure 5.7: Upward Deflection of North End of Specimen P0P1 due to Delamination..	97
Figure 5.8: Delamination from Support Beams at Northeast Corner of Specimen P0P1	97
Figure 5.9: Crack Patterns for Specimen P0P1 after Punching Shear Failure.....	98
Figure 5.10: Photographs of Specimen P0P1 after Punching Shear Failure.....	99
Figure 5.11: Measured Response of Specimen P0P2 during Initial Static Test	101
Figure 5.12: Measured Responses of Specimen P0P2 during Before Static Overload Tests	103
Figure 5.13: Measured Response of Specimen P0P2 during Static Overload Test.....	104
Figure 5.14: Cracks Observed during Static Overload Test for Specimen P0P2	105
Figure 5.15: Measured Response of Specimen P0P2 during Periodic Static Tests after Overload Test.....	106
Figure 5.16: Measured Response of Specimen P0P2 during Static Test to Failure	108
Figure 5.17: Upward Deflection of North End of Specimen P0P2 due to Delamination	109
Figure 5.18: Delamination from Support Beams at Northeast Corner of Specimen P0P2	109
Figure 5.19: Crack Patterns for Specimen P0P2 after Punching Shear Failure.....	110
Figure 5.20: Photographs of Specimen P0P2 after Punching Shear Failure.....	111
Figure 5.21: Cracks Observed in NOP1 before Initial Static Test.....	113
Figure 5.22: Shrinkage Cracks in Larger-Scale Specimen (Coselli 2004)	113
Figure 5.23: Measured Response of Specimen NOP1 during Initial Static Test.....	114
Figure 5.24: Measured Response of Specimen NOP1 during Periodic Static Tests	117
Figure 5.25: Measured Response of Specimen NOP1 during Static Test to Failure.....	119
Figure 5.26: Crack Maps for Specimen NOP1 Test to Failure.....	120
Figure 5.27: Photograph of Specimen NOP1 after Punching Shear Failure	120

Figure 5.28: Cracks Observed in NOP2 before Initial Static Test.....	122
Figure 5.29: Measured Response of Specimen NOP2 during Initial Static Test.....	123
Figure 5.30: Measured Response of Specimen NOP2 during Periodic Static Tests	125
Figure 5.31: Measured Response of Specimen NOP2 during Static Test to Failure.....	128
Figure 5.32: Crack Maps for Specimen NOP2 Test to Failure.....	129
Figure 5.33: Photograph of Specimen NOP2 after Punching Shear Failure	130
Figure 6.1: Comparison of Capacities of Specimens POP1 and POP2 with Larger-Scale Specimen.....	134
Figure 6.2: Comparison of Capacities of Specimens NOP1 and NOP2 with Larger-Scale Specimen.....	137
Figure A.1: Load vs. Deflection Response during Initial Static Test (POP1).....	143
Figure A.2: Load vs. Deflection Response during Static Test to Failure (POP1)	144
Figure A.3: Measured Strain Responses during Initial Static Test and Static Test to Failure (POP1).....	145
Figure A.4: Load vs. Deflection Response during Initial Static Test	146
Figure A.5: Load vs. Deflection Response during Static Test to Failure	146
Figure A.6: Load vs. Deflection Response Specimen NOP1	147
Figure A.7: Measured Strain Response Specimen NOP1.....	148
Figure A.8: Load vs. Deflection Response Specimen NOP1	149

List of Tables

Table 3.1: Maximum Values of Principal Stress from Elastic Finite Element Analyses of Bridge Deck	38
Table 3.2: Maximum Values of Principal Stress from Elastic Finite Element Analyses of Positive Moment Specimen	39
Table 3.3: Maximum Values of Principal Stress from Elastic Finite Element Analyses of Negative Moment Specimen.....	39
Table 3.4: Concrete Mixture Proportions	51
Table 3.5: Summary of Applied Load Histories	53
Table 5.1: Static Loading History for Specimen P0P1	88
Table 5.2: Static Loading History for Specimen P0P2	100
Table 5.3: Static Loading History for Specimen N0P1	112
Table 5.4: Static Loading History for Specimen N0P2	121
Table 6.1: Summary of Failure Response of Positive Moment Specimens.....	133
Table 6.2: Summary of Failure Response of Negative Moment Specimens	137

Chapter 1: Objectives and Scope

A framework for understanding the purpose of this experimental program and this thesis is presented in this Chapter. The background is presented in Section 1.1, and the primary research objectives are outlined in Section 1.2. Two site visits are documented in Section 1.3, and a general outline for this thesis is discussed in Section 1.4.

1.1 BACKGROUND

The Texas Department of Transportation (TxDOT) is constantly investigating new construction technologies for faster, safer and more economical bridge construction. One recent improvement has been the incorporation of precast, prestressed concrete (PC) panels as stay-in-place formwork for the bridge deck. The use of PC panels has improved worker safety and reduced construction time.

The construction sequence for a bridge deck is illustrated in Figure 1.1 and Figure 1.2. After completion of the supports (bent caps and abutments), the bridge girders are positioned in the longitudinal direction (Figure 1.1). The girder spacing typically varies between 6 and 10 ft.

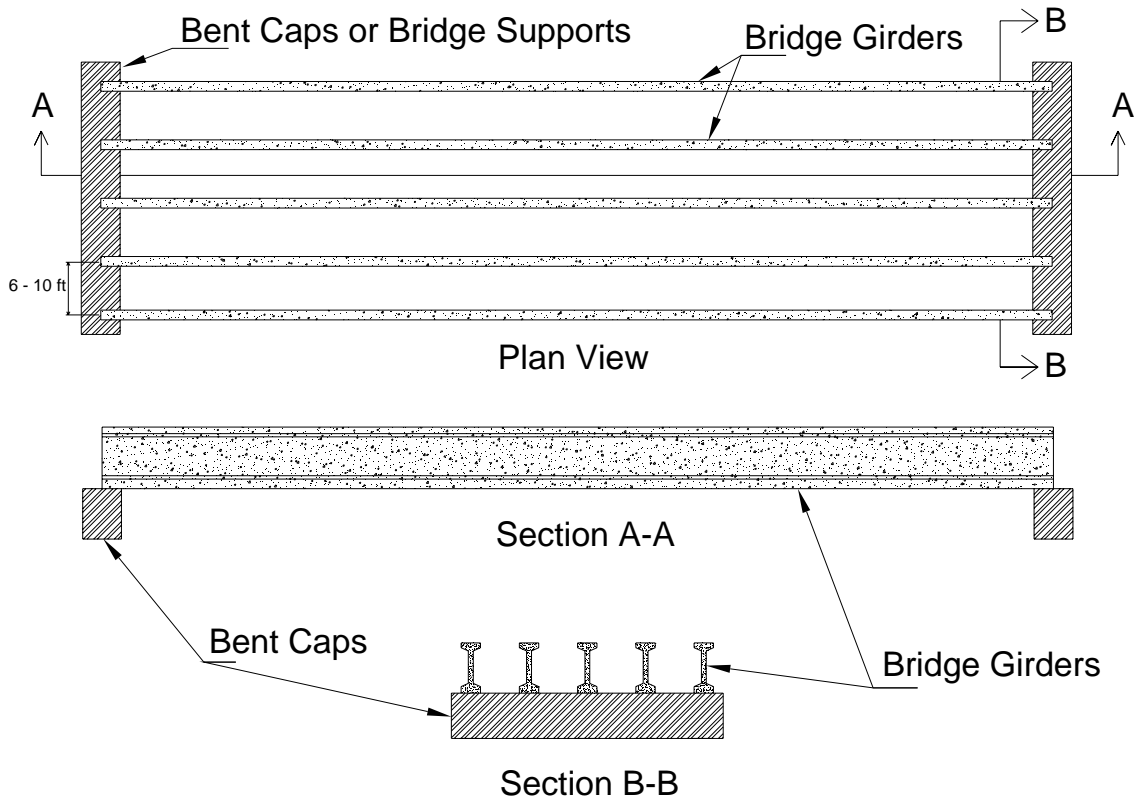


Figure 1.1: Typical Prestressed Concrete Bridge Construction Prior to Placing Bridge Deck

Rectangular PC panels are then placed on the top flanges of adjacent girders. These panels are typically 8 ft in the longitudinal direction and are prestressed in the transverse direction. As shown in Figure 1.2, the PC panels are not typically used over the supports or at expansion joints. A full-depth, cast-in-place (CIP) slab has traditionally been used at these locations. Once in place, the PC panels form a deck of stay-in-place formwork on which workers place the reinforcement for the CIP topping slab.

Figure 1.2 is a simple representation of a typical bridge as the PC panels are placed during construction. Figure 1.3 also shows a photograph of a TxDOT bridge deck prior to casting the topping slab, in which the PC panels can be seen underneath the mat

of top reinforcing steel. After the cast-in-place (CIP) concrete topping slab has been placed and cured, the PC panels and CIP slab form a composite 8-in. bridge deck.

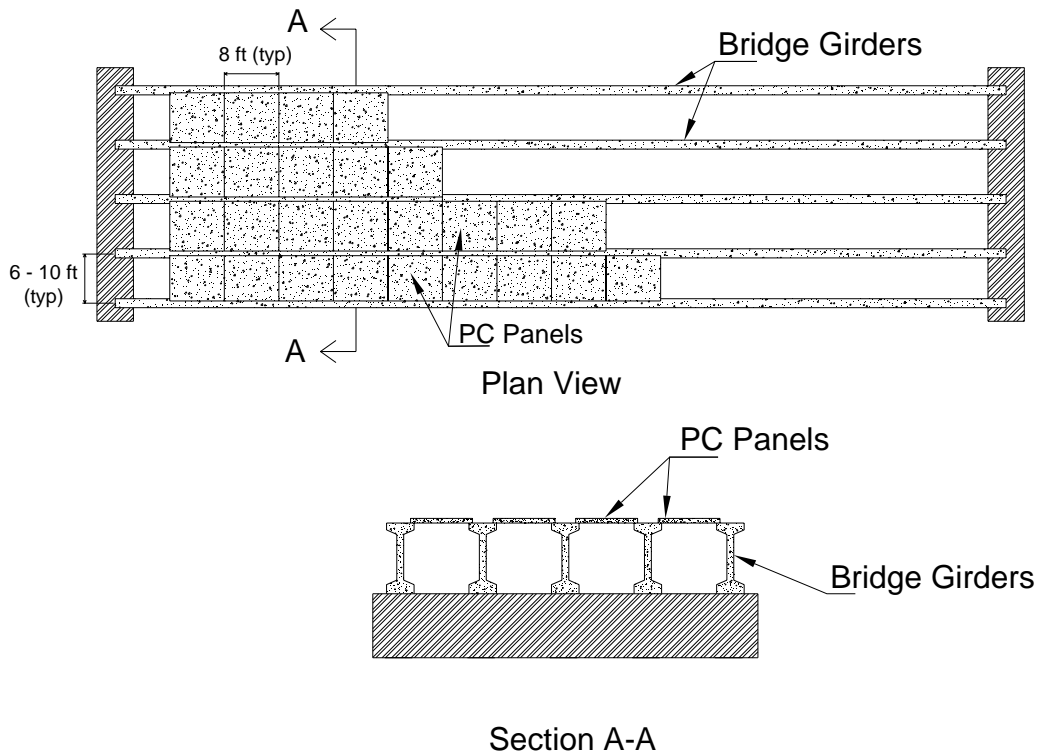


Figure 1.2: Typical Prestressed Concrete Bridge Construction during Placement of PC Panels



Figure 1.3: PC Panels and Reinforcing Steel Prior to Casting Topping Slab

There are a few challenges associated with this method of bridge construction. Bridges require expansion joints to allow for expansion and contraction due to thermal cycles. These expansion joints can be located at several points along the length of the bridge and often are located at the bent cap or bridge abutments. At the expansion joints, TxDOT typically uses a full-depth CIP strip. Until recently, the typical TxDOT detail at expansion joints, which is called the I-beam Thickened Slab (IBTS) detail, was a 10-in. thick CIP section that formed a 4-ft wide end diaphragm between the PC girders. More information about the IBTS detail is presented in Chapter 2, and the cross section of the IBTS detail is included in Figure 1.4.

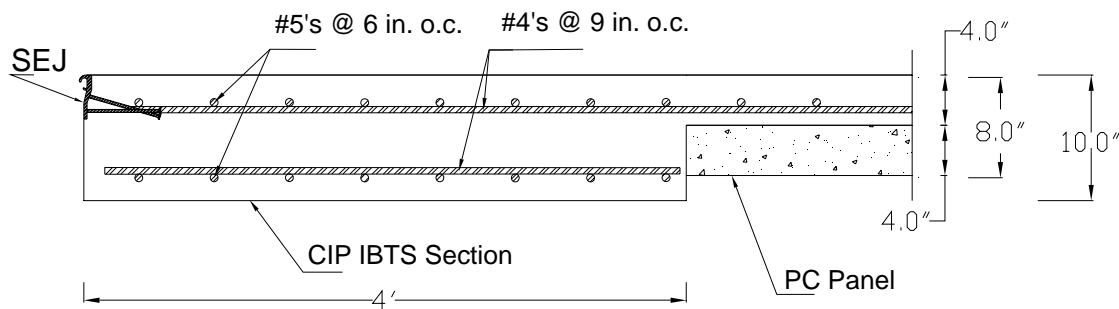


Figure 1.4: Cross Section of IBTS Detail

The primary construction difficulty associated with the IBTS detail is the temporary formwork that must be constructed to support the CIP concrete (Figure 1.5). Because bridge overpasses are often at an elevation high above grade, it is difficult and dangerous work to construct and remove this formwork.



Figure 1.5: View from Underneath Bridge of Formwork for IBTS Detail

A second construction challenge at expansion joints is that the longitudinal direction of the bridge might be skewed with respect to the abutments or bent caps. Figure 1.6 illustrates that skew angles can create complex geometries when using rectangular PC panels at expansion joints.

The configuration of PC beams shown in Figure 1.6 highlights another potential problem. If the lengths of the adjacent spans differ, the number of beams is likely to be different in the spans.



Figure 1.6: Construction of Expansion Joint with Skewed Angle Orientation

These construction challenges led to two research projects at the Ferguson Structural Engineering Laboratory (FSEL) at The University of Texas at Austin. In the first research project (0-4418), the behavior of the IBTS detail with a 0° and a 45° skew angle was evaluated. A simpler CIP detail was also investigated, as was the option of using PC panels at expansion joints. The results of project 0-4418 are discussed in Chapter 2.

The PC panel detail offers many advantages to TxDOT in terms of construction speed and worker safety, compared with the IBTS detail. The proposed detail places the PC panel at the expansion joint instead of forming and casting a thicker slab end section. The reinforcing steel in the topping slab is the same as that used in the rest of the bridge deck. The PC panel detail results in a composite, 8-in. thick section at the expansion joint.

At the conclusion of project 0-4418, the research team suggested that further research be conducted to evaluate the fatigue behavior of the PC panel detail at expansion joints in bridge decks. Project 0-5367 addresses this issue for both skewed and perpendicular bridges.

1.2 RESEARCH OBJECTIVES AND PROJECT SCOPE

The purpose of Project 0-5367 is to evaluate and develop a PC panel detail for use in both perpendicular and skewed bridges. This thesis documents the first phase of project 0-5367: large-scale fatigue tests of the proposed PC panel detail in bridge decks with 0° skew. In the second phase of 0-5367, the research team will develop new designs for skewed PC panels and will then evaluate the structural behavior of the new detail.

Four fatigue specimens were constructed using full-scale components (PC panels and expansion joints). The research team evaluated the specimens under both service-level and design-level loads and considered the possibility of overloads during the service life of the bridge. The results of these tests are presented, and the conclusions and recommendations address the future use of the PC panel detail at expansion joints.

1.3 SITE VISITS

The research team sought to simulate as-built conditions of typical TxDOT bridges as closely as possible in the laboratory specimens. The research team held several meetings with TxDOT personnel during the design of the test specimens and visited two sites in the Austin area where PC panels were used. These site visits were valuable educational experiences that allowed the research team to understand typical TxDOT construction practices and the practical ramifications of the research. One site was a bridge on Highway 183A in north Austin, and the other site was an overpass of Highway 130 over Highway 290 in east Austin.

Both bridges were constructed with PC girders, and PC panels were used as stay-in-place formwork for the interior portions of the bridge deck. Figure 1.7 shows the IBTS detail prior to casting the topping slab for a skewed bridge deck. The sealed

expansion joint can be seen along the upper left corner of the picture, and the reinforcing steel can be seen within the IBTS section.



Figure 1.7: IBTS Detail Prior to Casting Topping Slab

1.4 OUTLINE OF THESIS

This thesis has been divided into six chapters. In Chapter 2, a literature review summarizes the significance and correlation of previous research to the current experimental program. Chapter 3 presents the design of the test specimens used in this experimental program. The construction of the test specimens, the setup of the test, and the testing procedures are discussed in Chapter 4. In Chapter 5, the measured responses from the test specimens are presented. In Chapter 6 the results are discussed and compared with results from previous research projects. The conclusions of this investigation are summarized in Chapter 7.

Chapter 2: Literature Review

The background information related to the experimental program is presented in this Chapter. Research that was conducted prior to 1990 is presented in Section 2.1, and research that was conducted after 1990 is presented in Section 2.2. The significance of the previous research and the relevance to this experimental program are discussed in Section 2.3.

2.1 RESEARCH PRIOR TO 1990

A new construction method that used precast, prestressed concrete (PC) panels as stay-in-place formwork was investigated in early research. These evaluations focused on the fundamental behavior and properties of the bridge deck, and focused on the ability of the panels to act compositely with the cast-in-place (CIP) topping slab. Generally, all of these research projects concluded that the PC panel and CIP slab formed a composite bridge deck that provided sufficient strength and fatigue performance.

2.1.1 Buth, Furr, and Jones (1972)

In this research project, the capability of full-scale precast PC panels to act compositely with a CIP deck to distribute wheel loads under both static and fatigue loadings was evaluated. A full-scale bridge deck (Figure 2.1) was constructed in the laboratory, and was first subjected to cyclic applications of the design load amplified by the dynamic impact factor. The cyclical wheel load (20.8 kip) was one half of the axle load (41.6 kip) corresponding to the rear axle of the HS-20 Design Truck (32 kip) multiplied by $(1+I)$ to account for dynamic effects, where $I = 1.3$. Two million fatigue cycles were applied to the specimen at three locations: the center of the bridge span and at the butt-joints between adjacent PC panels. Expansion joint details were not evaluated.

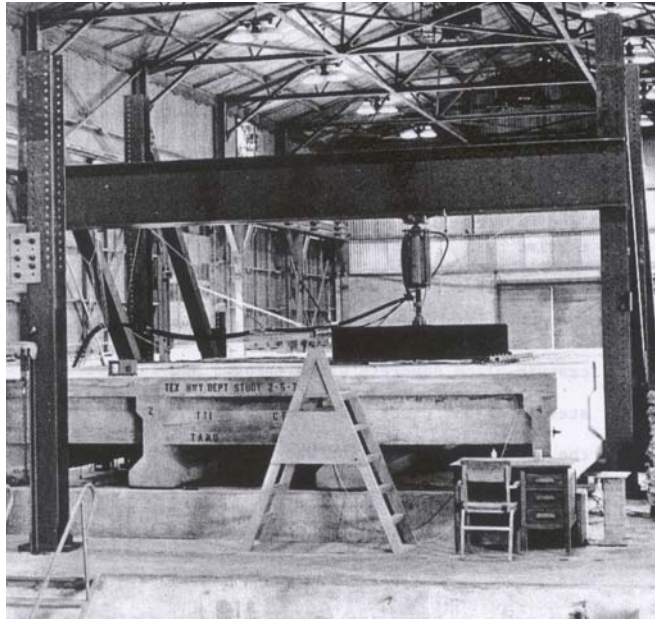


Figure 2.1: Full-scale Bridge Deck Specimen (Buth, et al. 1972)

The results of the fatigue tests indicated that the bond at the interface of the PC panel and CIP slab showed no signs of distress. Also, at the loading location near the butt-joints, the interface was not damaged. After the fatigue testing was concluded, the bridge deck was tested to failure. The lowest cracking load was 3.8 times the design wheel load, and the lowest measured failure load was 12.5 times the design wheel load.

The researchers concluded that the bond between PCP and CIP exhibited no problems under fatigue loading. They also concluded that the construction method using the PC panel and CIP composite bridge deck was an adequate method for bridge deck construction.

2.1.2 Kluge and Sawyer (1975)

This research project investigated if mechanical connectors were needed between the interface of PCP and CIP bridge decks. Using PC panels built compositely with a CIP topping slab, the researcher team designed and constructed 57 composite slabs that were 18-in. wide by 8-ft long. Four series of tests evaluated 7-in. thick deck specimens that consisted of a 3-in. thick PC panel built with a 4-in. thick CIP topping slab. The PC

panels were reinforced with 7/16-in. diameter prestressing strands placed at 9-in. on center.

The test specimens were loaded in simple beam bending to evaluate shear capacity, flexural strength, and bond capabilities at the interface of the PC panel and CIP slab. One series of tests included steel mechanical connectors between the PC panel and the CIP slab. Also, for one series of tests, the top surface of the PC panel was oiled before placing the CIP deck.

Overall, the research team concluded that the bond at the interface was sufficient without connectors, and that the PC panel and CIP composite bridge deck could be considered as a stress-resisting part of the deck for standard bridges, and the measured capacities significantly exceeded the required strength. However, they noted that a clean interface between the PC panel and CIP slab was necessary to achieve the full design strength because the oiled panel failed at a load 40% lower than the other specimens.

2.1.3 Fagundo, Tabatabai, Soongswang, Richardson, and Callis (1985)

The research team determined that previous research had neglected to evaluate the effects of the bearing of the PC panel on the bridge girders because cracks had been identified during forensic investigations of the bridge decks. The research team conducted a series of field tests and forensic repairs to investigate the effectiveness of fiberboard bedding strips that were placed along the bridge girders. These bedding strips allowed the CIP concrete to flow underneath the panel and provide positive bearing underneath for the PC panel. The field tests consisted of simple load tests at interior locations of bridge decks.

The research team concluded that positive bearing significantly improved the performance of the composite bridge decks. The causes of cracking at the girders were mostly attributed to creep and shrinkage of the topping slab, and the presence of strand extensions was shown to improve the resistance to creep and shrinkage cracking. When damaged bridge decks were repaired to provide positive bearing along the length of the panels, no additional cracking was observed.

2.2 RECENT RESEARCH: 1990-PRESENT

Research conducted in the past fifteen years has not addressed the fatigue performance of the PC panel at expansion joints. However, several studies have addressed relevant issues involved with the development of the PC panel detail for expansion joints. Also, the three experimental investigations included in TxDOT Project 0-4418 are discussed because the results from those studies contributed directly to the development of the current research project.

2.2.1 Dolan and Frank (1994)

In this research project, failures in bridge expansion joint rails were investigated. The use of steel armor joints and sealed expansion joints is a common construction practice for highway bridge decks (Figure 2.2 and Figure 2.3). The steel joints consist of steel studs welded to steel members and are cast compositely with the bridge slab at expansion joints.

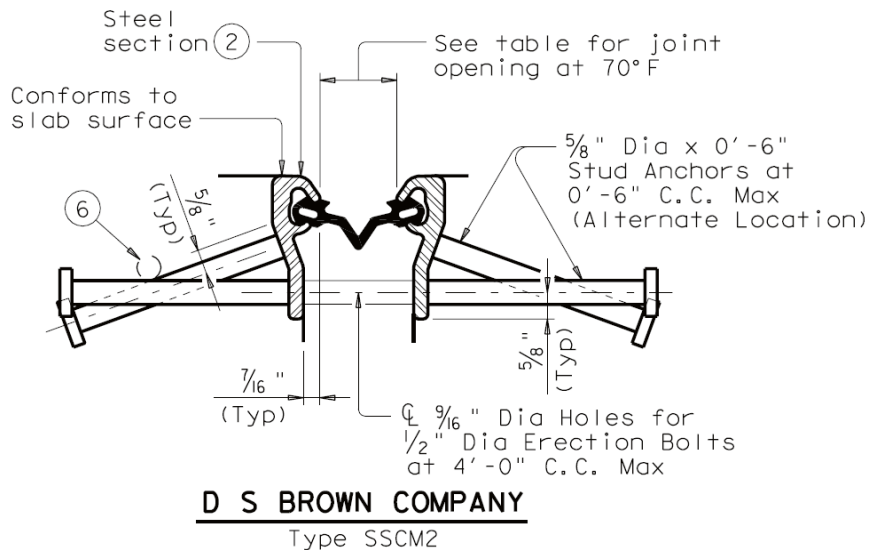


Figure 2.2: Sealed Expansion Joint (SEJ-A) Detail (TxDOT)

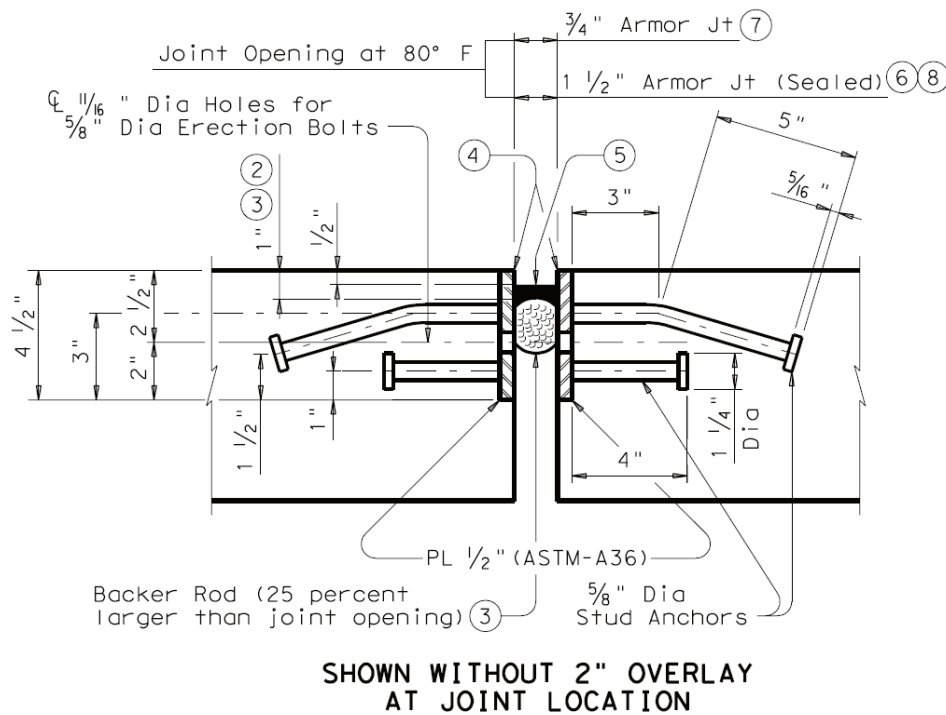


Figure 2.3: Cross Section of TxDOT Armor Joint Rail (TxDOT)

Several failures were reported where the steel studs had fractured from the steel sections. The research team removed samples of these failed joints from bridge decks to determine the cause of failure. They conducted several tests to measure the weld strength of the steel studs, and also measured the yield strengths of the steel sections and steel studs. They found that the yield strengths were sufficient and that all steel studs had been welded correctly. The conclusion of the research team was that the steel studs and expansion joint rails were sufficient, but the cause for failure was insufficient consolidation of the concrete around the steel studs. Insufficient consolidation resulted in uneven bearing of the steel studs that resulted in high stress concentrations at the weld, and under fatigue loading, the welds fractured.

2.2.2 Graddy, Kim, Burns, Whitt, and Klingner (2002)

In this project, the research team conducted an analytical and experimental investigation of the effects of arching action in bridge slabs, and how this concept applied

to punching shear capacities of bridge decks subjected to fatigue loading. The investigation included static tests and fatigue tests on full-scale bridge specimens constructed in the laboratory. The research team conducted fatigue tests of specimens with the PC panel compositely built with CIP topping slabs. The cyclic loading was approximately 9.4 x the rear axle from the HS-20 Design Truck.

The research team concluded from the static tests that the AASHTO and ACI formulas for punching shear were conservative, and that finite element analyses could be used to predict the behavior of bridge slabs. They also concluded that arching action exists in bridge decks but does not contribute significantly to the overall flexural capacity of the bridge slab.

The researchers concluded from the fatigue tests that horizontal shear could possibly be the mode of failure for the PC panel and CIP slab interface. At the interface, delamination and severe cracking was observed. However, the extremely high levels of the fatigue loading were not representative of service load behavior.

2.2.3 TxDOT Project 0-4418, Specimen 1 (Ryan 2003)

Ryan (2003) constructed a full-scale bridge deck to evaluate the behavior of the I-Beam Thickened Slab (IBTS) detail. The behavior of the IBTS detail was as a baseline for comparison with new details proposed for expansion joints. To reflect the conditions of a typical bridge deck with 0° skew the test specimen included two girder spacings (8 ft and 10 ft) and two construction details at the expansion joint (the IBTS detail and an alternative detail, the Uniform Thickness Slab Edge Detail (UTSE)).

A plan view of the IBTS detail, according to TxDOT standard details, is shown in Figure 2.4, and three cross section views are included in Figure 2.5 and Figure 2.6. These figures show that the IBTS detail consists of a slight deviation from the typical bridge deck detail because PC panels are not incorporated into the construction of expansion joints. The IBTS consists of a 10-in. CIP slab region, which is thicker than the 8-in. composite slab which is used in the interior portions of the bridge deck. The IBTS detail forms a 4-ft wide edge beam at the slab end that is designed to carry load between

the girders. To sustain both the positive and negative moments in this slab end region, the IBTS detail is reinforced with top and bottom reinforcement in both the longitudinal and transverse directions. Typical bridge decks are constructed with the PC panels placed in the interior portions of bridge. However, the only area that was evaluated during this test was the expansion joint, and PC panels were not used for the interior portion of the test specimen.

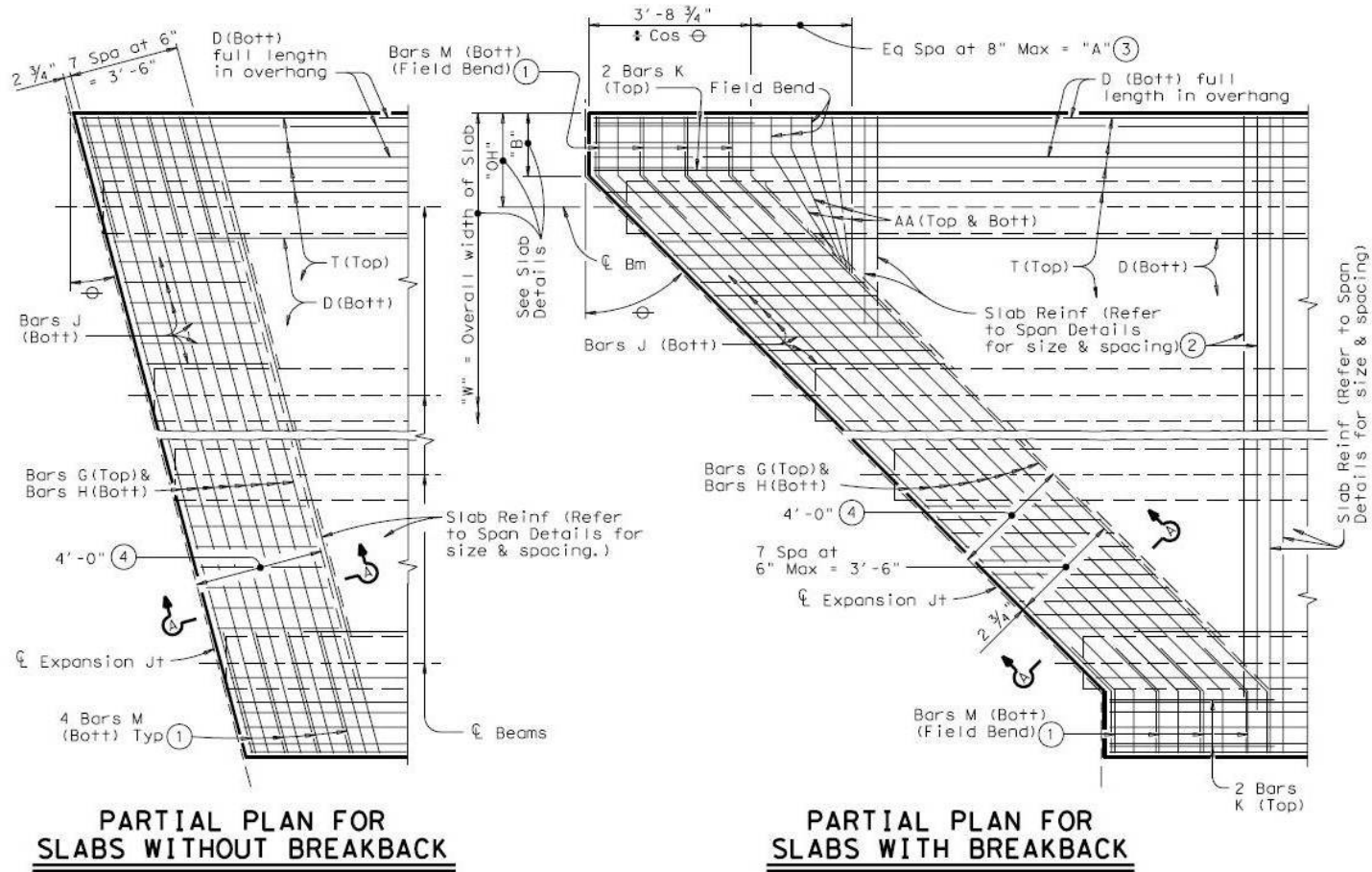


Figure 2.4: Plan View of IBTS Detail at Expansion Joints (TxDOT)

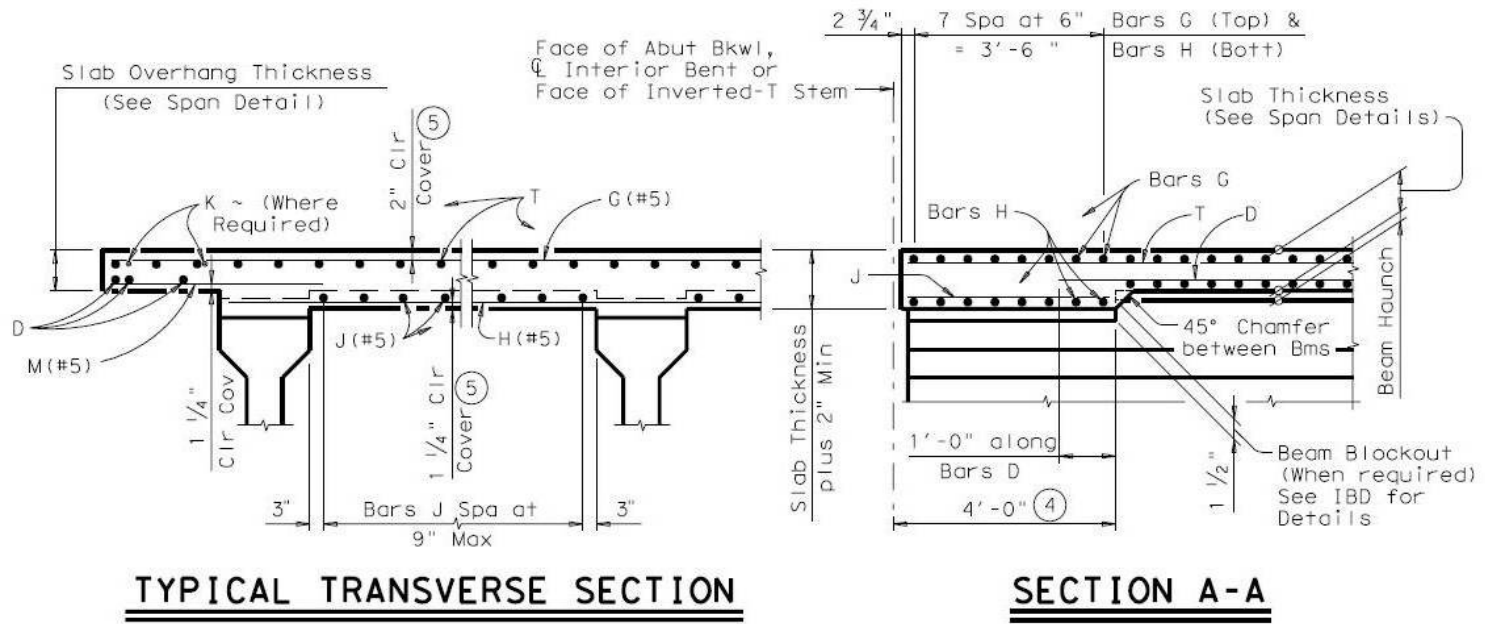


Figure 2.5: Cross Section Views of IBTS Detail (TxDOT)

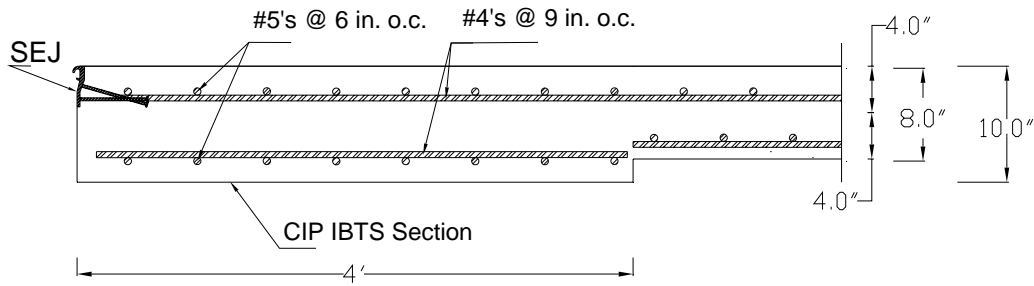


Figure 2.6: Simple Cross Section View of the IBTS Detail at Expansion Joints

The second detail evaluated in this test specimen was the UTSE detail. The UTSE detail was designed to reduce the cost of the expansion joint by maintaining a constant thickness of 8 in. (Figure 2.7). The UTSE detail includes a 4-ft wide edge beam at the slab end, which is similar to the IBTS detail in plan view. The difference between the IBTS and UTSE was that the UTSE was constructed with a uniform 8-in. slab thickness, and more reinforcing steel than the IBTS detail. The additional reinforcement in the UTSE detail was selected to achieve the same flexural capacity as the IBTS detail.

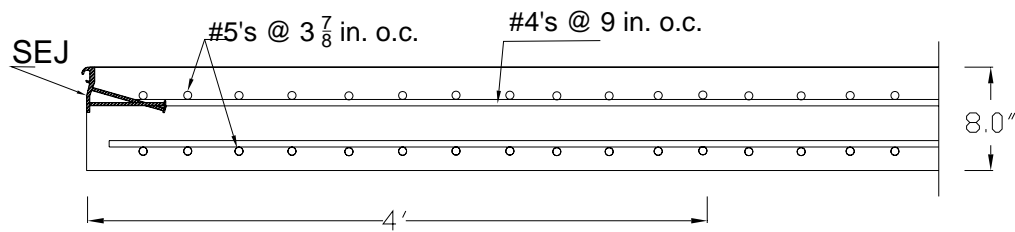


Figure 2.7: Cross Section of UTSE Detail

The full-scale bridge deck specimen was built with a 0° skew orientation. The IBTS detail was used along the south end of the specimen, and the UTSE detail was used along the north end. The specimen was 18-ft long by 32-ft wide and consisted of three spans of slab deck compositely built with four steel girders. The beam spacing on the western edge of the specimen was 10 ft, and the spacing of the two beams on the eastern edge was 8 ft (Figure 2.8). Four critical loading patterns, or test areas, were developed by using influence lines to maximize the positive and negative moments experienced by the bridge slab in each slab end detail. The maximum positive moment in the slab occurred

within the 10-ft span, while the maximum negative moment in the slab occurred when the design vehicle axle load was centered over Beam 3.

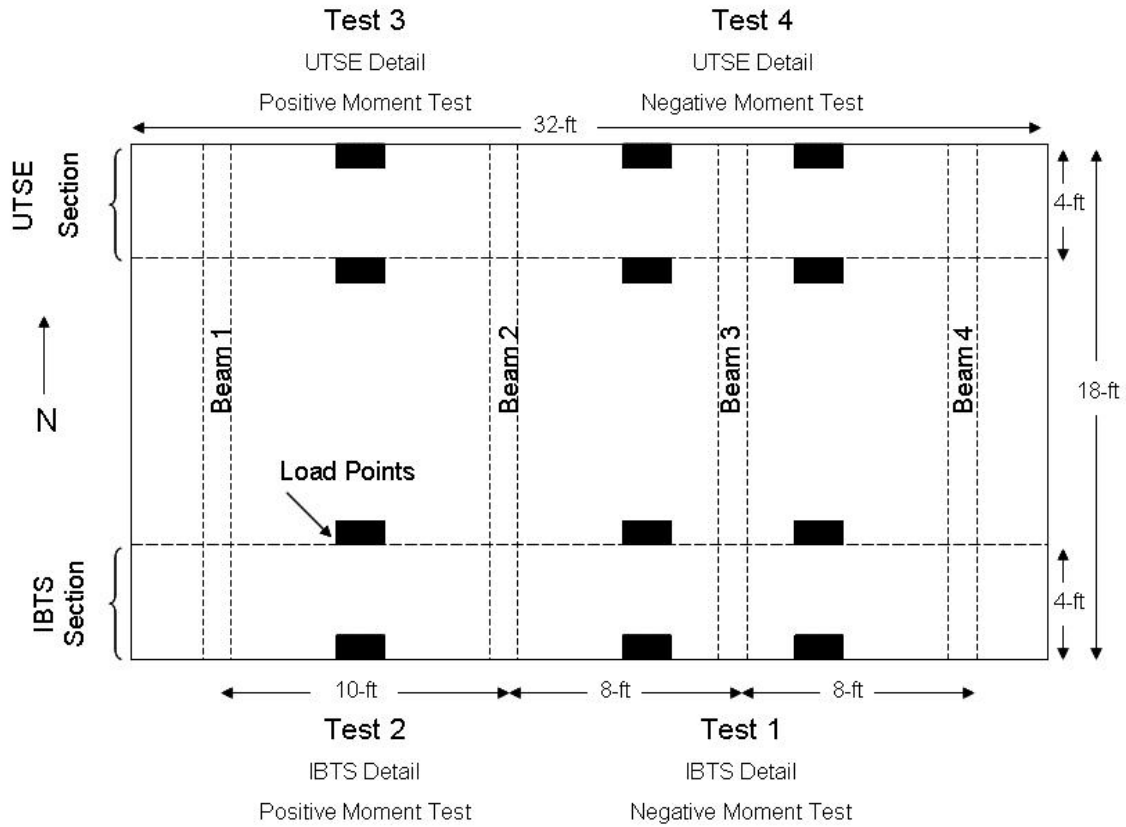


Figure 2.8: Plan View of 0° Skew Bridge Deck Specimen (Ryan 2003)

In Figure 2.8, the black rectangles denote load points representative of the design vehicle wheel contact area, which is 20-in. wide by 10-in. long. The loads applied to the test specimen corresponded to the rear axle loads of the AASHTO LRFD HL-93 Design Vehicle and the HL-93 Design Tandem. Figure 2.9 and Figure 2.10 summarize the configurations of the AASHTO HL-93 Design Truck and HL-93 Design Tandem.

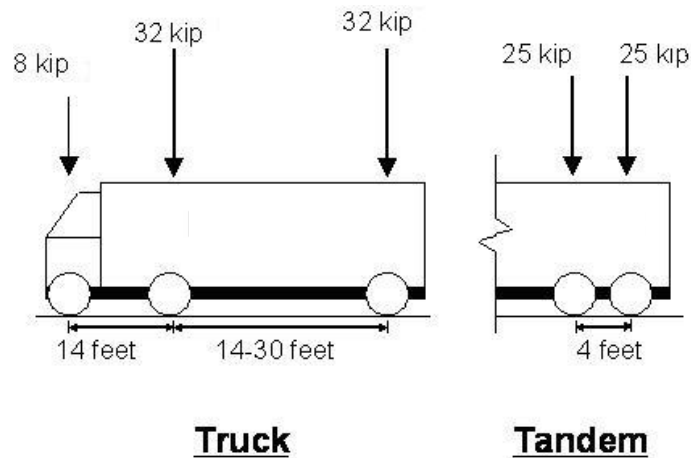


Figure 2.9: HL-93 Design Truck and Design Tandem (AASHTO)

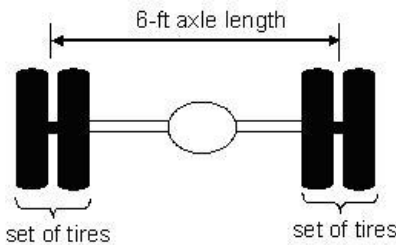


Figure 2.10: Design Vehicle Axle Width (AASHTO)

For the Test 1 and Test 4, the entire design axle was centered over Beam 3 to achieve the maximum negative moment within the slab. When the HL-93 Design Truck loading was applied, two wheel loads corresponding to the rear axle were placed at the slab edge. When the HL-93 Design Tandem loading was applied, two wheel loads were placed at the slab edge and two wheel loads were located four feet from the edge. Test 1 evaluated the IBTS detail and Test 4 evaluated the UTSE detail

For the Test 2 and Test 3, the loads were placed at midspan of the 10-ft span to achieve the maximum positive moment within the slab, and the load points represented wheel loads from either the rear axle of the HL-93 Design Truck or the HL-93 Design Tandem. When the HL-93 Design Truck loading was applied, only one wheel load was placed at midspan of the slab edge detail. When the HL-93 Design Tandem loading was applied, one wheel load was located at midspan of the slab edge, and the second wheel

load was located four feet from the edge wheel. Test 2 evaluated the IBTS detail and Test 3 evaluated the UTSE detail.

In all four test areas, the specimen was loaded first with the loads corresponding to the rear axle from the HL-93 Design Truck and then with the HL-93 Design Tandem. After sustaining the design loads, it was concluded that the HL-93 Design Tandem was the critical load condition, and for the various test locations the specimen was loaded to failure using the tandem configuration.

Overall, the IBTS and UTSE details performed satisfactorily. Under design-level loads, no cracking was observed when negative moments were induced. Minor cracks were observed when positive moments were induced. Extensive cracks were not observed until the applied loads exceeded two times the design loads.

The performance at failure was also satisfactory for both the IBTS and UTSE details. The failure mechanism was punching shear for all test areas, and the maximum loads ranged from 5.5 to 7 x HL-93 Design Tandem.

2.2.4 TxDOT Project 0-4418, Specimen 2 (Griffith 2003)

A second test specimen was constructed during project 0-4418 with many construction details similar to the first specimen. However, this specimen incorporated a 45° skew angle (Figure 2.11). The IBTS detail was used along the south edge of the specimen and the UTSE detail was used along the north edge.

The skew angle of 45° was chosen because more than 96% of TxDOT bridges have a skew angle of 45% or less (Van Landuyt 2006).

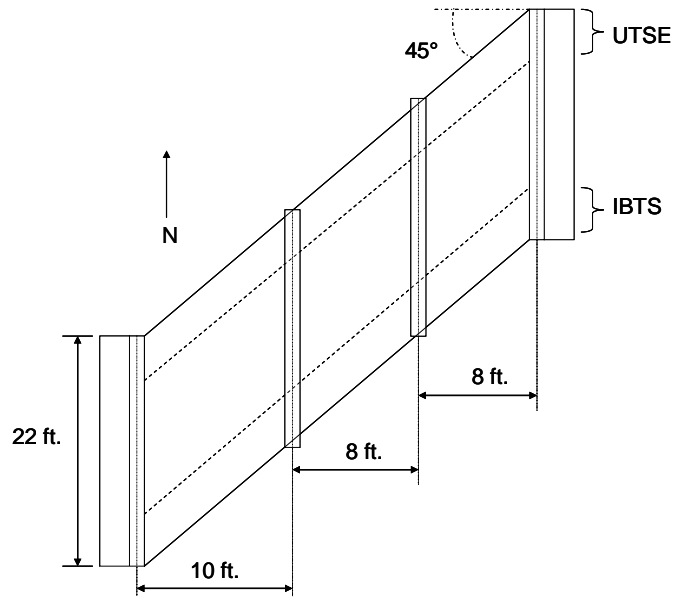
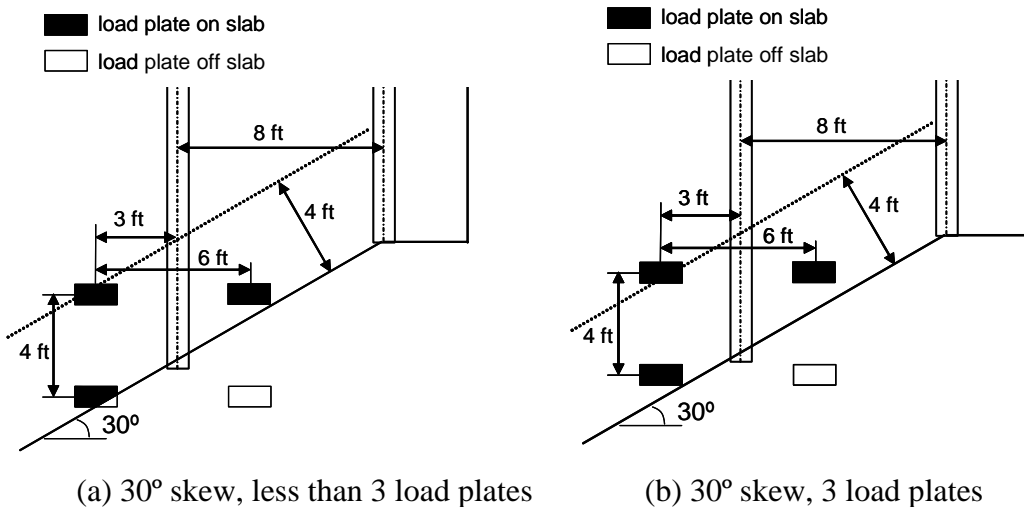


Figure 2.11: Plan View of 45° Skew Specimen

Because the HL-93 Design Tandem loading produced the most critical results for the first test specimen with 0° skew, the HL-93 Design Tandem was the only load configuration that was considered for the 45° skew specimen. However, the skew angle affected the loading configuration because all four wheel loads could not be placed on the specimen simultaneously (Figure 2.12).



(a) 30° skew, less than 3 load plates

(b) 30° skew, 3 load plates

Figure 2.12: Placement of Load Plates in Relation to Skew Angles (Griffith 2003)

After the relationship between the skew angle and the loading configuration was determined, four specific test areas were designed for the skewed specimen (Figure 2.13). Tests 2 and 3 evaluated the maximum positive moment experienced by the slab within the 10-ft span by placing at midspan two wheel loads from the HL-93 Design Tandem. Tests 1 and 4 investigated the maximum negative moment within the 8-ft span by centering the HL-93 Design Tandem across a beam, but only three wheel loads were located on the slab, as shown in Figure 2.13.

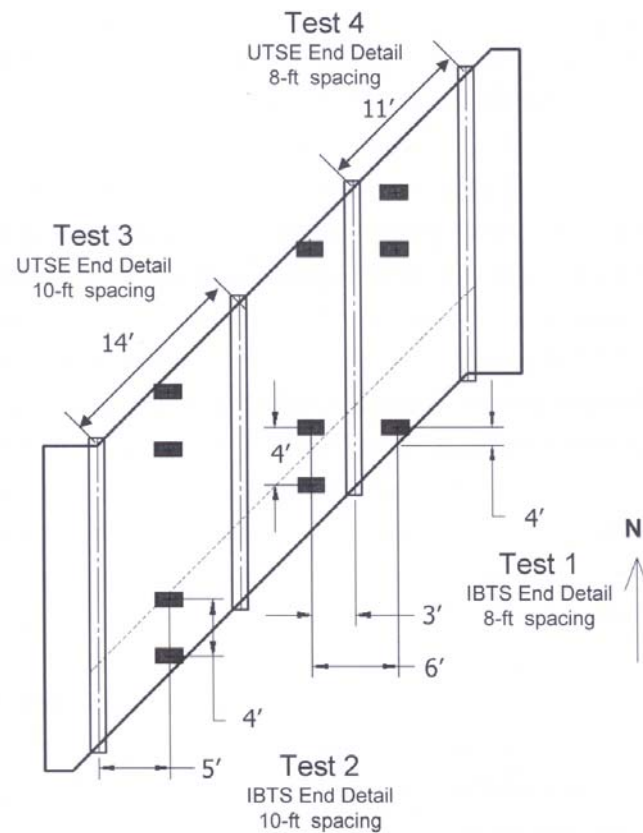


Figure 2.13: Second Specimen Loading Configurations (Griffith 2003)

Overall, the behavior of both the IBTS and UTSE details was satisfactory at design-level loads. All of the measured strain responses and the deflections were very small, and for most of the tests, cracks were not observed until 2 x HS-20 Design Tandem. In Test 2, minor cracking was observed at 1.25 x HS-20 Design Tandem. The mode of failure was punching shear for most of the test areas except for a one way shear

failure in the IBTS 10-ft span. The research team concluded that the effects of skew increased the deflections when compared with the same test in the 0° skew specimen, and that the effect of skew decreased the ultimate capacity when compared with the same test in the 0° skew specimen. However, they concluded the effects of skew were not significant, because all of the specimens failed at load levels exceeding 3.75 x HS-20 Design Tandem.

2.2.5 TxDOT Project 0-4418, Specimen 3 (Coselli 2004)

In the third phase of TxDOT project 0-4418, Coselli (2004) investigated a PC construction detail for 0° skew bridge decks at expansion joints. Instead of casting a thicker slab end, this new detail used the PC panels up to the edge of the expansion joint and then placed a cast-in-place topping over the panel (Figure 2.14 and Figure 2.15). Other test variables at the slab end included the use of expansion joint rails and the spacing of the top transverse reinforcement.

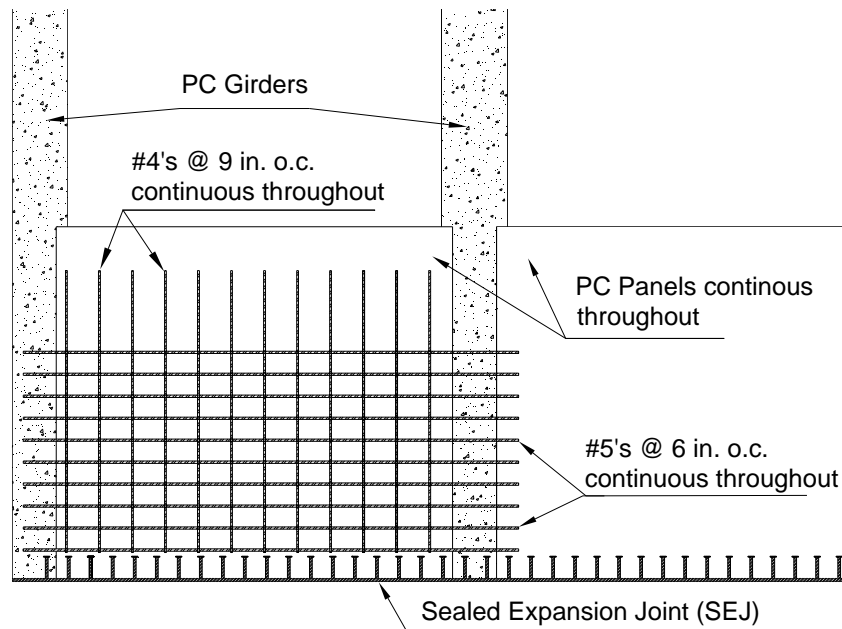


Figure 2.14: Plan View of PC Panel Detail

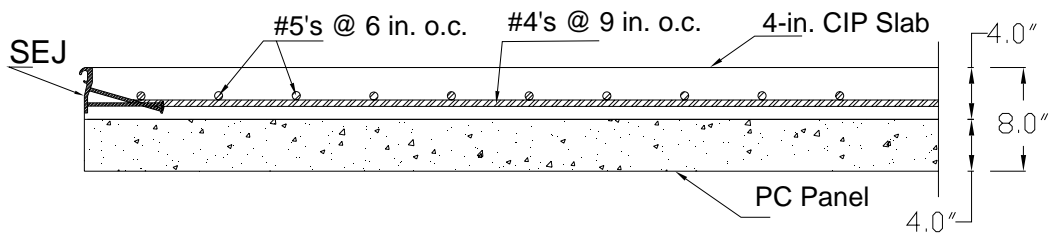


Figure 2.15: Cross Section view of Proposed PC Panel Detail

The plan of the test specimen is shown in Figure 2.16. The north end of the specimen was constructed with an armor joint rail (Figure 2.3) along the east half and a sealed expansion joint rail (Figure 2.3) along the west half. The south end was constructed without an expansion rail.

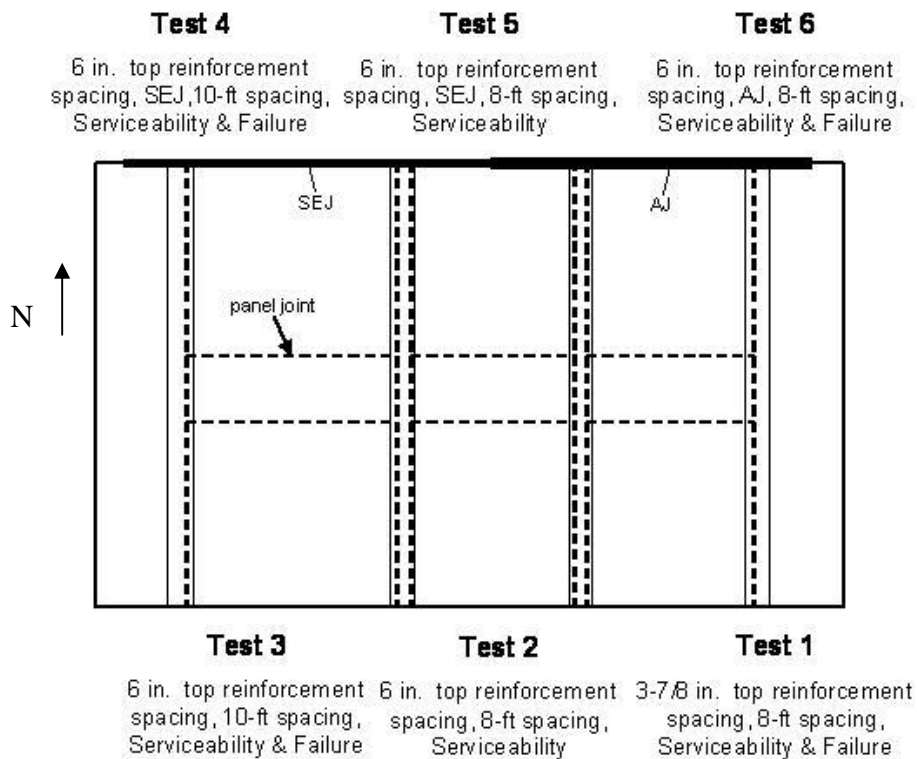


Figure 2.16: Plan View of PC specimen (Coselli 2004)

Because the PC detail was similar in depth to the UTSE detail, the top transverse reinforcement was spaced at 3-7/8 in. in the 4-ft wide end region at the southeast corner of the specimen. In the remainder of the specimen, the 6-in. spacing of the #5 bars was continued throughout the end detail.

Six tests were conducted to evaluate the design variables. First, each test area was loaded to design-level loads and typical overload levels. Next, four test locations were loaded incrementally until the specimen failed.

The results from the third test specimen indicate that the PC panel detail performed excellently when subjected to design level loads. In all of the test regions, with and without expansion joint rails, deflections were less than 0.06 in., and all transverse reinforcement strain values were less than 15% of yield strain at the design levels. Significant cracks were not observed until the applied loads exceeded two times the design levels. All tests failed in punching shear at applied loads more than five times the design tandem.

In test regions where an expansion joint rail was included, the midspan deflections were lower, and the maximum loads were 20% – 25% higher than test regions without a joint rail. The measured strains in the top transverse reinforcement were also lower when an expansion joint rail was included.

The spacing of the top reinforcement did not influence the failure load appreciably; however, the cracks were narrower and more uniformly distributed when the spacing of the transverse reinforcement was reduced.

2.3 SUMMARY

The research conducted prior to 1990 demonstrated that PC panels act compositely with the CIP topping slab, and that the interface between the panel and the CIP slab does not need additional reinforcement. However, all specimens included diaphragms at the end of the span. Most specimens were loaded in the middle of the deck, and few experimental programs evaluated full-scale specimens. No research has included tests of bridge deck details that included skewed angle orientations, and no research prior to 2003 had evaluated the IBTS detail at expansion joints.

Recently, researchers have continued to support the use of PC panels in bridge deck construction. The results from Dolan (1994) emphasized that proper consolidation around the expansion joint rails is an important construction detail.

The results from TxDOT project 0-4418 hold the most relevance to the current research project because they have led to this research project.

The tests reported by Ryan (2003) demonstrated that both the IBTS detail and the UTSE detail in bridges with 0° skew had capacities that greatly exceeded the required strength.

The tests reported by Griffith (2003) demonstrated that the skew angle decreased the capacity of the expansion joint details, but the capacities were still significantly higher than the required strengths.

The tests reported by Coselli (2004) demonstrated that the PC panel detail had sufficient strength. Coselli (2004) also suggested that further research be conducted to evaluate the fatigue behavior of the new PC panel detail at expansion joints in bridge decks with a 0° skew angle.

Because fatigue behavior is often important to bridge design, this behavior was considered a necessary research topic to be investigated in this current experimental series. Furthermore, no previous research has investigated fatigue behavior of expansion joints that have included armor joints or sealed expansion joints at the slab edge. Overall, the fatigue behavior of the proposed PC panel detail at expansion joint edges was not known, and there was a clear need to conduct this experimental program.

Chapter 3: Design of Test Specimens

Four sections of full-scale bridge slabs were designed and constructed to evaluate the fatigue performance of the PC panel detail at expansion joints. The preliminary design is discussed in Section 3.1 and the final design details are presented in Section 3.2. The loading history is discussed in Section 3.3, and the configuration of the reaction frame is presented in Section 3.4.

3.1 PRELIMINARY DESIGN

Issues considered during the preliminary design included the size of the test specimens required to evaluate the fatigue behavior of the PC panel detail. The research team decided that it was necessary to test specimens that reproduced the as-built conditions for TxDOT bridges. Therefore, full-scale PC panels and expansion joints were used to construct the test specimens. The research team conducted preliminary analyses to establish the dimensions of the specimens and then considered the constructability and costs involved with the proposed sizes.

The three specimens tested during TxDOT project 0-4418 (Ryan 2003, Griffith 2003, Coselli 2004) were constructed at full-scale and each specimen included sections of four longitudinal girders and a 32-ft wide bridge deck. Wheel loads were applied at multiple locations on each specimen to evaluate the behavior of the expansion joint details under both positive and negative moment. A similar construction arrangement was considered for the fatigue test specimens. An alternative arrangement was also proposed for the fatigue specimens that involved the construction of multiple, smaller sections of the bridge deck and testing those sections individually.

To determine the most practical specimen size, the cost involved with construction of a large full-width bridge deck was weighed against the potential benefits offered by testing multiple sections of a smaller, full-scale specimen. The research team concluded that testing smaller sections of a full-scale bridge deck was a better investment of time and resources, because more information would be generated. Smaller sections

were more economical to construct, and several specimens could be built more efficiently than one large bridge deck. Multiple test specimens would also allow for the repeatability of the test results to be evaluated.

As shown in Figure 2.8, a 10-ft girder spacing was used to evaluate the performance of the expansion joint details under positive moments in TxDOT project 0-4418 and an 8-ft girder spacing was used to evaluate the performance under negative moments. A similar plan was developed for this investigation. The positive moment specimen included two longitudinal girders, spaced at 10-ft on center, with a single precast PC panel spanning between the girders. The negative moment specimen included three longitudinal girders, spaced at 10-ft on center, with two precast PC panels. In both cases, the wheel loads were applied at the end of the PC panels, immediately adjacent to the expansion joint. Generally, it was desirable to evaluate the worse cases during the investigations, and various analyses were conducted to demonstrate that the moments induced in the test specimens were representative of those induced in the prototype bridge. The results were then used to indicate whether or not the test specimens were within the bounds of practical conditions. These analyses are discussed in the following sections.

3.1.1 Number of Spans in Transverse Direction

A transverse cross section of a typical bridge deck is presented in Figure 3.1, where the direction of traffic flow is perpendicular to the plane of the page. One way to analyze this three-dimensional structure under traffic loads is to idealize the slab as a continuous beam in the transverse direction of the bridge. The slab spans between the girders and experiences negative moments in the vicinity of the girders and positive moments at mid-span. A two-dimensional model of a three-span continuous slab supported by four girders was developed using SAP 2000. The slab was modeled using beam elements and the girders were idealized as pinned supports or roller supports.

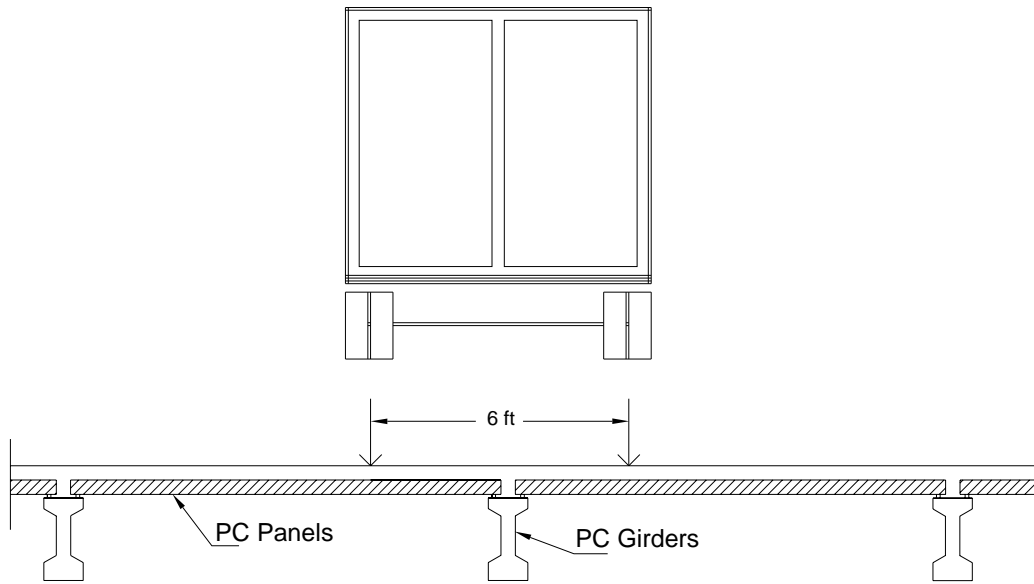


Figure 3.1: Transverse Cross Section of Typical Bridge Deck

The transverse placement of the design vehicle on the bridge deck influences the amplitude of the moments induced in the slab (Figure 3.1). The transverse spacing of wheel loads is 6 ft for both the HL-93 Design Truck and the HL-93 Design Tandem; therefore, this spacing was used in all analyses. The transverse locations of the wheel loads corresponding to the maximum positive and negative moments are shown in Figure 3.2.

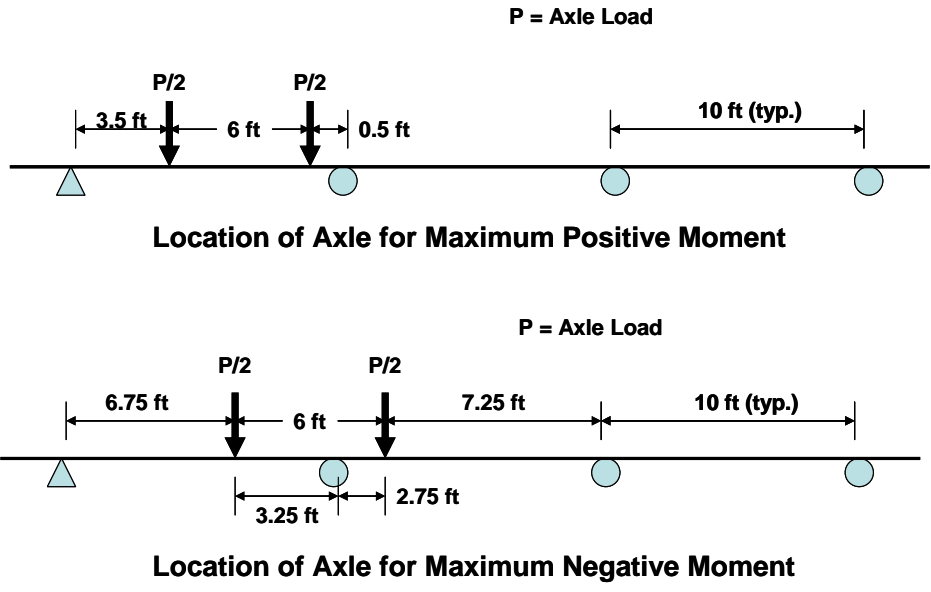


Figure 3.2: Locations of the Axle Loads Used in SAP Analysis

A two-dimensional representation of the positive moment specimen is shown in Figure 3.3. A single wheel load was positioned at mid-span. The maximum positive moment induced in the two-dimensional model of the test specimen (Figure 3.3) was 20% larger than the maximum positive moment induced in the continuous bridge deck model (Figure 3.2).

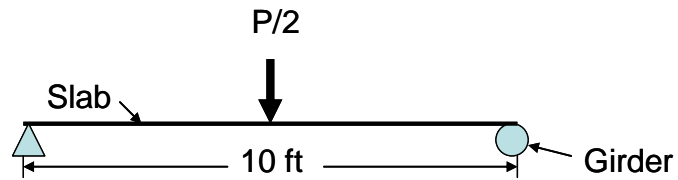


Figure 3.3: Cross Section Idealization of Proposed Positive Moment Specimen

A similar analysis was conducted for the negative moment specimen (Figure 3.4). Two wheel loads were applied to the specimen, which were centered about the center support. The maximum negative moment induced in the two-dimensional model of the test specimen was 9% larger than the maximum negative moment induced in the continuous bridge deck model (Figure 3.2).

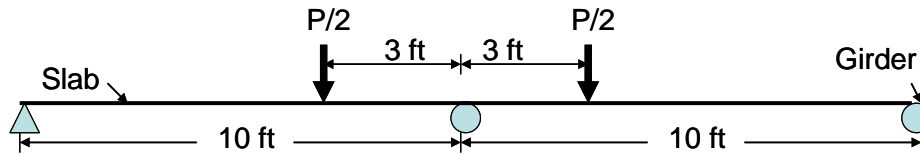


Figure 3.4: Idealization of Proposed Negative Moment Specimen

The results of the two-dimensional SAP analyses indicated that the proposed test specimens would develop moments that are comparable to those in a continuous bridge deck. However, three-dimensional elastic analyses were also conducted to verify that the applied loads were distributed as intended.

3.1.2 Length of Test Specimens in the Longitudinal Direction

In TxDOT project 0-4418, Ryan (2003) developed a three-dimensional model of the bridge deck and concluded that the magnitude of the moments in the slab decreased rapidly with distance from the expansion joint (Figure 3.5) when the design tandem was applied at the expansion joint. In these analyses, the moments 8 ft from the expansion joint were less than 10% of the moments at the expansion joint. Therefore, the lengths of the test specimens for this investigation were taken as 8 ft. A series of three-dimensional analyses were then conducted to verify that the moments induced in the test specimens were representative of those in the prototype structures.

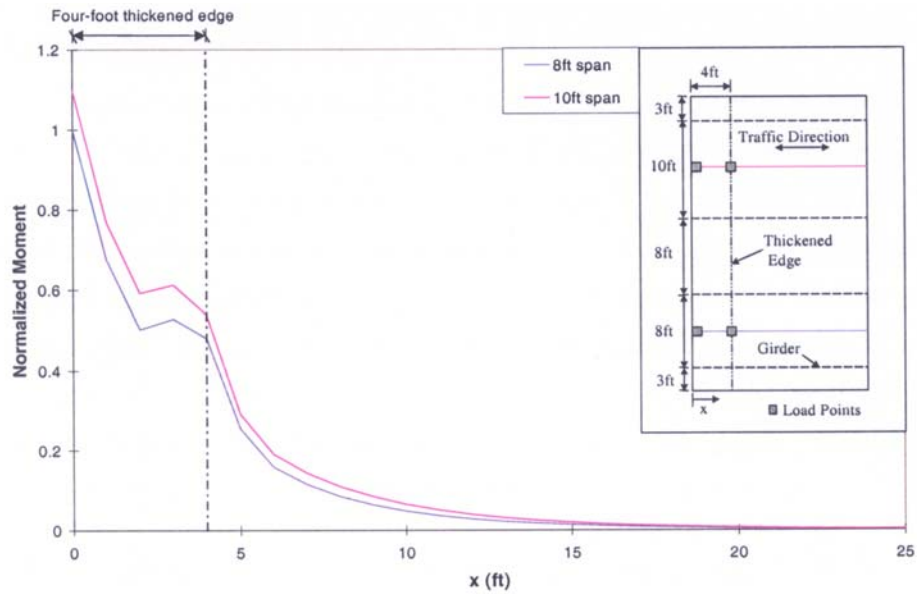


Figure 3.5: Slab Moment versus Longitudinal Distance (Ryan 2003)

3.1.2.1 Computational Models

Three-dimensional, elastic models were developed using ABAQUS. The finite element models were constructed using solid, eight-noded elements with reduced integration. Nodes were spaced at approximately 4 in. in all directions, except the vertical spacing was reduced to 1 in. within the depth of the slab. No attempt was made to model the reinforcement embedded in the concrete or cracking of the concrete.

The first model was a 32-ft wide bridge deck with four longitudinal girders (Figure 3.6.) The model was 20 ft in the longitudinal direction. The 8-in. slab was assumed to be monolithic with the girders. Each girder was 12 in. wide and extended 12 in. below the slab. The nodes at each end of the centerline of the beams were restrained against translation in all three directions.

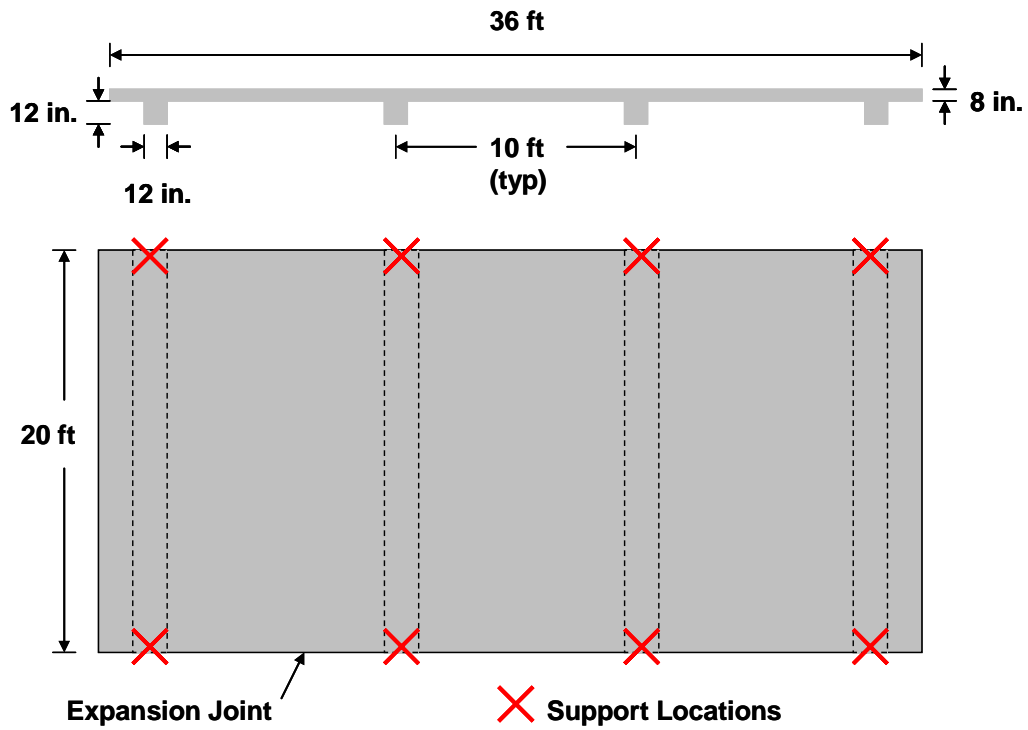
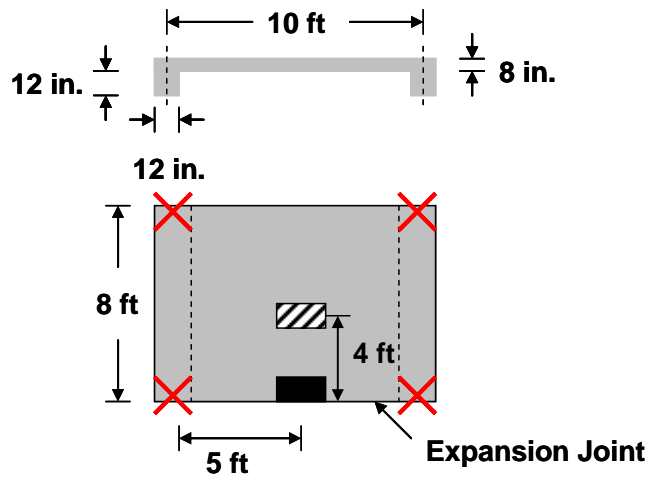


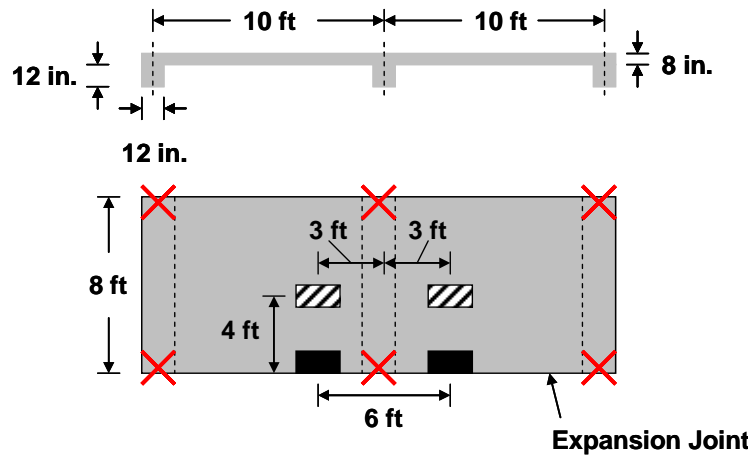
Figure 3.6: Cross Section and Plan Views of 3-D Model of Bridge Deck

Similar models were developed for the positive moment test specimen (Figure 3.7) and the negative moment test specimen (Figure 3.8). In both cases, the slab was assumed to be monolithic with the beams and the beams were supported only at the ends. In the analyses, the supports were restrained from translation in all directions.



- Load Point for Rear Axle of HL-93 Design Truck
- Additional Load Point for HL-93 Design Tandem
- ✗ Support Locations

Figure 3.7: Cross Section and Plan Views of 3-D Model of Positive Moment Specimen



- Load Point for Rear Axle of HL-93 Design Truck
- Additional Load Point for HL-93 Design Tandem
- ✗ Support Locations

Figure 3.8: Cross Section and Plan Views of 3-D Model of Negative Moment Specimen

3.1.2.2 Applied Loads

For the full-width model, two load cases were considered to maximize the induced moments, and a total of four analyses were run. First, the rear axle of the HL-93 Design Truck was analyzed. The axle load was placed adjacent to the expansion joint in the longitudinal direction, and in the transverse direction the wheel loads were positioned to induce the maximum moments based on the two-dimensional analysis Figure 3.2. Figure 3.9 shows the loading used to determine the maximum the positive moment, and Figure 3.10 shows the loading used to determine the maximum negative moment.

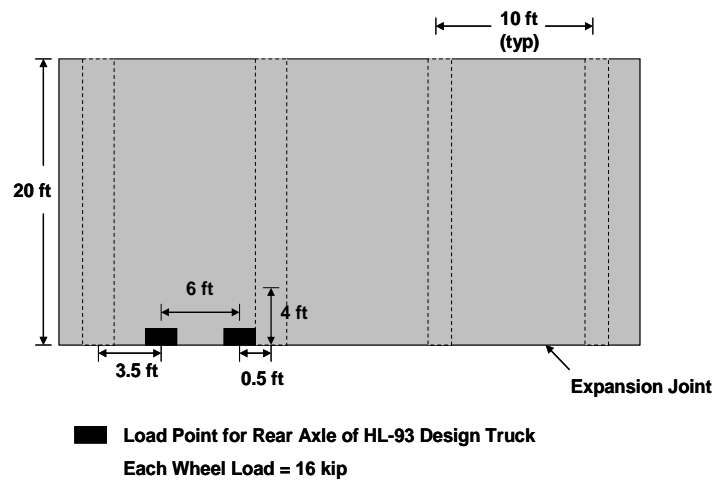


Figure 3.9: 3-D Model for Maximum Positive Moment with HL-93 Design Truck

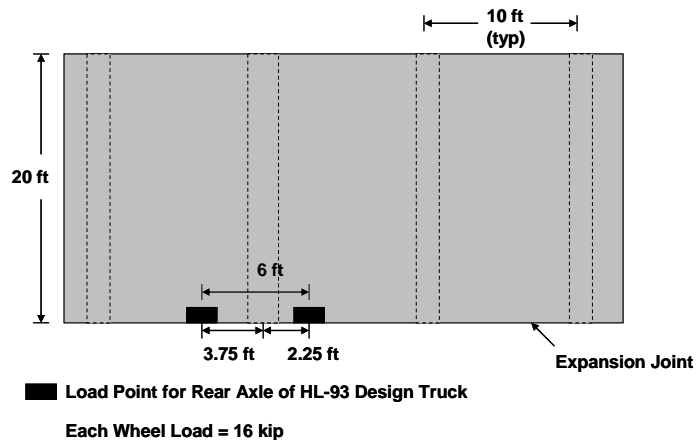


Figure 3.10: 3-D Model for Maximum Negative Moment with HL-93 Design Truck

In the second set of analyses, the HL-93 Design Tandem was analyzed to maximize the positive and negative moments. The first axle load was placed adjacent to the expansion joint in the longitudinal direction, and the second axle load was placed four feet from the edge. In the transverse direction the locations were identical to those shown in Figure 3.2. Figure 3.11 shows the loading used to determine the maximum the positive moment, and Figure 3.12 shows the loading used to determine the maximum negative moment.

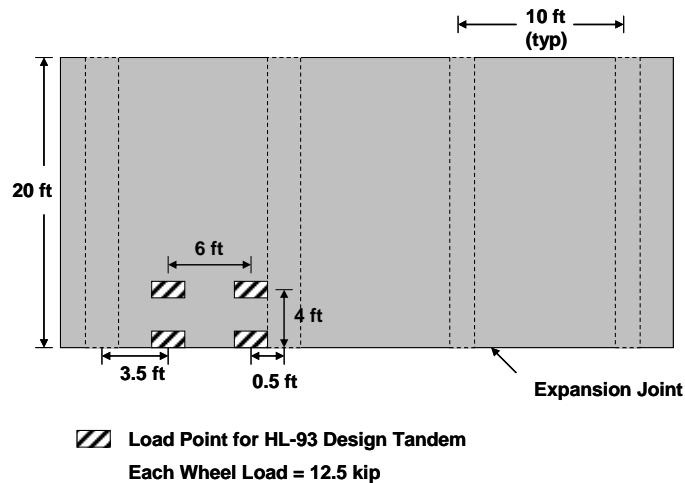


Figure 3.11: 3-D Model for Maximum Positive Moment with HL-93 Design Tandem

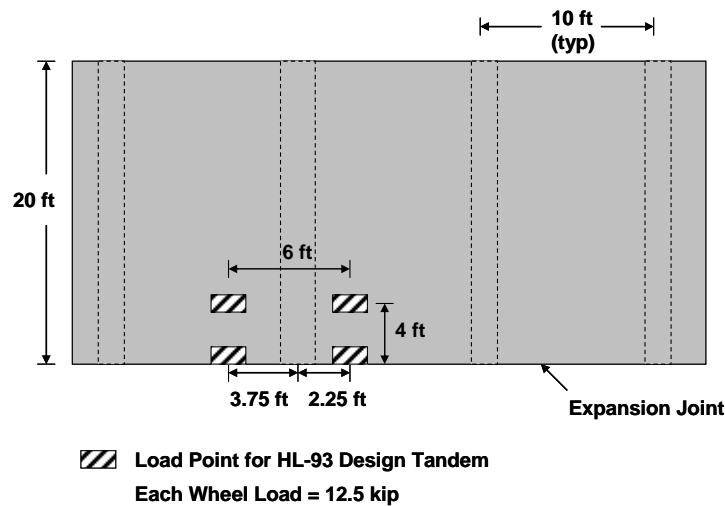


Figure 3.12: 3-D Model for Maximum Negative Moment with HL-93 Design Tandem

In the finite-element models, each wheel load was assumed to be uniformly distributed over a 10 in. by 20 in. area. The HL-93 Design Tandem configuration resulted in a loading of 12.5 kip per load plate (62.5 psi over the loaded area), and the HL-93 Design Truck resulted in a loading of 16 kip per load plate (80 psi over the loaded area).

3.1.2.3 Calculated Response

The four loading configurations described in Section 3.1.2.2 were analyzed, and the results are discussed in this section. For an example of one load case analysis, the two views in Figure 3.13 provide a general illustration of the principal stresses in the bridge deck when the HL-93 Design Truck loading was applied (Figure 3.9) to induce the maximum positive moment. The green color represents zero stress and the varying shades of blue represent compressive stresses with the darkest blue representing the maximum compressive stress. Similarly, the shades of red and yellow represent tensile stresses, and the darkest red represents the maximum tensile stress. As expected, the results of the analyses indicate that the maximum principal stresses occur at the slab edge. The results of the four analyses are summarized in Table 3.1.

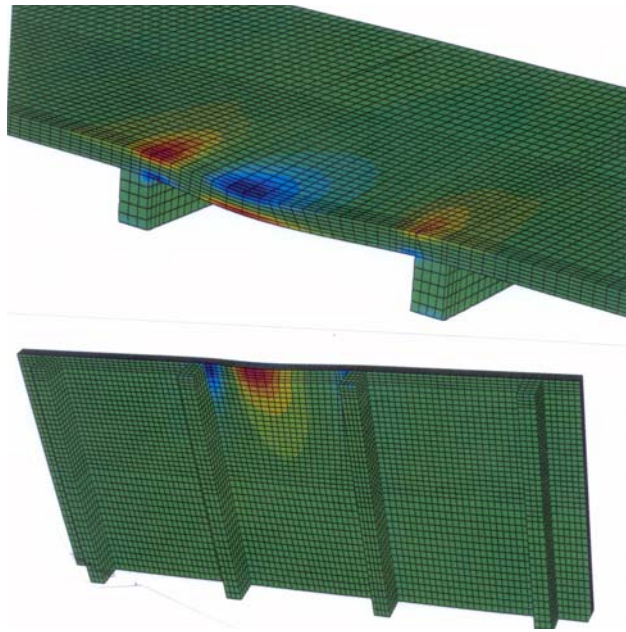


Figure 3.13: Plots of Maximum Principal Stresses in Full-Width Model

Table 3.1: Maximum Values of Principal Stress from Elastic Finite Element Analyses of Bridge Deck

	Load Placed to Maximize Positive Moment		Load Placed to Maximize Negative Moment	
	HL-93 Design Truck	HL-93 Design Tandem	HL-93 Design Truck	HL-93 Design Tandem
Compressive Stress (psi)	555	581	617	620
Tensile Stress (psi)	498	492	522	466

The results from Table 3.1 show that for the load case shown in Figure 3.13, the maximum compressive stress (555 psi) occurred beneath the load point at the top of the specimen, and the maximum negative stress (498 psi) occurred beneath the load point on the bottom side of the slab.

For the proposed positive moment test specimen, two load cases were analyzed to compare with the results from the full-width bridge deck. These results are presented in

Table 3.2, and show that the HL-93 Design Truck resulted in higher maximum principal stresses than the HL-93 Design Tandem.

Table 3.2: Maximum Values of Principal Stress from Elastic Finite Element Analyses of Positive Moment Specimen

	Load Placed to Maximize Positive Moment	
	HL-93 Design Truck	HL-93 Design Tandem
Compressive Stress (psi)	648	603
Tensile Stress (psi)	544	508

Similarly, for the proposed negative moment specimen, two load cases were analyzed, and the results are presented in Table 3.3. The results also showed that the HL-93 Design Truck resulted in higher maximum principal stresses than the HL-93 Design Tandem.

Table 3.3: Maximum Values of Principal Stress from Elastic Finite Element Analyses of Negative Moment Specimen

	Load Placed to Maximize Positive Moment	
	HL-93 Design Truck	HL-93 Design Tandem
Compressive Stress (psi)	682	640
Tensile Stress (psi)	540	485

The maximum principal stresses calculated in the proposed test specimens were compared with the maximum principal stresses calculated for the full-size model. The results in Table 3.1, Table 3.2, and Table 3.3 illustrate that the 8-ft long test specimens experienced realistic values of maximum principal stresses when compared to the full-size model. For example, when loaded with the HL-93 Design Truck, the maximum tensile stress in the positive moment specimen (544 psi) was about 9% higher than the maximum tensile stress that occurred in the full-size deck (498 psi). These result also confirmed the previous conclusion that the test specimens represented more critical loading conditions than the full-width specimens.

The HL-93 Design Truck loading was compared with the HL-93 Design Tandem loading for both specimens. The ABAQUS analysis allowed the research team to determine which load configuration created higher principal stress values at the slab edge. In all three ABAQUS models, the HL-93 Design Truck resulted in higher maximum tensile stresses at the slab edge. The HL-93 Design Truck also induced larger compressive stresses in the test specimens, but the HL-93 Design Tandem induced larger compressive stresses in the full deck model. Because the HL-93 Design Truck was determined to be the critical load configuration, it was applied to the test specimens for this research project.

A visual inspection of Figure 3.14 reveals that the distribution of calculated stresses in the test specimen resembled the response of the full deck shown in Figure 3.13. This figure had a different color legend for the stress values, but the locations of the maximum principal stresses and the area affected by the loading were essentially the same as the full-width model. The magnitudes of the computed stresses have been presented in Table 3.2, but this figure was included to illustrate the flow of stresses throughout the depth of the positive moment test specimen.

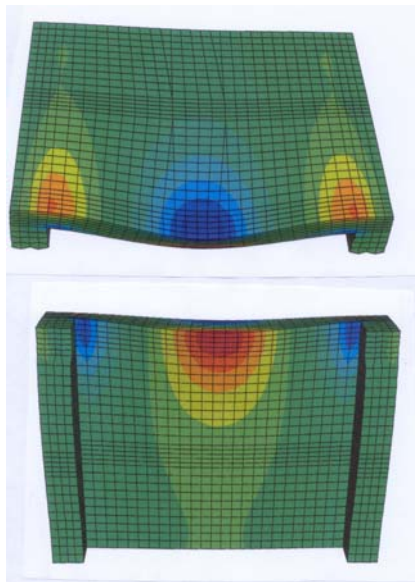


Figure 3.14: Plots of Maximum Principal Stresses in Positive Moment Specimen

Because the test specimens was loaded at the edge, the reactions at the back corners of the specimen were investigated to determine if the back corners would lift up during testing. A secondary investigation was conducted using the ABAQUS analyses. A simple check of the support reactions showed that all supports remained in compression under the applied loads. This result indicated that no additional tie-downs were required for the test specimens if the longitudinal dimension was 8-ft.

Based on the comparisons of the ABAQUS results, it was concluded that 8-ft was an appropriate length for the test specimens in the longitudinal dimension.

3.2 FINAL DESIGN OF TEST SPECIMENS

During the final design stage, the research team selected the final dimensions of the specimens, construction details, construction sequence, and specified material properties.

Two positive moment specimens were designed, and two negative moment specimens were designed. The nomenclature used to identify the test specimens is as follows: 1) positive (P) or negative (N) moment, 2) 0° skew (0), 3) PC panel detail (P), and 4) the specimen number (1 or 2). For example, the first positive specimen was designated POP1, the second positive moment specimen was designated POP2, the first negative moment specimen was NOP1, and the second negative moment specimen was NOP2.

The girder spacing was 10-ft for all specimens, and the specimen length was 8-ft. A cross section of the positive moment specimen is presented in Figure 3.15, and a plan view is presented in Figure 3.16. Similarly, a cross section of the negative moment specimen is presented in Figure 3.17, and a plan view is presented in Figure 3.18.

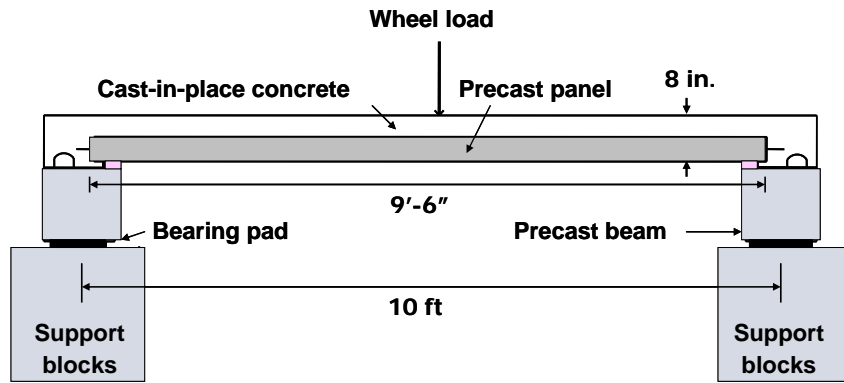


Figure 3.15: Cross Section of Positive Moment Specimens (Not to Scale)

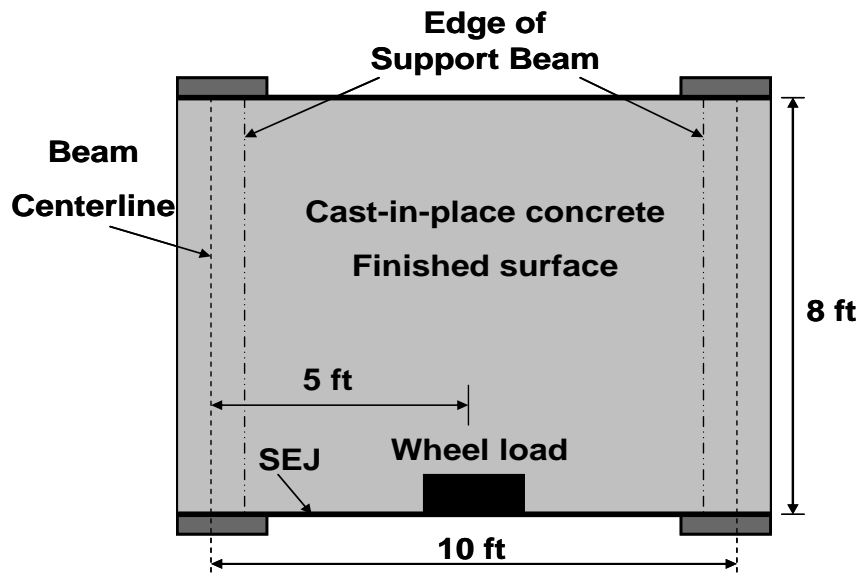


Figure 3.16: Plan View of Positive Moment Specimens (Not to Scale)

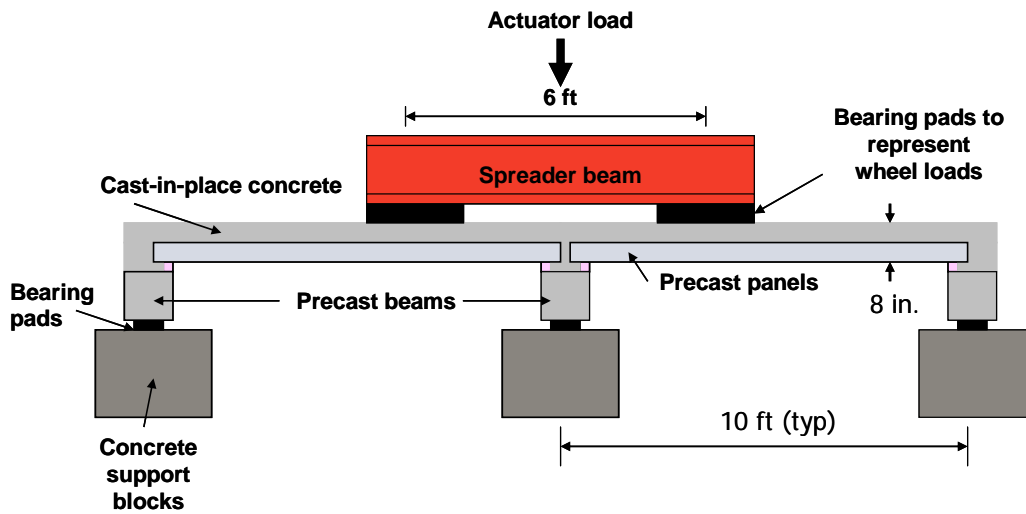


Figure 3.17: Cross Section View of Negative Moment Specimens (Not to Scale)

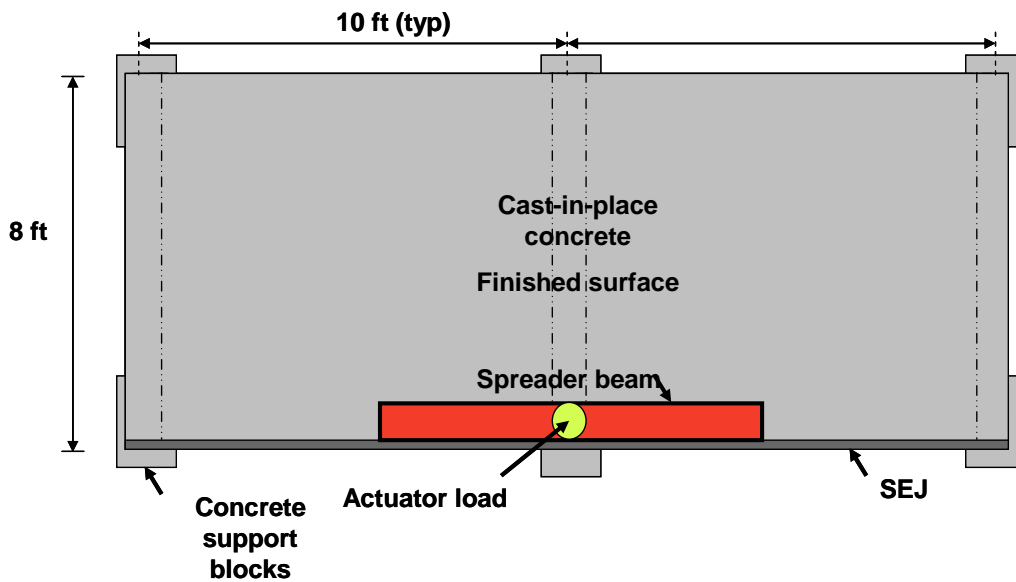


Figure 3.18: Plan View of Negative Moment Specimens (Not to Scale)

3.2.1 Precast Concrete Support Blocks

The test specimens were designed to provide access to the research team to mark cracks on the bottom surface of the slab. Concrete blocks (30-in. long, 20-in. wide, and

20-in. tall) were positioned at each end of each beam. These blocks served to elevate the test specimens to a practical height (Figure 3.19).



Figure 3.19: Concrete Support Block and Bearing Pad

3.2.2 Precast Support Beams

In typical TxDOT bridge construction practice, the PC panels are placed on top of the PC bridge girders. As mentioned in Chapter 1, the PC panels are placed along the length of each side of bridge girders (Figure 3.20). Furthermore, a standard TxDOT detail for PC beams is included in Figure 3.21, and shows that the top width of typical PC girders ranges from 12-in. to 20-in. Figure 3.21 also illustrates that shear reinforcement protrudes from the top of these beams to provide horizontal shear reinforcement and to ensure composite action between the girder and the CIP topping slab.

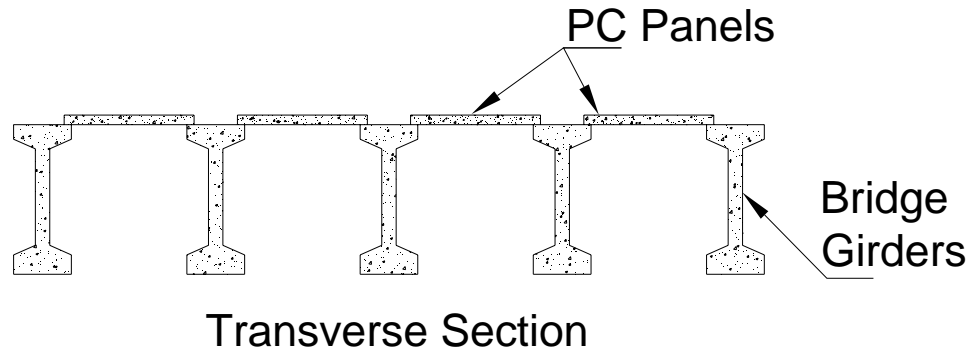


Figure 3.20: Typical Placement of PC Panels on Edge of PC Girders

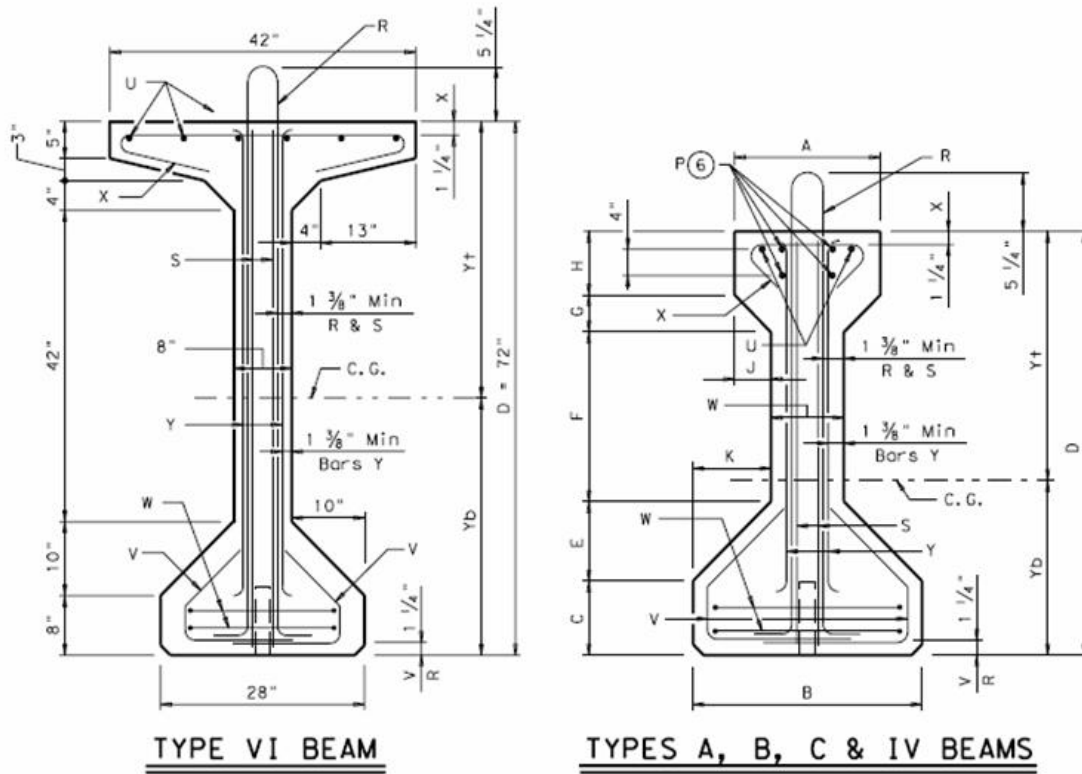


TABLE OF BEAM DIMENSIONS AND SECTION PROPERTIES																
BEAM TYPE	A in.	B in.	C in.	D in.	E in.	F in.	G in.	H in.	J in.	K in.	W in.	Yt in.	Yb in.	AREA in. ²	I in. ⁴	Weight plf
A	12	16	5	28	5	11	3	4	3	5	6	15.39	12.61	275.4	22,658	287
B	12	18	6	34	5 3/4	14	2 3/4	5 1/2	2 3/4	5 3/4	6 1/2	19.07	14.93	360.3	43,177	375
C	14	22	7	40	7 1/2	16	3 1/2	6	3 1/2	7 1/2	7	22.91	17.09	494.9	82,602	516
IV	20	26	8	54	9	23	6	8	6	9	8	29.25	24.75	788.4	260,403	821
VI	See section for beam dimensions											35.60	36.40	1,084.4	732,586	1,130

Figure 3.21: Cross Section of Typical PC Girder Dimensions (TxDOT)

For the test specimens, the support beams were designed to have a top width that would represent the top flange dimensions of typical TxDOT beams. A 12-in. width was selected because it provided sufficient bearing area for the PC panel.

Because the test specimens would only be loaded along the edge of the slab parallel to the expansion joint, the support beams would not experience large bending moments or shear forces. The depth of the beam was designed to be 12-in. because the required nominal capacity was low. Also, the beams were designed to be 8-ft long, the same length as the PC panels. Three #8 reinforcing bars were placed as tension reinforcement, and #3 stirrups were placed as shear reinforcement at a constant spacing of 4-in. on center throughout the length of the support beam.

The main purpose of these beams was to support the edges of the PC panel and to reproduce typical TxDOT conditions. In most TxDOT PC girders, horizontal shear reinforcement is included to resist the shear at the interface of the PC girder and the CIP deck. Therefore, #4 U-bars were cast in the support beams to reflect typical TxDOT conditions (Figure 3.22).

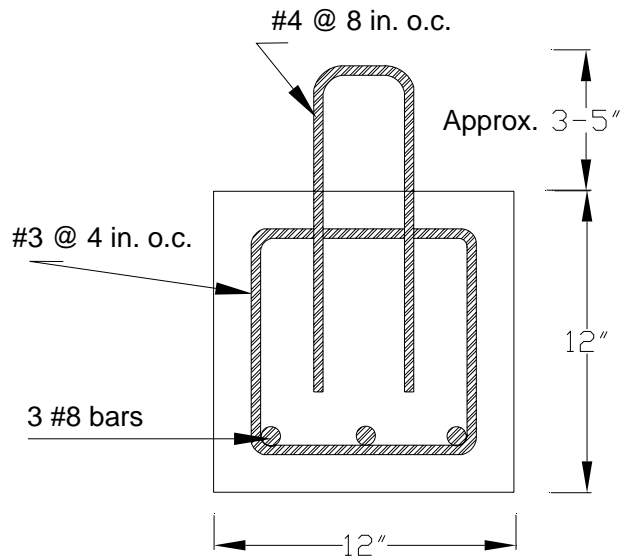


Figure 3.22: Cross Section of Precast Support Beams

3.2.3 Bearing Pads

TxDOT bridge girders typically are supported by steel reinforced, elastomeric bearing pads at the ends of the simply-supported bridge spans. To reproduce these conditions, the test specimens incorporated this same construction detail. Bearing pads (2.5-in. thick, 9-in. wide, and 13-in. long) were used at the ends of all the precast beams (Figure 3.19).

3.2.4 Bedding Strips

When the PC panels are placed on top of the bridge girders, the panels do not rest directly on the concrete surface of the bridge girder. The panels bear upon a continuous foam strip, or bedding strip, that is glued to the edges of the top flanges of the PC girder. Part of the panel extends beyond the bedding strip towards the center of the beam which creates a gap that allows the cast-in-place concrete to flow underneath the panel to provide uniform bearing. In the field, the bedding strips are cut from sheets of Foamular 400, a type of extruded polystyrene insulation manufactured by Owens Corning. As shown in Figure 3.23, the height and width of the bedding strips are varied in the field to account for camber in the prestressed girders or the grading of the bridge deck surface. At expansion joints, the typical dimensions of bedding strips approach the maximum allowable dimensions listed in Figure 3.23, because, if the top surface of the bridge deck is level, and the panels bear directly on the beams, the camber in the beams will cause a thicker slab at the supports and a thinner slab at mid-span.

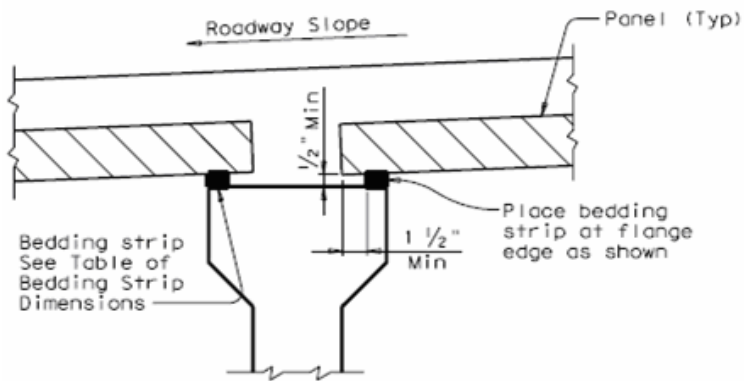


TABLE OF BEDDING STRIP DIMENSIONS		
WIDTH	HEIGHT (2)	
	Min	Max
1" (Min)	1/2"	2"
1 1/4"	1/2"	2 1/2"
1 1/2"	1/2"	3"
1 3/4"	1/2"	3 1/2"
2" (Max)	1/2"	4"

Figure 3.23: Cross Section and Limits of Bedding Strip Detail (TxDOT)

The research team desired to recreate typical bridge conditions, but also wanted to test the most severe conditions. The most severe condition corresponded to the minimum bedding strip height that would make it more difficult to place concrete underneath the panel. Initially, a 1-in. wide by 1/2-in. tall bedding strip was chosen, but during construction of the first specimen, the bedding strip was heavily compressed and deemed unacceptable. The bedding strip dimensions were then increased to 1 1/2-in. wide by 1-in. tall. This larger dimension was acceptable because the dimensions of the bedding strip at typical expansion joints are often larger.

Another factor involved with the bedding strip detail is the overhang distance of the PC panel past the bedding strip. As indicated in the table in Figure 3.23, the minimum allowable overhang distance is 1 1/2-in. To create a more critical condition, the final overlap distance was designed to be the minimum distance of 1 1/2-in. The construction photograph (Figure 3.24) of the bedding strip detail shows that the panel overlap exceeded 1 1/2 in. and had to be repositioned accordingly.

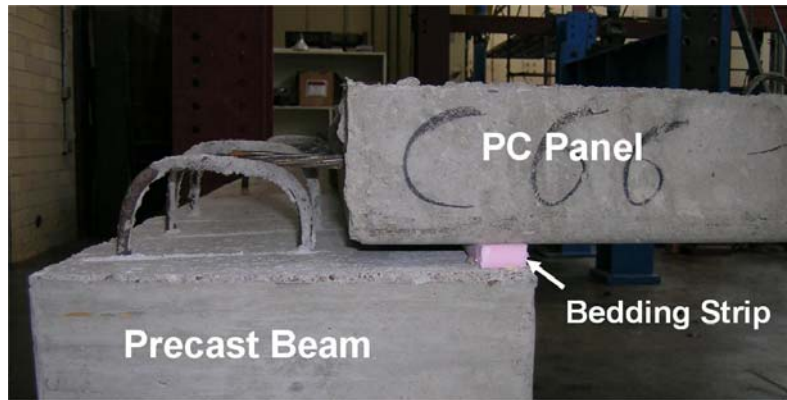


Figure 3.24: Test Specimen Bedding Strip and PC Panel Cross Section

3.2.5 Precast Prestressed Concrete Panels

The girder spacing was 10 ft in all test specimens. Therefore, PC panels with a width of 9 ft- 6 in. were selected. Each panel was 8 ft long, which is the typical length. The panels were 4 in. thick and contained 3/8-in. diameter prestressed steel strands at 6 in. on center in the transverse direction. Welded wire fabric provided the minimum temperature and shrinkage reinforcement in the direction of the girders. All panels were constructed by a local prestressed concrete producer.

3.2.6 Steel Reinforcement

The layout of the Grade 60 steel reinforcement was designed according to standard TxDOT details. In the longitudinal direction of the slab, #4 bars were placed at 9 in. on center throughout the entire 10 ft width. In the transverse direction, #5 bars were placed at 6-in. on center throughout the entire 8 ft length. The bars were placed on 7/8-in. rebar chairs to provide a 2-in. clear cover to the top surface of the slab (Figure 3.25).

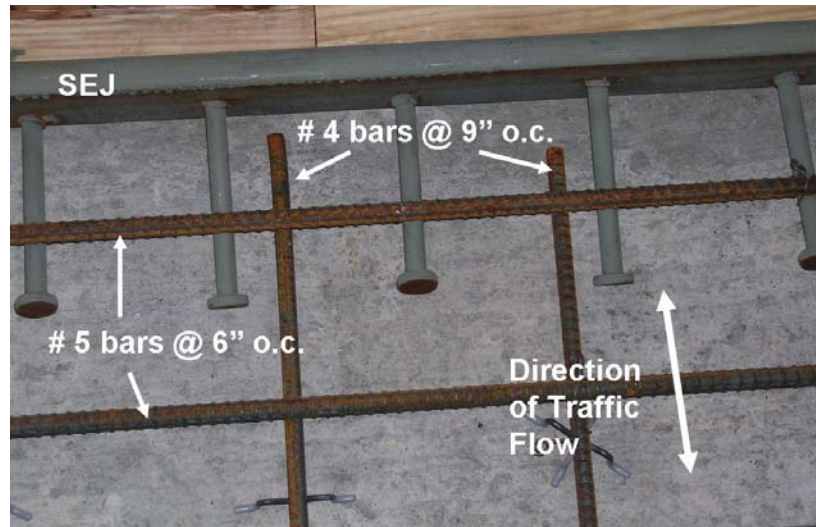


Figure 3.25: Steel Reinforcement for Positive Moment Specimen

3.2.7 Sealed Expansion Joint (SEJ)

According to TxDOT, the most common expansion joint rail used in bridge slabs is the SEJ-A detail (Figure 2.2). Therefore, the SEJ-A section was chosen for the final design. The SEJ-A section is 3½ in. deep and fits within the space allowed by a 4-in. thick CIP topping. In the previous specimen tested by Coselli (2004), the SEJ-P was used, which required the studs to be bent because the SEJ-P section is deeper than the allowable 4-in. depth of the CIP topping. For this investigation, 6-in. steel studs were welded to the SEJ section at a spacing of 6 in. on center (Figure 3.26). Erection bolt holes were drilled every 4 ft along the member to connect to the formwork prior to placing the CIP topping.



Figure 3.26: SEJ-A Steel Studs Prior to Casting

3.2.8 Concrete Mixture

The design mixture for all test specimens was based on TxDOT specifications for Class “S” structural concrete which is used for all bridge slabs. The minimum specified compressive strength was 4000 psi, and the maximum water to cementitious material (w/cm) ratio was 0.45. All concrete was provided by a ready-mix plant, and a summary of a cubic-yard batch weights is included in Table 3.4. The weights for the fine aggregates and the course aggregates are based on a saturated surface dry (SSD) condition.

Table 3.4: Concrete Mixture Proportions

Cement (lb/yd ³)	SSD Fine Aggregate (lb/yd ³)	SSD Course Aggregate (lb/yd ³)	Water (lb/yd ³)	Fly Ash (lb/yd ³)
479	1350	1857	250	85

3.3 LOAD HISTORY

The primary objective of the investigation was to evaluate the performance of the expansion joint detail subjected to fatigue loading. However, it was not possible to measure the response of the specimens during the fatigue tests; therefore, the tests were stopped periodically to perform static tests. Displacements and strains were recorded

during the periodic tests. At the conclusion of the fatigue tests, each specimen was loaded statically to failure. Each type of test is discussed in the sections below.

3.3.1 Fatigue Loading

The fatigue loadings were initially selected to represent service-level traffic loadings. Because the specimens exhibited excellent fatigue response, the fatigue loads were gradually increased until design-level loads were used for the last specimen.

Service-level axle loads were determined from weigh-in-motion (WIM) data from I-35 South of San Antonio (Wood, et al. 2007). A histogram of axle weights measured over a 50-day period is shown in Figure 3.27, and the effective axle weight was 12 kip.

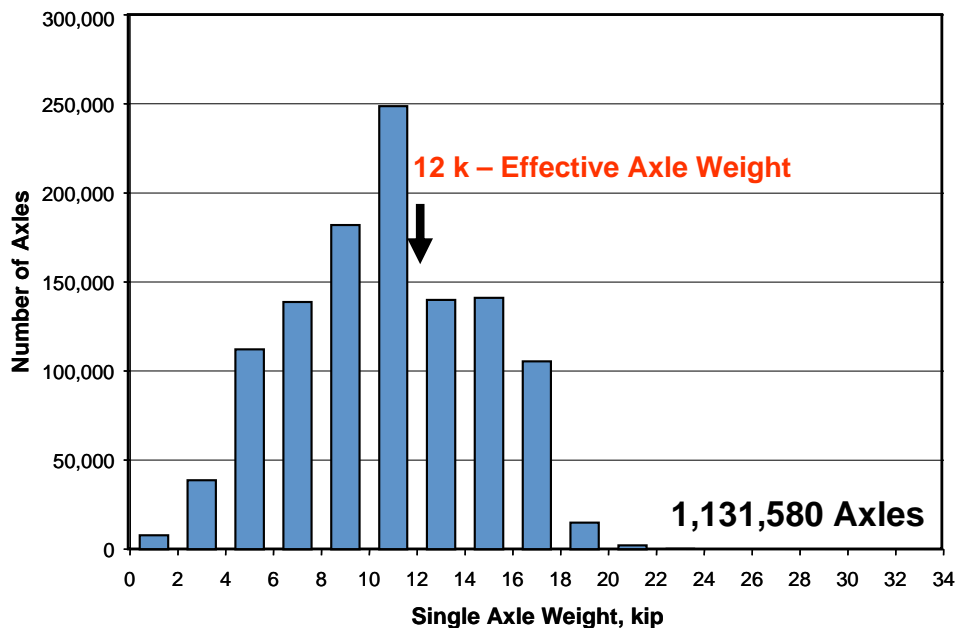


Figure 3.27: Histogram of Weigh-In-Motion Data (Wood, et al. 2007)

As determined in previous sections, wheel loads were applied to the two positive moment specimens (POP1 and POP2). The applied wheel load for specimen POP1 (6 kip) corresponded to one half of the effective axle load from the WIM data. Because of the excellent fatigue response of specimen POP1, the design-level fatigue load for specimen POP2 (16 kip) corresponded to one half of the rear axle from the HL-93 Design Truck.

For the two negative moment specimens (N0P1 and N0P2), the full axle load was placed across the central support beam. Because of the excellent fatigue response of specimen P0P2, the load for specimen N0P1 (32 kip) corresponded to the rear axle of the HL-93 Design Truck. Again, the fatigue response of specimen N0P1 was excellent, so the fatigue load for the specimen N0P2 was increased to represent an amplification factor and a dynamic impact factor. The amplification factor of 1.25 was used to represent an overload truck, which has been used often in Texas to represent heavier loaded trucks due to the NAFTA trade agreements. The dynamic impact factor ($1+I = 1.15$) is specified for fatigue design of bridge decks in the AASHTO LRFD Design Specifications.

The target length of the fatigue tests was 5 million cycles, and Table 3.5 presents a summary of the load histories applied to the four test specimens.

Table 3.5: Summary of Applied Load Histories

Specimen	Fatigue Level	Load Type	Cyclic Load (kip)
P0P1	Service	Wheel Load	6
P0P2	Design	Wheel Load	16
N0P1	Design	Axle Load	32
N0P2	Overload	Axle Load	46

3.3.2 Periodic Static Loads

The periodic static tests served two purposes. The first purpose was to record data at regular intervals throughout the fatigue loading in order to observe the structural behavior of the bridge slab at different points throughout the fatigue loading history. The load for the static tests was the HL-93 Design Truck load: 16 kip per wheel load for the positive moment specimens and 32 kip per axle load for the negative moment specimens.

The second purpose of the periodic static tests was to apply a static overload to initiate cracks in the test specimen. This 50-kip overload was applied after 2,000,000 fatigue cycles. It was desirable to crack the specimen because it was assumed that most bridge slabs experience an overload at some point in their design life, and the research team sought to evaluate the fatigue performance of a cracked test specimen after the overload event.

3.3.3 Load to Failure

The purpose of the load to failure was to compare the data from the smaller specimens considered in this research project with the data from the full-size specimen constructed by Coselli (2004). After the fatigue tests were completed, the test specimens were loaded to failure with a hydraulic ram.

3.4 REACTION FRAME

A reaction frame was designed to support the actuators used to load the test specimens. Two W12x65 columns were used for the reaction frame columns. Bolted to the columns were two W30x108 beams with coped flanges to allow the web of the beams to be bolted directly to the flanges of the columns. The reaction frame was bolted to the strong floor at Ferguson Structural Engineering Laboratory.

The fatigue loads were applied using a 50-kip MTS hydraulic actuator. The 73-in. tall actuator was bolted to a steel plate that was bolted to the reaction frame. For the positive moment specimens, a 10-in. by 20-in. load plate was bolted to the head of the actuator to apply load to the slab. For the negative moment specimens, the actuator was bolted to a spreader beam that was welded to two load plates, which were supported on rubber bearing pads.

Figure 3.28 through Figure 3.33 provide several views of the reaction frame used for the positive and negative moment test specimens.

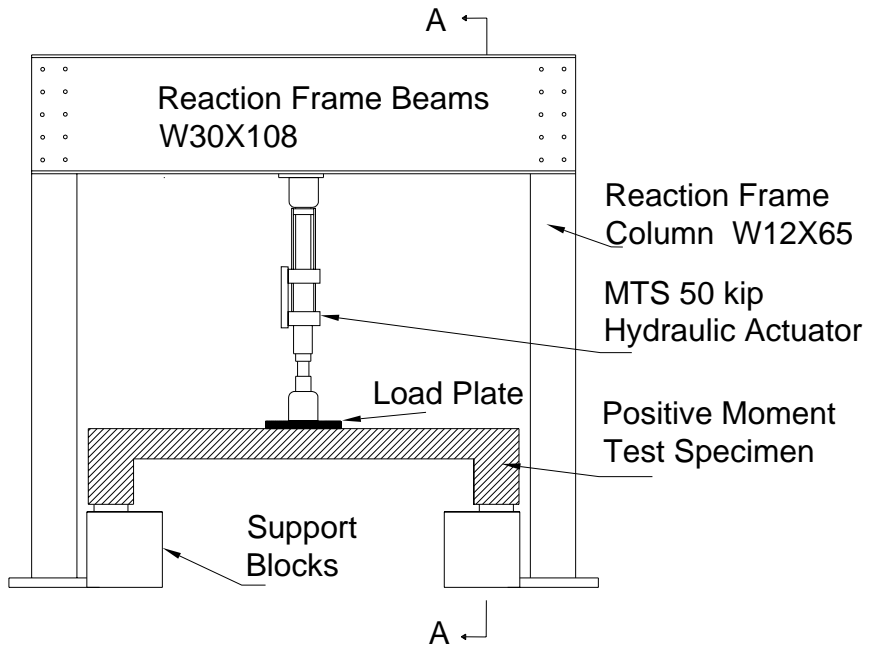


Figure 3.28: Elevation of Positive Moment Specimen Reaction Frame

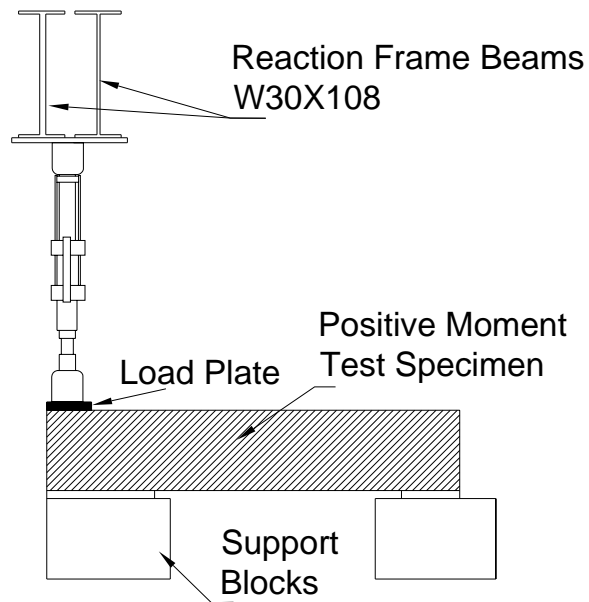


Figure 3.29: Section A-A Positive Moment Specimen Reaction Frame

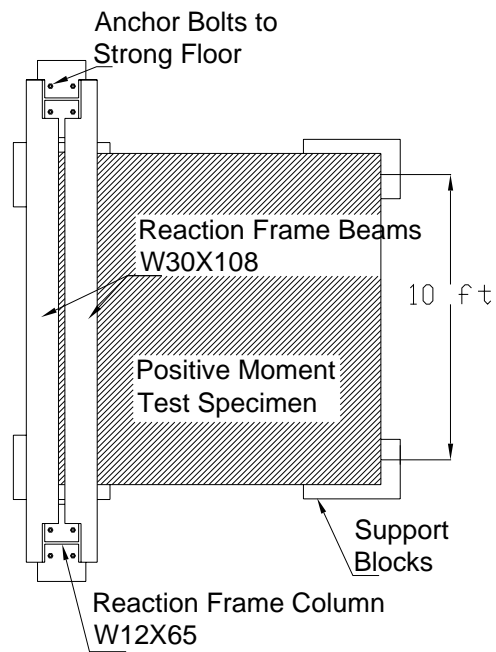


Figure 3.30: Plan View of Positive Moment Test Specimen Reaction Frame

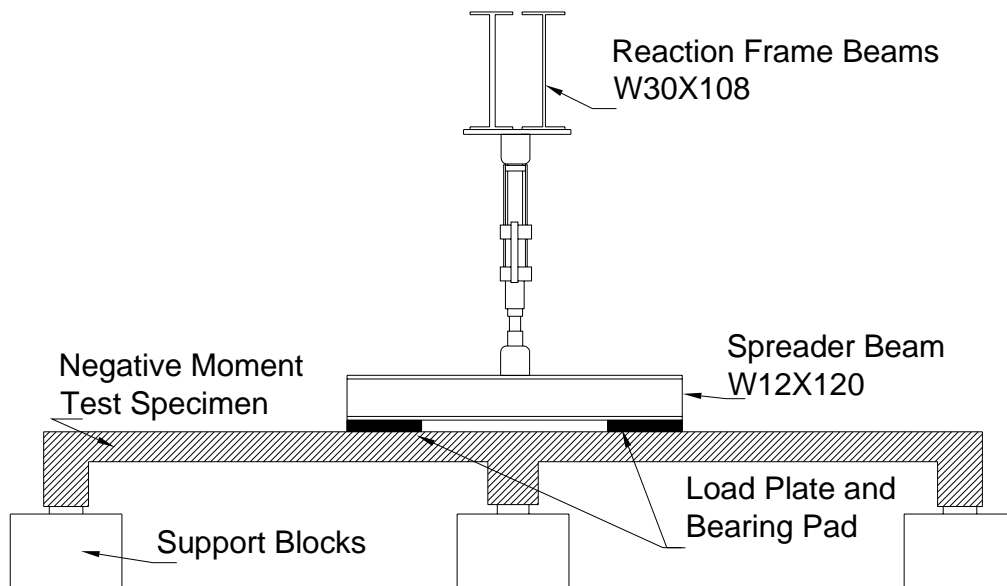


Figure 3.31: Elevation of Negative Moment Specimen Reaction Frame (Section B-B)

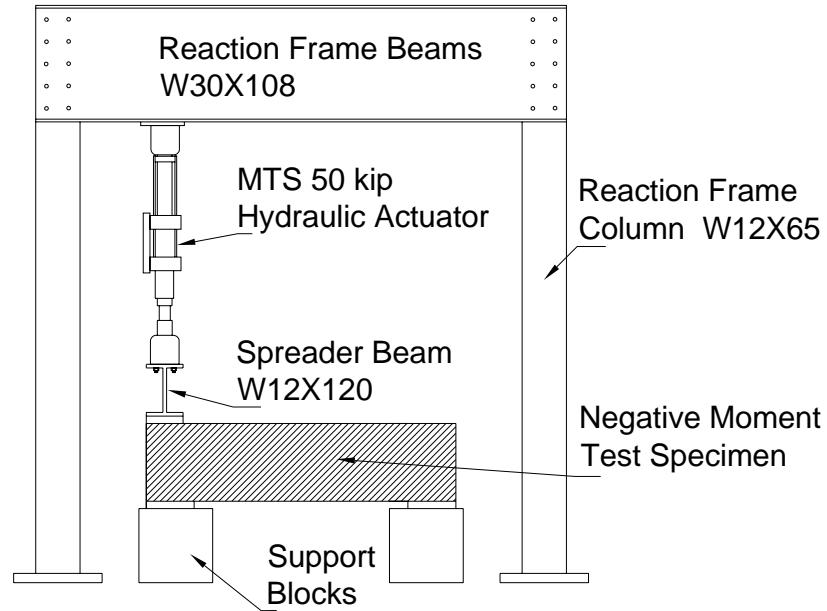


Figure 3.32: Longitudinal Elevation of Negative Moment Specimen Reaction Frame

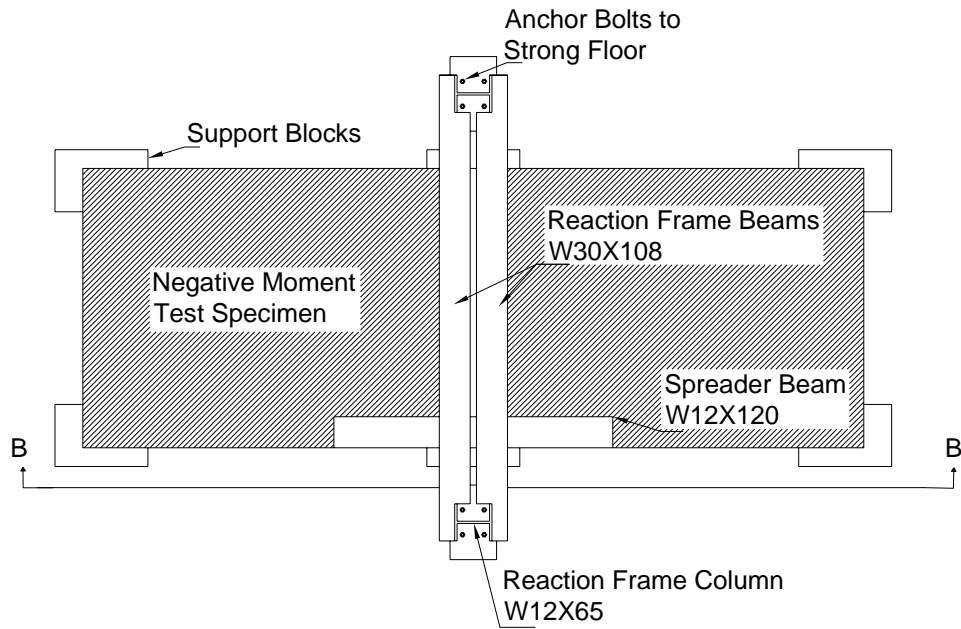


Figure 3.33: Plan View of Negative Moment Specimen Reaction Frame

Chapter 4: Experimental Program

In this chapter, the construction of the test specimens is documented in Section 4.1, the reaction frame construction is documented in Section 4.2, and the measured material properties are included in Section 4.3. The instrumentation of the test specimen is discussed in Section 4.4, and the general test procedure is outlined in Section 4.5.

4.1 CONSTRUCTION OF TEST SPECIMENS

Four test specimens were constructed: two specimens to test positive moment in the slab, and two to test negative moment in the slab. The construction of the positive moment specimens is presented in Section 4.1.1, and the construction of the negative moment specimens is presented in Section 4.1.2.

4.1.1 Specimens P0P1 and P0P2

For the specimens subjected to positive moment, the first step was to cast the concrete blocks and beams used to support the slabs. As shown in Figure 4.1, the blocks and beams were then positioned on the strong floor at Ferguson Structural Engineering Laboratory (FSEL). The concrete support blocks were placed at the corners of the specimen, and bridge bearing pads were placed on top of the blocks. The precast beams were then positioned on the bearing pads.

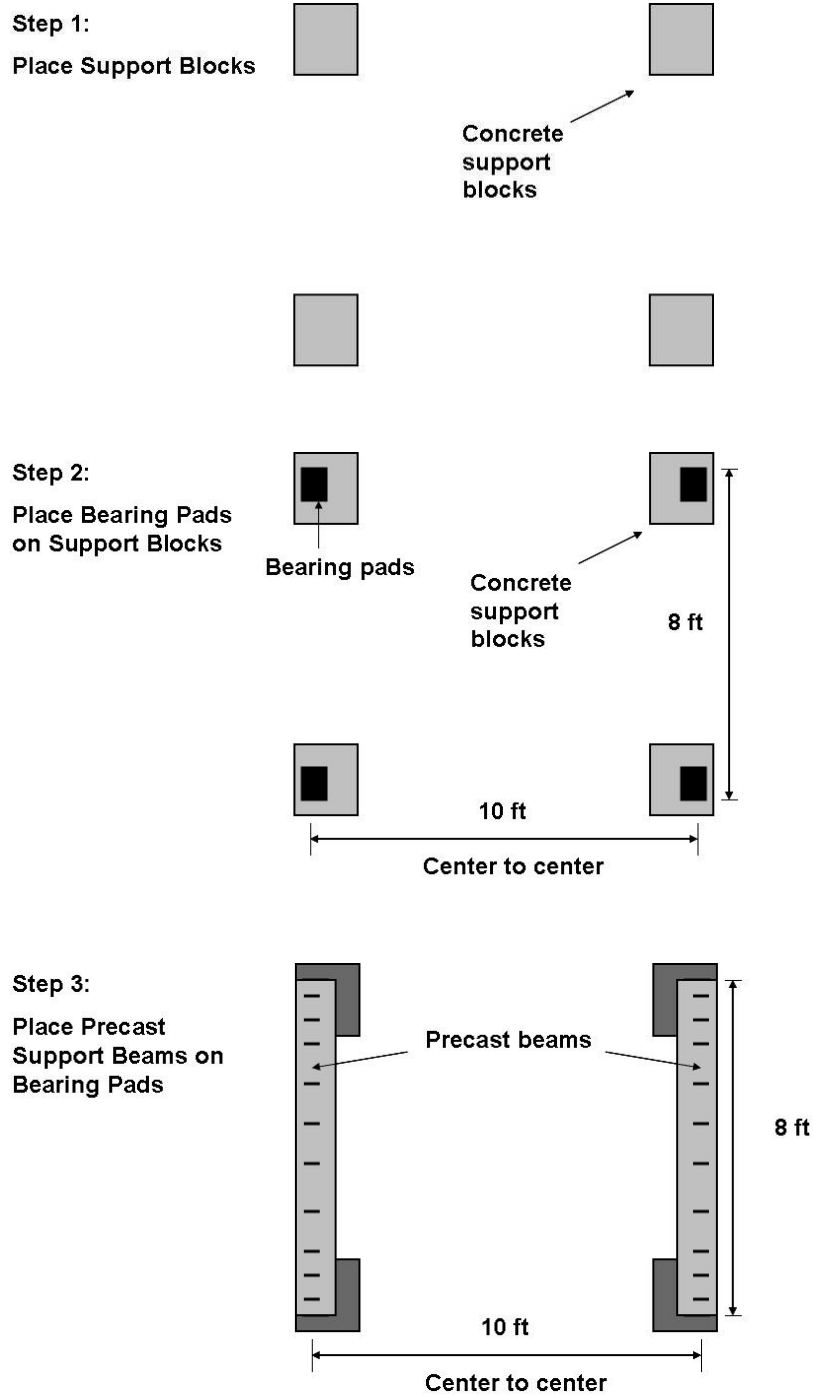
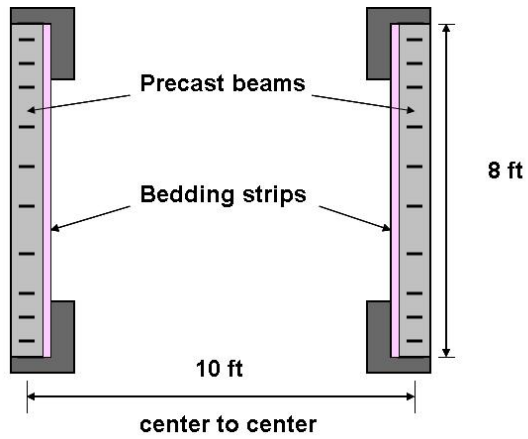
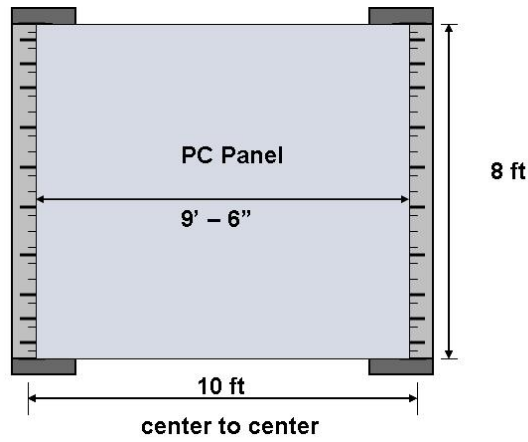


Figure 4.1: Construction of Positive Moment Specimens (Plan View)

Step 4:
Glue Bedding Strips
to Support Beams



Step 5:
Place PC Panel
on Bedding Strips



Step 6:
Cast Concrete
Topping Slab

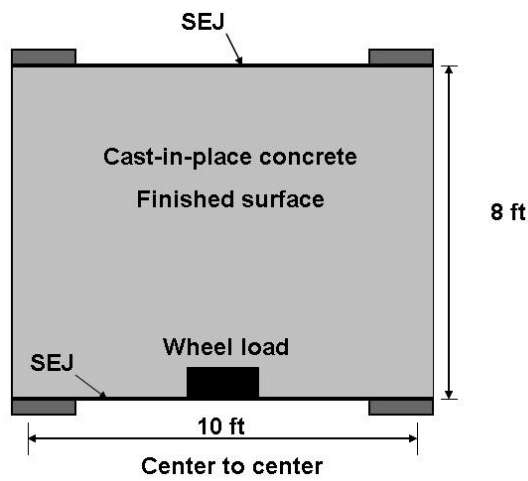


Figure 4.2: Construction of Positive Moment Specimens (Plan View)

Bedding strips were then glued in place along the edge of each beam, and the PC panels were placed on the beams, as shown in Figure 4.2. Figure 4.3 shows specimen P0P1 after the PC panel had been placed on top of the support beams, and the wide flange columns of the reaction frame bolted to the floor prior to building the test specimen.



Figure 4.3: Specimen P0P1 After Placing PC Panel

After the PC panel had been placed, formwork was constructed for the 4-in. topping slab. The formwork was braced by the strong floor, and the SEJ was attached to the formwork with erection bolts. Next, the steel reinforcement was placed and tied. In accordance with typical TxDOT standards, #4 bars were placed at 9 in. on center in the longitudinal direction. In the transverse direction, #5 bars were placed at 6 in. on center, and all reinforcing steel was supported on 7/8-in. high rebar chairs. A photograph of the SEJ and reinforcing steel is shown in Figure 4.4, and the entire specimen is shown prior to casting in Figure 4.5.



Figure 4.4: SEJ and Reinforcing Steel Prior to Casting Topping Slab



Figure 4.5: Specimen P0P1 Prior to Casting

TxDOT Class “S” structural concrete was provided by a local ready-mix supplier to cast the slab. As shown in Figure 4.6, a slump test was conducted before placing the concrete to determine if the batch was acceptable. Figure 4.7 shows the placement of the concrete for the topping slab and the consolidation of the concrete using hand-operated vibrators. After the concrete was placed, a screed was used to level the top surface, and the concrete was finished with hand trowels.

TxDOT typically cures the bridge slabs for 10 days by covering the slab with burlap sacks and/or plastic. For all test specimens, large sheets of plastic were cut and placed over the specimens, and the slab was allowed to cure for 10 days before removing the plastic. A photograph of the specimen POP1 before testing is presented in Figure 4.8.



Figure 4.6: Slump Test for specimen POP1



Figure 4.7: Placing Topping Slab for Specimen POP1



Figure 4.8: Specimen POP1 Before Testing

Specimen POP2 was constructed similarly to specimen POP1, as shown in Figure 4.1 and Figure 4.2. However, specimen POP2 was constructed in a different location while the fatigue test of specimen POP1 was ongoing. Lifting inserts were cast in the support beams so that the completed specimen could be moved with the crane. The photograph in Figure 4.9 shows specimen POP2 immediately after casting the topping slab with specimen POP1 in the background.



Figure 4.9: Specimen POP2 Curing While Testing Specimen POP1

4.1.2 Specimens N0P1 and N0P2

The negative moment specimens, N0P1 and N0P2, were the third and fourth specimens constructed, and these specimens were built in a similar manner to the positive moment specimens. Different design details required three support beams and two PC panels for the negative moment specimens. To support the three beams, six support blocks were positioned on the strong floor, and then six bearing pads were placed on the blocks. Once the bearing pads were placed, the construction sequence was identical to the first two test specimens. Figure 4.10 and Figure 4.11 illustrate the construction of the negative moment specimens, and Figure 4.12 shows researchers consolidating the concrete and leveling the surface of the slab of specimen N0P1.

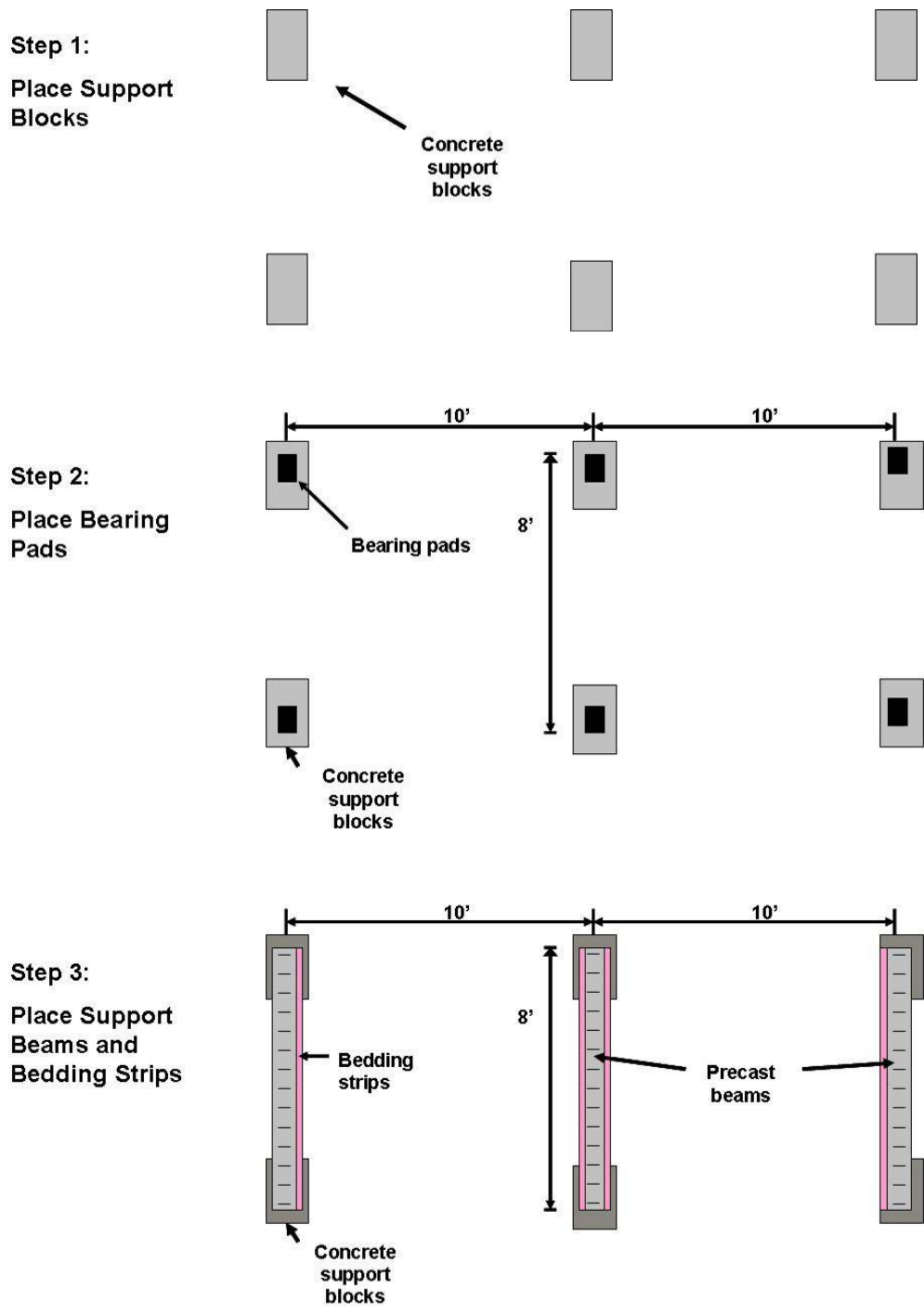
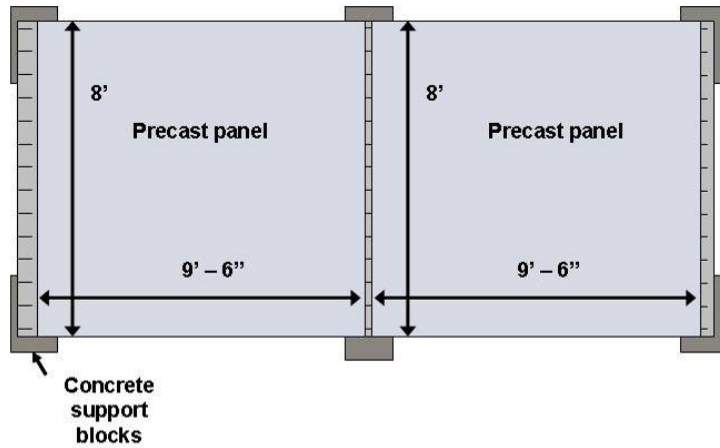
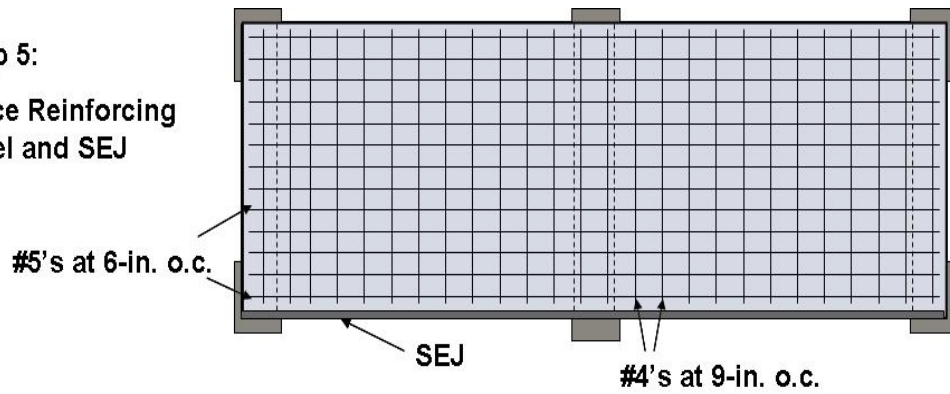


Figure 4.10: Construction Sequence for Negative Moment Specimens (Plan View)

Step 4:
Place PC Panels



Step 5:
Place Reinforcing
Steel and SEJ



Step 6:
Cast Topping Slab

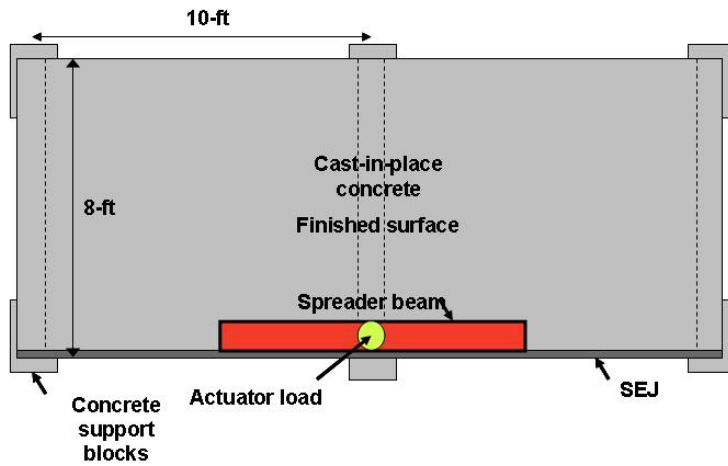


Figure 4.11: Construction Sequence for Negative Moment Specimens (Plan View)



Figure 4.12: Placing Topping Slab on Specimen NOP1

Once testing had been initiated for specimen NOP1, construction began for specimen NOP2, and the photograph included in Figure 4.13 shows an overhead view of specimen NOP1 during testing, and the support beams for the construction of specimen NOP2.



Figure 4.13: Construction of Specimen NOP2

4.2 REACTION FRAME

The reaction frame was designed to be disassembled and reassembled easily for each test specimen. Using resources provided by the Ferguson Structural Engineering Laboratory, two columns and cross beams spanned across each specimen to apply the design loads at the edge of the expansion joint. Each column was bolted to the strong floor with four $\frac{3}{4}$ -in. diameter threaded rods, and the cross beams were bolted to the columns with six $\frac{7}{8}$ -in. diameter A325 bolts. Photographs of the assembly of the reaction frame for specimen NOP1 are shown in Figure 4.14.



Figure 4.14: Assembling the Reaction Frame for Specimen NOP1

4.2.1 Load Application During Fatigue Tests

The fatigue loads were applied to the specimens by a 50-kip, MTS hydraulic actuator with a 10-in. stroke. The actuator was bolted to a steel plate which was then bolted into place on the reaction frame. Oversize holes were drilled into the bottom flanges of the cross beams to allow the actuator to be placed directly above the designed load point. For the positive moment specimens, a 2.5-in. thick load plate was bolted to the actuator to represent the 10-in. by 20-in. wheel load area. The actuator and load plate can be seen on specimen POP1 in Figure 4.15. To represent an axle loading for the negative moment test specimens, the actuator was bolted to a spreader beam that

distributed the applied load to the ends of the beam. Figure 4.16 shows the actuator, spreader beam, and load plates used for the negative moment specimens.



Figure 4.15: MTS Actuator and Load Plate for Positive Moment Specimens



Figure 4.16: Actuator and Spreader Beam for Negative Moment Specimens

4.2.2 Load Application During Static Tests to Failure

The reaction frame had to be modified when each specimen was tested to failure, because the MTS actuator did not have the capacity necessary to fail the specimens. For the positive moment specimens, a hydraulic ram with a 150-kip capacity was used, and for the negative moment specimens, a 300-kip hydraulic ram was used. Each of the hydraulic rams was about 50 in. shorter than the actuator; therefore, the cross beams of the reaction frame had to be lowered by 50 in. Once the cross beams had been lowered, a 1-in. thick steel plate was attached to the ram, and the ram was then bolted in place on the cross beams. Figure 4.17 shows the hydraulic ram and spreader beam used for the test to failure of specimen NOP2.



Figure 4.17: Hydraulic Ram Setup Used to Test Specimen NOP2 to Failure

4.2.3 Load Plates

The AASHTO LRFD Bridge Design Specification defines the tire contact area to be 20 in. wide and 10 in. long. For the test specimens, two 2.5-in. thick steel plates were cut to these dimensions (Figure 4.18). To provide uniform bearing underneath the steel plate, high-strength, quick-setting grout material was cast underneath the load plate for

the positive moment specimens. For the negative moment specimens, 1-in. thick elastomeric pads served the same purpose.

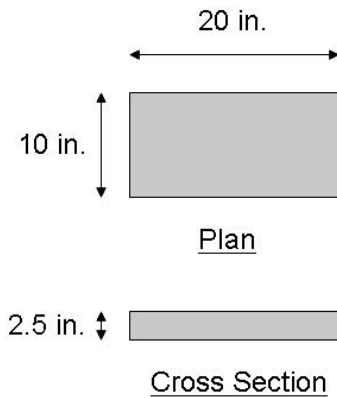


Figure 4.18: Load Plate

4.3 MATERIAL PROPERTIES

4.3.1 Concrete

Approximately twenty concrete cylinders were cast for each of the topping slabs. These 6-in. diameter cylinders were then tested in accordance with ASTM standards to determine the compressive strength. At least three cylinders were tested at various ages after casting the concrete (Figure 4.19). After 28 days, the compressive strength of the concrete used in all the slabs exceeded the required minimum for TxDOT Class “S” structural concrete.

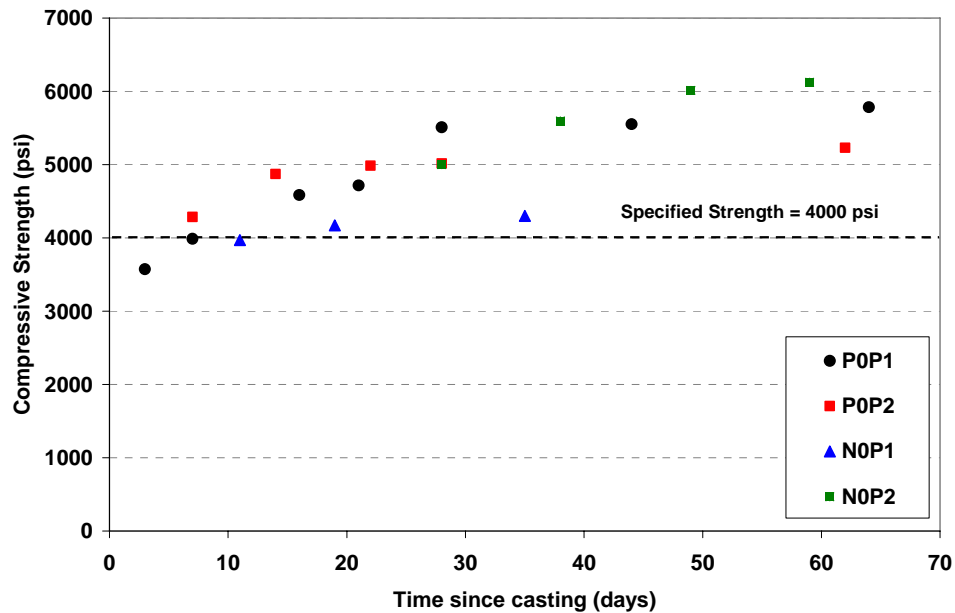


Figure 4.19: Compressive Strength of Concrete Used for Topping Slabs

4.3.2 Steel

All of the reinforcing steel bars were delivered by a local steel supplier, and Grade 60 reinforcing steel was specified. The mill report provided by Capital City Steel indicated that the yield strength was 65.9 ksi, and the tensile strength was 102 ksi. A36 steel was used for the sealed expansion joint section.

4.3.3 Prestressed Concrete Panels

The PC panels were constructed off-site and delivered by a local precast concrete supplier. TxDOT specifies a minimum 28-day compressive strength of 5000 psi and a compressive strength of 4000 psi at release. The panels were reinforced with 3/8-in. diameter prestressing strand that was stressed with an initial average stress of 189 ksi per strand. The material properties of the concrete and strand were not measured by the research team.

4.4 INSTRUMENTATION

For the fatigue evaluation of the test specimens, several different parameters required instrumentation. Inspections of the test specimens throughout the fatigue tests provided qualitative, visual information. The research team marked and measured cracks, and inspected the interface between the CIP slab and the PC panel for any signs of deterioration.

It was also important to determine if the response of the specimens deteriorated during the fatigue tests. The cyclic loading was stopped periodically to measure strains and deflections during static tests. Plots of this data would indicate the changes in the structural response throughout the fatigue tests.

4.4.1 Deflection Measurements

To measure deflections, 6-in. and 2-in. linear potentiometers were placed beneath the test specimen near the supports and underneath the point of load application. The locations of the linear potentiometers for the positive moment specimens are presented in Figure 4.20, and the locations of the linear potentiometers for the negative moment specimens are presented in Figure 4.21.

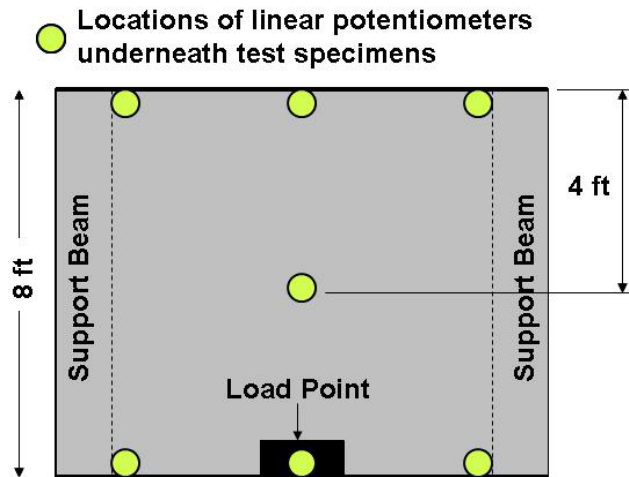


Figure 4.20: Locations of Linear Potentiometer for Positive Moment Specimens

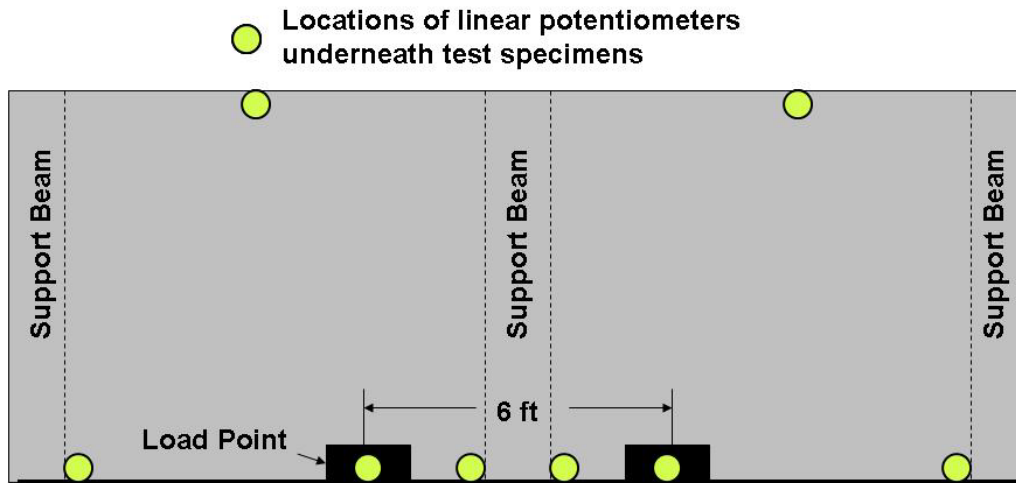


Figure 4.21: Locations of Linear Potentiometers for Negative Moment Specimens

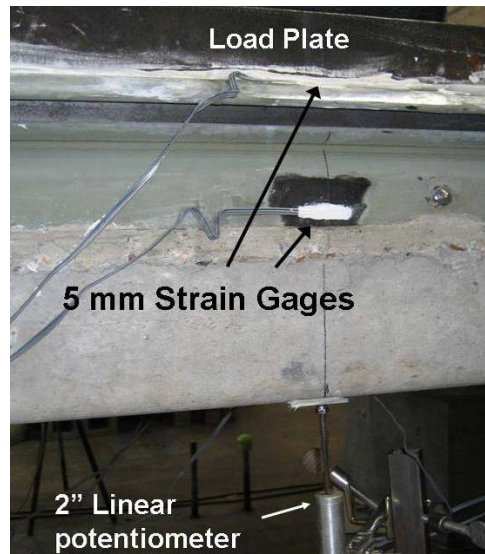


Figure 4.22: Photograph of Instrumentation of Specimen P0P1

4.4.2 Strain Measurement

Strain gages were used to evaluate the strain at several locations on the specimens, including the PC panel, the SEJ, and the reinforcing bars. All of the strain gages were 120-ohm, temperature compensating, three-wire strain gages.

4.4.2.1 Positive Moment Specimens

The extreme tensile fiber in the positive moment specimens was located on the bottom of the PC panels. Because the PC panels were not constructed at the laboratory, it was not possible to install strain gages on the prestressing strand; therefore, 60-mm strain gages were installed directly onto the bottom surface of the precast concrete panel. The 60-mm strain gages are designed for measuring strain on concrete surfaces, and Figure 4.23 presents the locations of the PL-60 strain gages used to measure the response of specimen POP1.

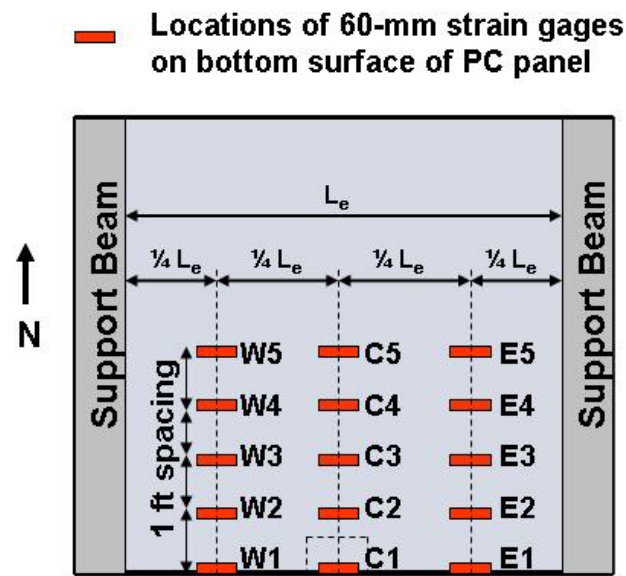


Figure 4.23: Strain Gage Locations for Specimen POP1 Plan View

Strains were recorded in the steel sealed expansion joint (SEJ). Five-mm strain gages were placed at mid-height of the section and at the top of the section (extreme compression fiber). Two strain gages, designated as FLA-5 strain gages, were positioned at each of the quarter points, and two were placed at midspan (Figure 4.24).

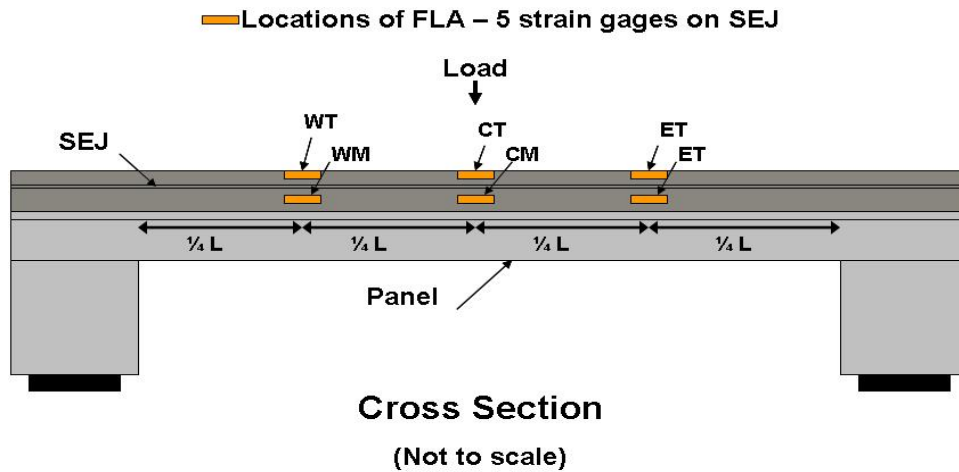


Figure 4.24: Locations of Strain Gages on SEJ for Specimen P0P1

After examining the data from specimen P0P1, it was decided that fewer strain gages could be used to monitor the response of specimen P0P2. Information about the measured strain response is presented in Chapter 5. Therefore, only four strain gages were installed along the center line of the panel for specimen P0P2. The first strain gage was located at the edge, beneath the load point, and the next three strain gages were spaced at 1-ft increments (Figure 4.25).

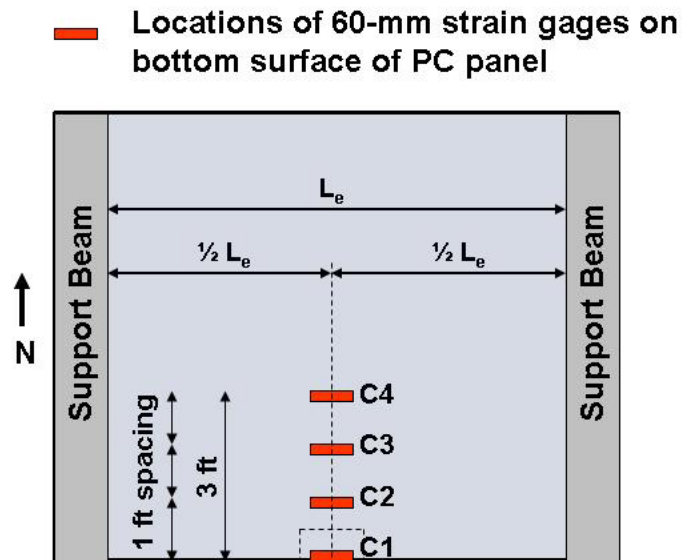


Figure 4.25: Strain Gage Locations for Specimen P0P2

It was also decided to reduce the number of 5-mm strain gages installed along the SEJ for specimen POP2. Only two FLA-5 strain gages were installed at midspan, as shown in Figure 4.25.

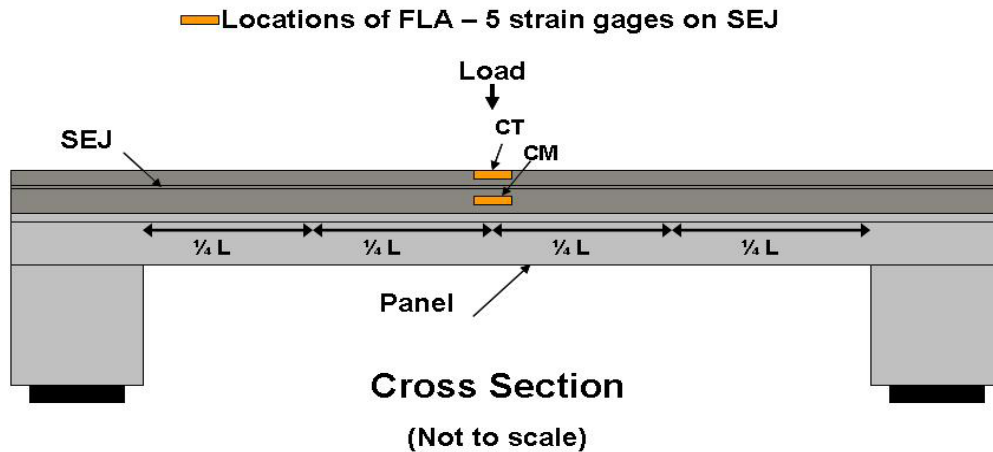


Figure 4.26: Locations of Strain Gages on SEJ for Specimen POP2

4.4.2.2 Negative Moment Specimens

Because the third and fourth test specimens were subjected to negative moments, the extreme tension fiber was located at the top of the cross section. Fifteen, 5-mm strain gages were installed on the transverse reinforcement (parallel to the SEJ) in specimen NOP1. The strain gages were installed near the locations of the maximum negative moment, and were placed directly over the outer edges of the supporting beam, and along the centerline of the supporting beam. Figure 4.27 provides the locations and nomenclature of the strain gages on the #5 reinforcing steel bars in Specimen NOP1. To measure the strain in the SEJ, one strain gage was placed at the top of the SEJ section directly over the centerline of the central support beam.

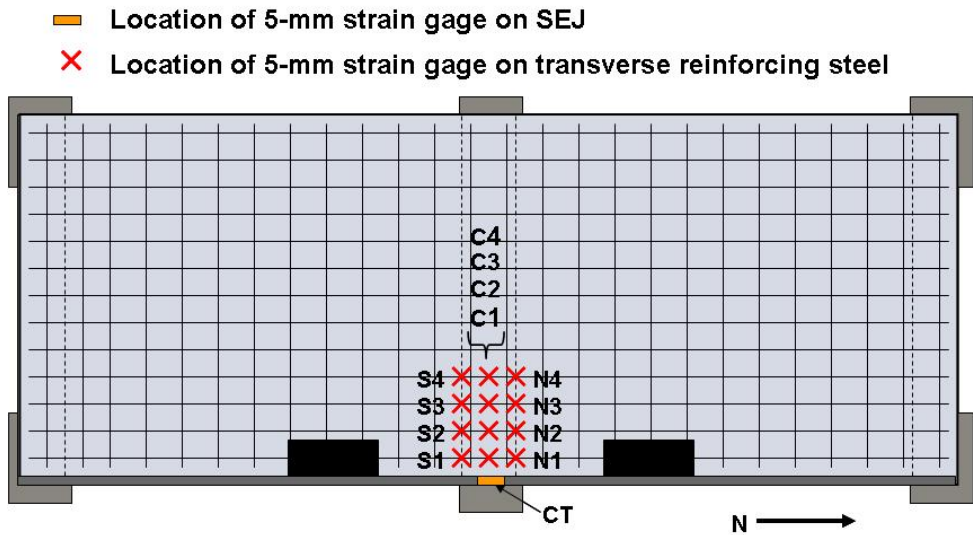


Figure 4.27: Layout of Strain Gages for Specimen N0P1

When specimen N0P1 was loaded, cracks formed directly above the outer edges of the support beam. The results indicated that the strain gages located along the center line of the support beam, and on the fourth reinforcing bar, were experiencing low levels of stress. Therefore, it was decided to use fewer strain gages to measure the response of specimen N0P2. Figure 4.28 shows the layout of the seven strain gages attached to specimen N0P2.

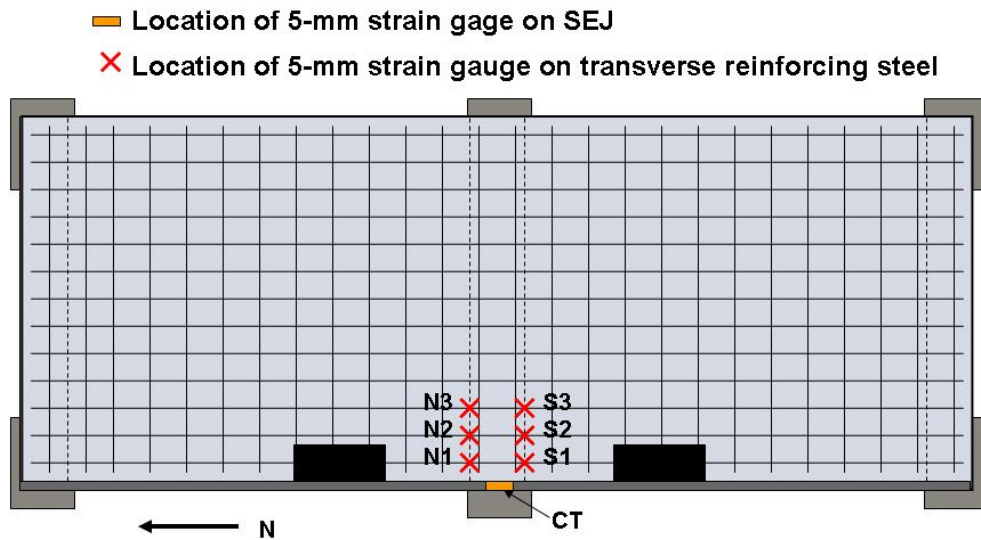


Figure 4.28: Layout and Nomenclature for Strain Gages in Specimen N0P2

4.4.3 Load Measurement

For all fatigue cycles and periodic static tests, the magnitude of the applied loads was measured by the internal load cell in the MTS actuator. For the tests to failure, hydraulic rams were used to apply the load. For the positive moment tests, a 100-kip load cell was placed beneath the ram, and for the negative moment specimens a 200-kip load cell was used.

4.4.4 Data Acquisition System

A data acquisition system was assembled to record the data from the strain gages, linear potentiometers, and load cells during testing. All instruments were connected to “quarter bridge” or “full bridge” transfer boxes that were wired to an HP scanner that converted the data to a digital format. A LabView program was used to monitor and record the data during the tests.

4.5 TEST PROCEDURE

As mentioned in Chapter 3, the general procedure used to evaluate deterioration of the specimen response under fatigue loads was to conduct periodic static tests during the fatigue testing. Static overloads were applied after 2 million cycles, and after 5 million fatigue cycles, the specimens were tested to failure. The actual load histories varied for the different test specimens, but the general test procedure is outlined below:

1. Initial static test
 - a. Place instrumentation
 - b. Zero data acquisition system, begin recording data
 - c. Load specimen using the rear axle load from the HL-93 design truck
 - d. Unload specimen
 - e. Repeat test
 - f. Remove linear potentiometers and turn off DAQ
2. Fatigue cycles
 - a. Setup controls for fatigue tests (set point, span, frequency)

- b. Establish limits
 - c. Begin fatigue cycles
- 3. Periodic static tests
 - a. After approximately 250,000 cycles, stop fatigue test
 - b. Repeat initial static test procedure
- 4. Static overload test
 - a. After approximately 2,000,000 cycles, stop fatigue test
 - b. Load specimen to 50 kip
 - c. Mark cracks
 - d. Inspect interface of CIP/PC panel
 - e. Unload specimen
 - f. Repeat overload test
- 5. Continue fatigue cycling, with period static tests at every 250,000 cycles
- 6. Test to failure
 - a. Stop fatigue test after approximately 5,000,000 cycles
 - b. Modify reaction frame, replace MTS actuator with hydraulic ram
 - c. Apply load incrementally until specimen failed

4.5.1 Load Control Program

An MTS closed-loop controller was programmed to apply the desired cyclic loads to the test specimens. An input signal was delivered to a hydraulic manifold, which controlled the hydraulic flow to the actuator.

The first step in controlling the fatigue loads was to program the input signal as the sine function. Next, a “set point” was established that represented the baseline load around which the fatigue loading was cycled. Only downward loads were applied to the specimens because truck loads are gravity loads. The magnitude, or “span,” of the load that cycled around the set point was established, and then the testing frequency was established. After the control limits had been established, the fatigue cycling was begun.

4.5.1.1 Control Limits

The control program required the establishment of limits for the input and feedback signals. The limits were used as a safety precaution that the specimen would be loaded as designed. If the feedback signal exceeded the maximum or minimum limits for load or displacement, the hydraulic system would shut down immediately. In addition, a limit on the maximum error between the input signal and the feedback was set at 1.0 kip for the specimens P0P1 and P0P2 and at 1.8 kip for specimens N0P1 and N0P2. If power was lost to the controller, or if a leak occurred in the hydraulic hoses, the difference between the input signal and the feedback would trigger an immediate termination of the load program. Also, if the response of the specimen changed significantly, the error between the input and feedback signals would terminate the fatigue cycling. Figure 4.29 through Figure 4.32 illustrate the limits and input signals that were applied to the control programs for each test specimen.

4.5.1.2 Specimen P0P1

For specimen P0P1, the load history was based on the effective axle load of 12 kip from the WIM data (Wood, et al. 2007). The set point was 4 kip in compression, and the span was 3 kip. This input signal cycled the loading from the baseline of 4 kip down to 1 kip and up to 7 kip using a sinusoidal pattern. The load limits were 0.2 kip and 7.8 kips, and the error limit was 1 kip. The input signal, associated feedback, and control limits for specimen P0P1 are shown in Figure 4.29.

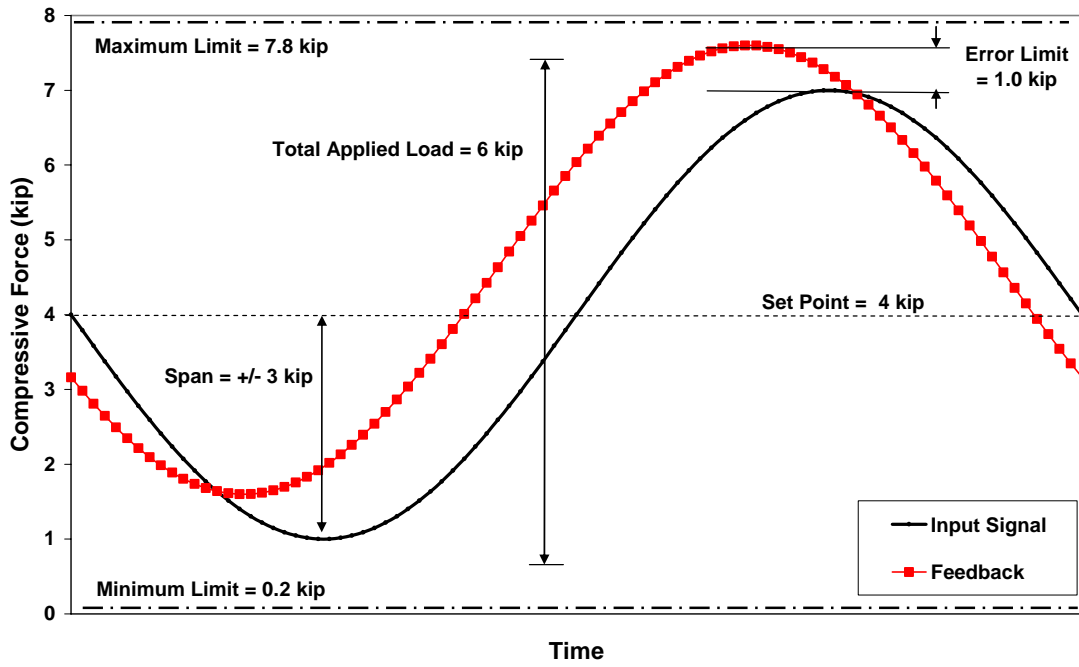


Figure 4.29: Input and Feedback Signals for Specimen P0P1

4.5.1.3 Specimen P0P2

The input signal for specimen P0P2 was similar to specimen P0P1, except that set point and span were modified to correspond to a wheel load of the rear axle from the HL-93 Design Truck. The set point was 9 kip in compression, and the span was 8 kip. This input signal cycled the loading from the baseline of 9 kip down to 1 kip and up to 17 kip using a sinusoidal pattern. The load limits were 0.2 kip and 17.8 kips, and the error limit was 1 kip. The input signal, associated feedback, and control limits for specimen P0P2 are shown in Figure 4.30.

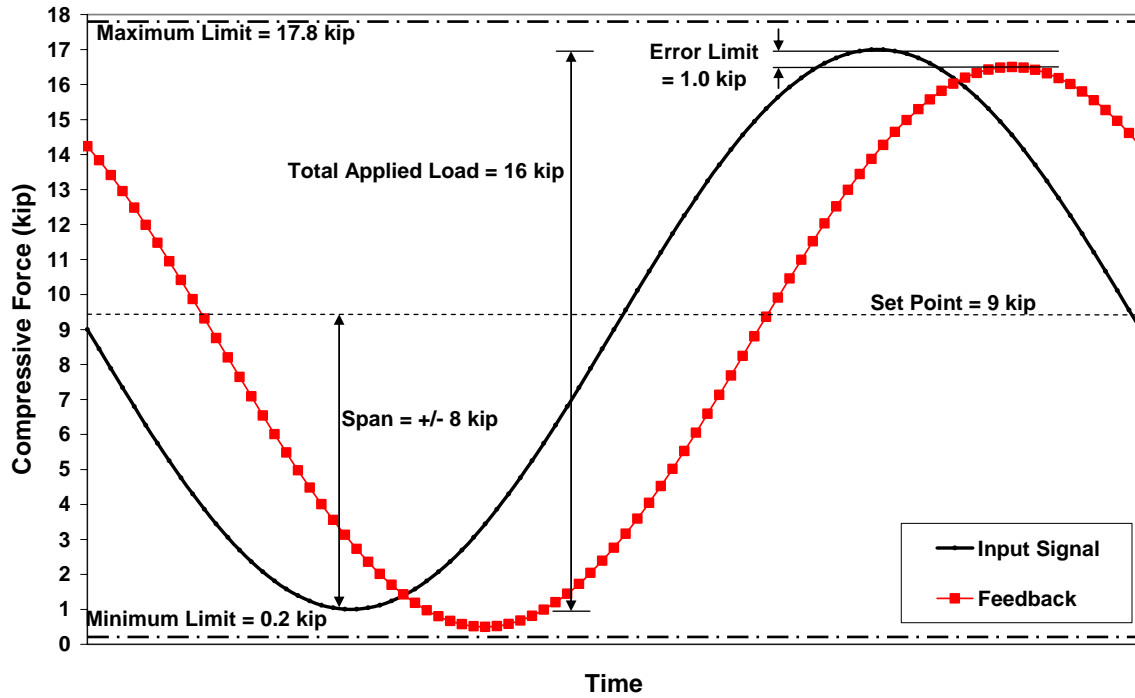


Figure 4.30: Input and Feedback Signals for Specimen P0P2

4.5.1.4 Specimen N0P1

For the negative moment test specimens, the input signal was increased because the actuator load represented the entire axle loading (two wheel loads). For specimen N0P1, the input signal was based on the HL-93 Design Truck, with a set point equal to 18 kip, and a span of 16 kip. This input signal cycled the loading from the baseline of 18 kip down to 2 kip and up to 34 kip using a sinusoidal pattern. The load limits were 0.2 kip and 35.8 kips, and the error limit was 1.8 kip. The input signal, associated feedback, and control limits for specimen N0P1 are shown in Figure 4.31.

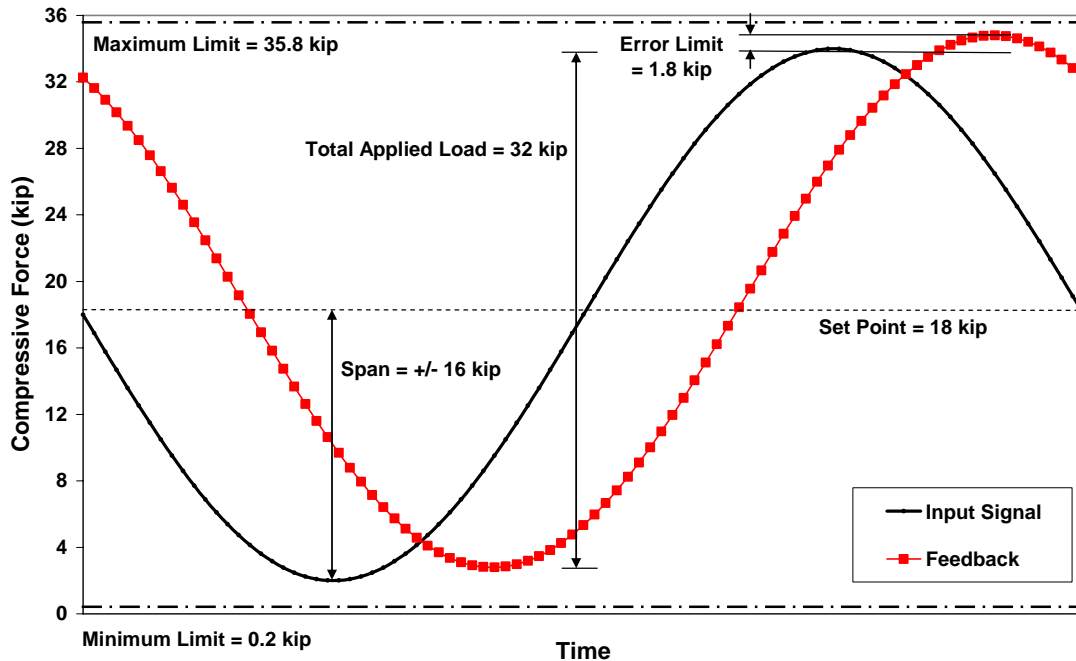


Figure 4.31: Input and Feedback Signals for Specimen N0P1

4.5.1.5 Specimen N0P2

The input signal for specimen N0P2 was increased because the first three specimens had exhibited very little deterioration due to the fatigue loadings, and the results are presented in Chapter 5. The design loading for specimen N0P2 was 46 kip which represented the HL-93 Design Truck load multiplied by two load factors. The first load factor, 1.25, represented an overloaded truck, and the second load factor, 1.15, represented the dynamic impact factor used for fatigue in the AASHTO LRFD Specification. For specimen N0P2, the input signal was based on the HL-93 Design Truck, with a set point equal to 25 kip, and a span of 23 kip. This input signal cycled the loading from the baseline of 25 kip down to 2 kip and up to 48 kip using a sinusoidal pattern. The load limits were 0.2 kip and 49.8 kips, and the error limit was 1.8 kip. The input signal, associated feedback, and control limits for specimen N0P2 are shown in Figure 4.32.

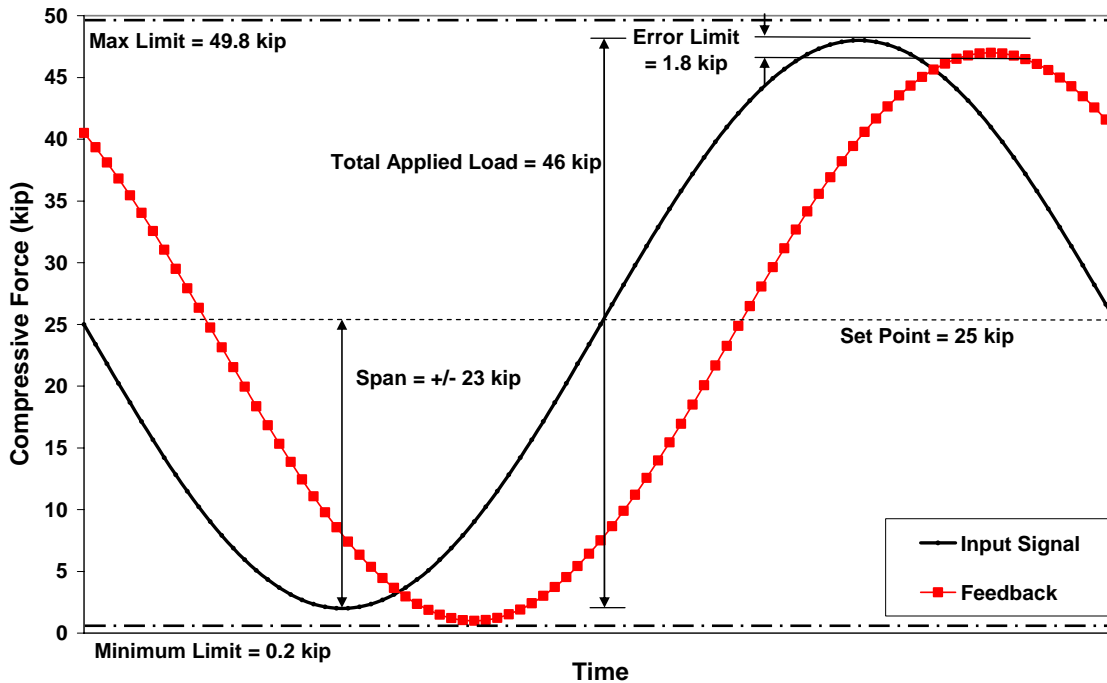


Figure 4.32: Input and Feedback Signals for Specimen N0P2

Chapter 5: Measured Response of Test Specimens

The measured response of the four test specimens are summarized in this Chapter. The results from the positive moment specimens, POP1 and POP2, are discussed in Section 5.1 and Section 5.2, respectively. The results from the negative moment specimens, NOP1 and NOP2, are presented in Section 5.3 and Section 5.4, respectively.

The same general loading history was used for each test specimen; therefore, the discussion of the measured response is divided into sections corresponding to the applied loading histories: initial static test, periodic static tests, static overload test (after at least two million fatigue cycles), additional periodic static tests, and static test to failure (after at least five million fatigue cycles). Key sets of data are discussed in this chapter. The displacements and strains recorded by many of the instruments in the static tests were essentially zero at locations away from the point of the applied load. These records are not discussed in this chapter, but are presented in Appendix A.

Wherever displacements are discussed in this chapter, the data have been adjusted to correspond to the relative displacement of the test specimen. As discussed in Chapters 3 and 4, each specimen was supported on bearing pads, and these pads compressed under the applied loads. Therefore, the average of the displacements measured at the supports was subtracted from each of the displacement readings recorded by the linear potentiometers to determine the relative displacement.

5.1 SPECIMEN POP1

Specimen POP1 was subjected to a total of eleven static tests before, during, and after the fatigue test (Table 5.1). During the fatigue test, the applied loads varied between 1 and 7 kip at a frequency of 2 Hz. During the periodic static tests, a maximum load of 16 kip was applied, which corresponds to the wheel load for the rear axle of the HL-93 Design Truck. It was originally planned to apply a maximum load of 32 kip during the overload test, but flexural cracks were not observed at this level of load. Therefore, a maximum applied load of 50 kip was applied.

Table 5.1: Static Loading History for Specimen P0P1

Type of Static Test	Accumulated Fatigue Cycles*	Maximum Applied Load (kip)	Condition at Conclusion of Test
Initial	0	16	Uncracked
Periodic	250,000	16	
Periodic	1,240,000	16	
Periodic	2,000,000	16	
Overload	2,000,000	50	Cracked
Periodic	2,200,000	16	
Periodic	3,000,000	16	
Periodic	3,500,000	16	
Periodic	4,750,000	16	
Periodic	5,000,000	16	
Failure	5,000,000	88	Punching Failure

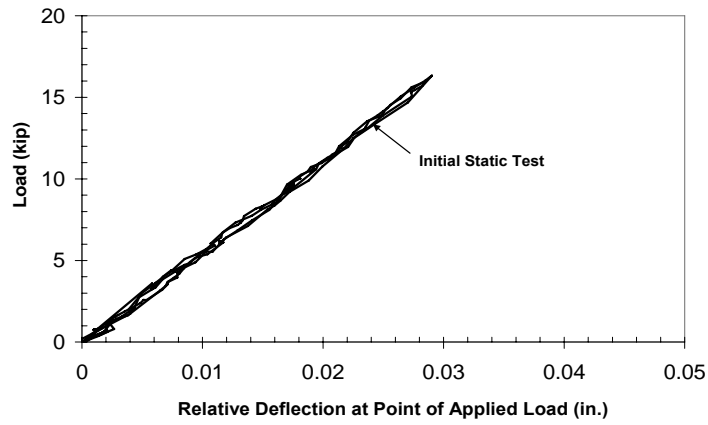
* Limiting fatigue loads: $P_{\min} = 1$ kip and $P_{\max} = 7$ kip

5.1.1 Initial Static Test

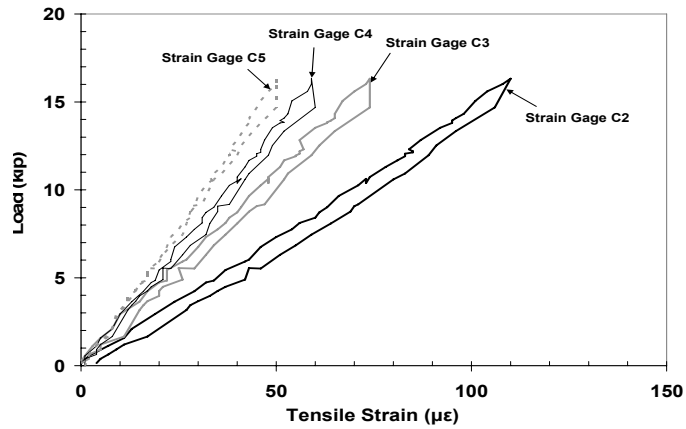
Key elements of the response of specimen P0P1 during the initial static test are presented in Figure 5.1. The overall load-displacement response was linear (Figure 5.1a), and the maximum displacement of the specimen under the point of the applied load was less than 0.03 in.

Strains were measured at fifteen locations on the tension face of the precast concrete panel for specimen P0P1. The nomenclature used to identify each of the strain gages is given in Figure 4.23. The measured strains were largest along the panel centerline, and are shown in Figure 5.1b. The strain gage closest to the expansion joint, C1, was damaged during installation and no strain data were obtained from this location; however, strain data from the other four gages along the panel centerline are shown in Figure 5.1b. All strains increased linearly with increasing load.

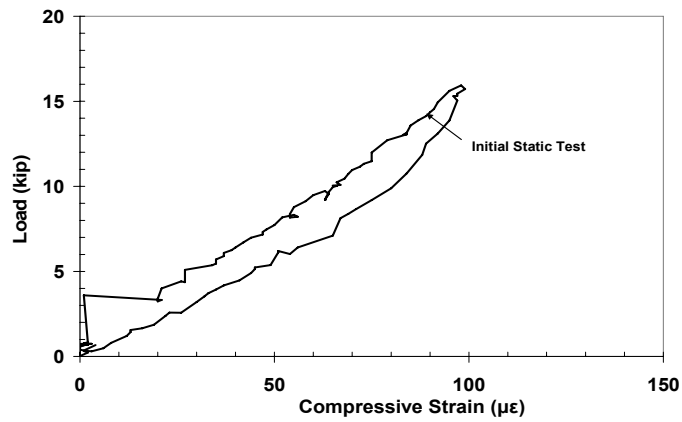
Strains were measured at six locations along the SEJ (Figure 4.24), with the largest strains recorded by the top gage at the centerline of the panel. The steel strains also increased linearly with the applied load (Figure 5.1c). The maximum strain was less than $110 \mu\epsilon$, which corresponds to a maximum compressive stress of approximately 3 ksi.



(a) Load-Deflection Response



(b) Tensile Strains on Surface of Concrete along Panel Centerline



(c) Compressive Strains on SEJ (Gage CT)

Figure 5.1: Measured Response of Specimen P0P1 during Initial Static Test

5.1.2 Periodic Static Tests

As indicated in Table 5.1, the fatigue test was stopped three times during the first 2 million cycles. The measured response during these three tests is compared with the response during the initial static test in Figure 5.2.

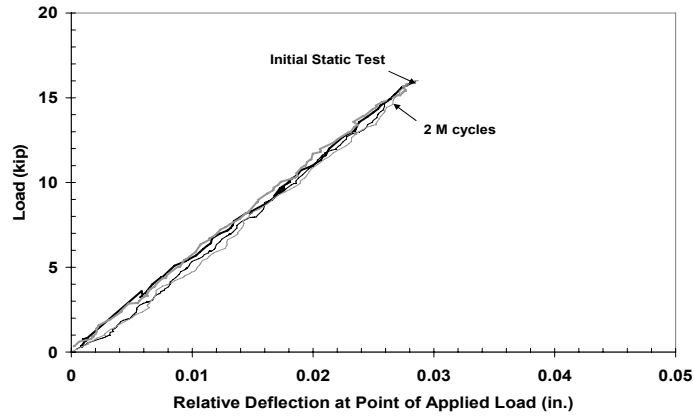
The load-deflection response was not sensitive to the number of fatigue cycles. The maximum deflection was less than 0.03 in. at an applied load of 16 kip during all four static tests. The tensile strains measured on the surface of the PC panel were also independent of the number of loading cycles. Slight variations were observed in the strain response of the SEJ, but these were considered to be insignificant.

5.1.3 Static Overload Test

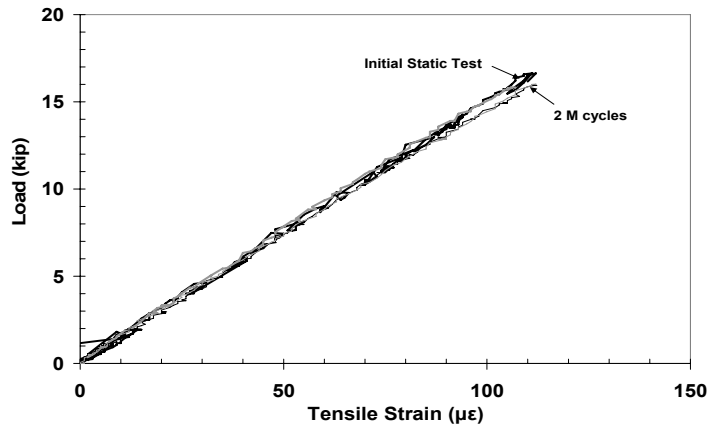
After 2 million fatigue cycles, a static overload test was conducted to crack the test specimen. It is expected that a bridge deck will crack at some point during its service life due to an overload vehicle. Subsequent fatigue tests were used to determine if the stiffness of the cracked slab deteriorated under fatigue loading. The measured response during the static overload test is shown in Figure 5.3.

Specimen POP1 was subjected to two loading cycles during the overload test. The maximum load during the first cycle was 32 kip, which corresponds to two times the wheel load for the rear axle of the HL-93 Design Truck. The overall load-deflection response was nearly linear during this cycle, as was the strain response in the SEJ. In contrast, the stiffness of the tensile strain response of the PC panel changed abruptly at an applied load of 20 kip. No cracks were observed in specimen POP1 during this first loading cycle. Therefore, the maximum load was increased to 50 kip in the second cycle. The overall stiffness decreased gradually with increasing load during this cycle.

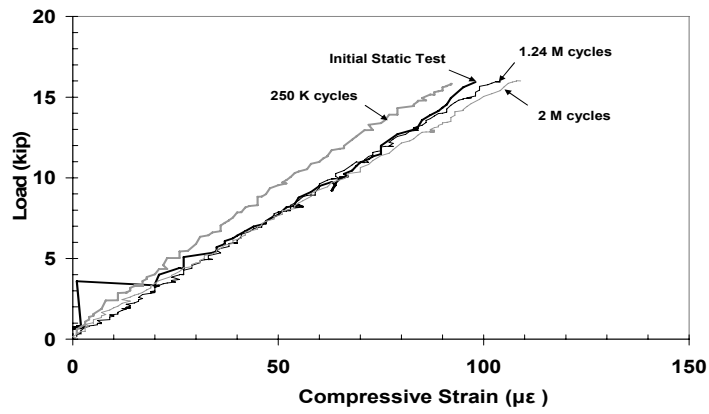
The crack patterns observed after the overload test are shown in Figure 5.4. No cracks were observed on the top of the slab, but several cracks were observed on the bottom of the PC panel.



(a) Load-Deflection Response

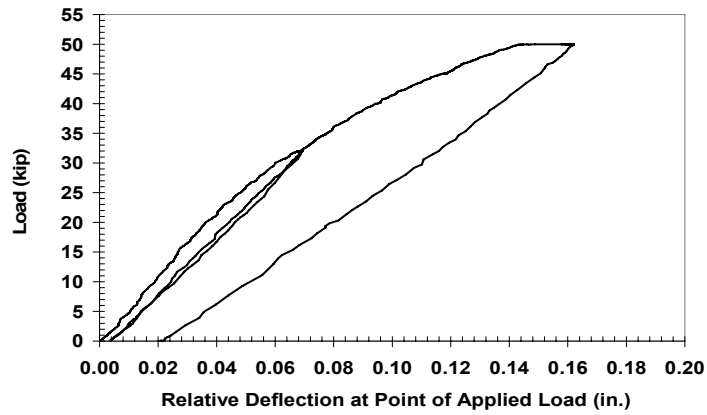


(b) Tensile Strains on Surface of Concrete (Gage C2)

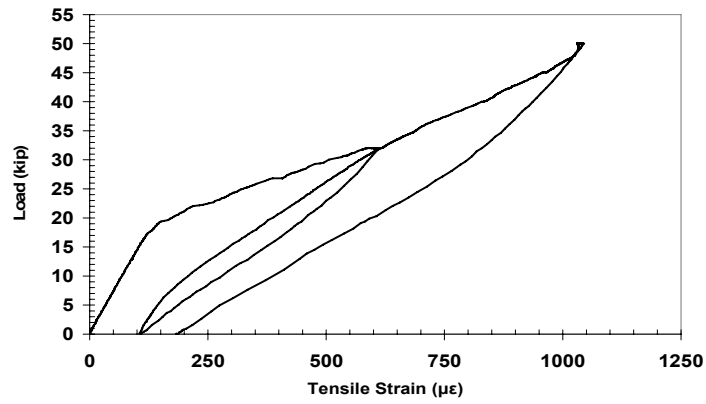


(c) Compressive Strains on SEJ (Gage CT)

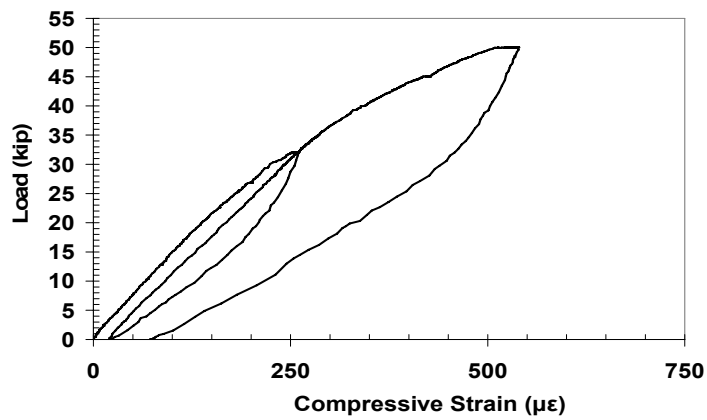
Figure 5.2: Measured Response of Specimen P0P1 during First Four Static Test



(a) Load-Deflection Response



(b) Tensile Strains on Surface of Concrete (Gage C2)



(c) Compressive Strains on SEJ (Gage CT)

Figure 5.3: Measured Response of Specimen P0P1 during Static Overload Test

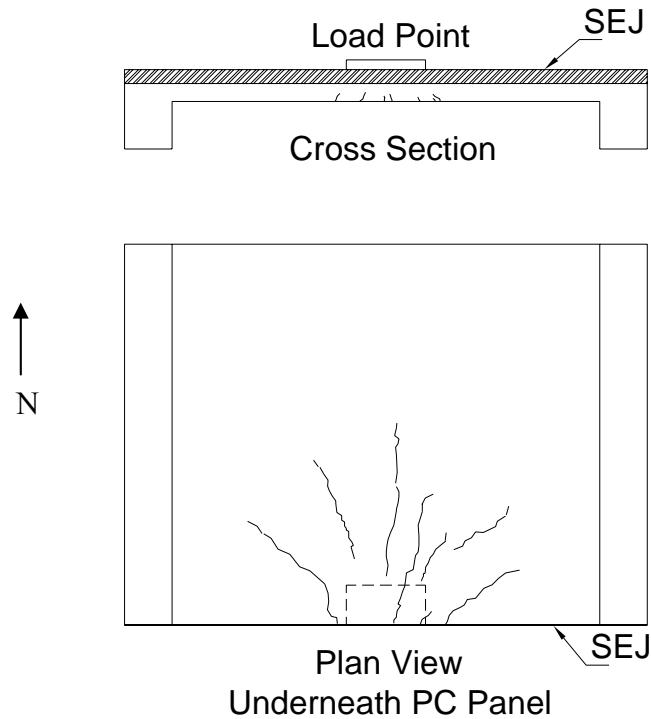
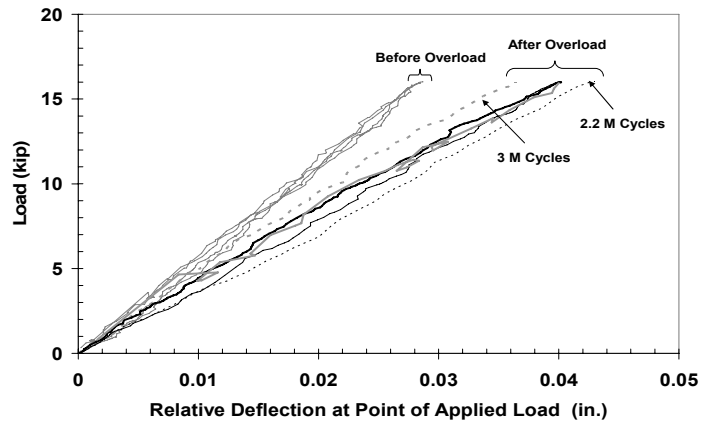


Figure 5.4: Cracks Observed during Static Overload Test for Specimen P0P1

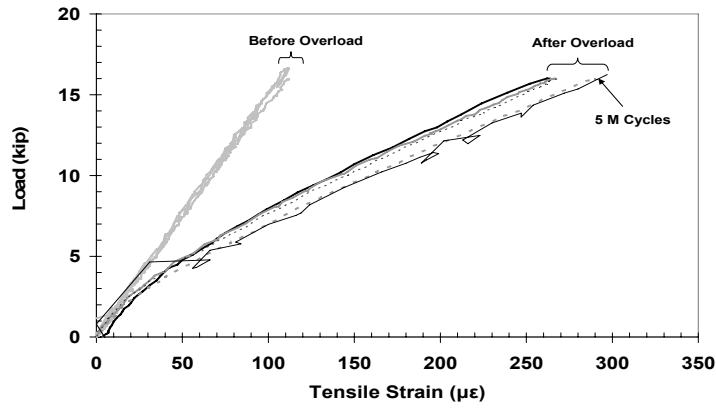
5.1.4 Additional Periodic Tests

After the overload test, the fatigue test was stopped five times between two million and five million cycles for additional static tests. The specimen was loaded statically to a maximum of 16 kip during each static test. The measured response during these static tests is shown in Figure 5.5.

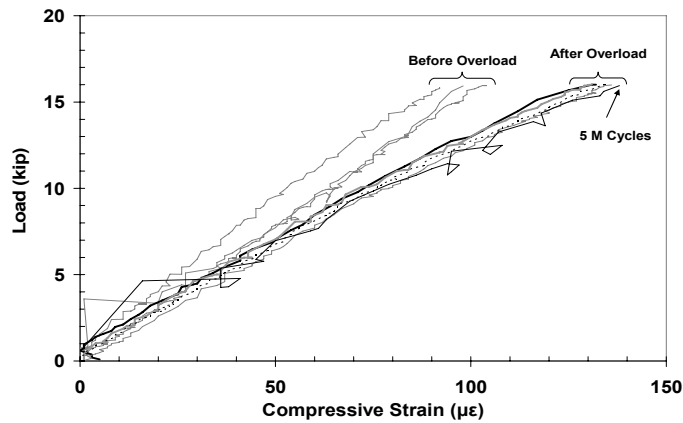
The stiffness of the specimen was less after cracks formed during the static overload test, but the nature of the response did not change appreciably as the number of loading cycles increased. The overall load-displacement response was linear and the compressive strains in the SEJ increased linearly with increasing load.



(a) Load-Deflection Response



(b) Tensile Strains on Surface of Concrete (Gage C2)



(c) Compressive Strains on SEJ (Gage CT)

Figure 5.5: Measured Response of Specimen P0P1 during Periodic Static Tests after Overload Test

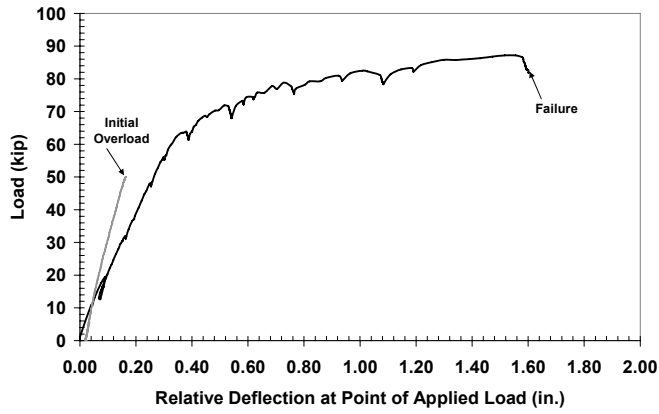
5.1.5 Test to Failure

After completion of the fatigue test, the specimen was tested to failure. The measured response is shown in Figure 5.6. The specimen failed in punching shear at an applied load of 88 kip, which corresponds to more than 5 times the wheel load for the rear axle of the HL-93 Design Truck. However, the ductile response of the specimen was the result of delamination near the north corners of the specimen, where large cracks formed as the CIP slab pulled away from the support beams. The linear potentiometer (Figure 5.7) located at the north edge of specimen POP1 indicated that the specimen was experiencing slight downward deflections until these cracks (Figure 5.8) formed at an applied load of 77 kip.

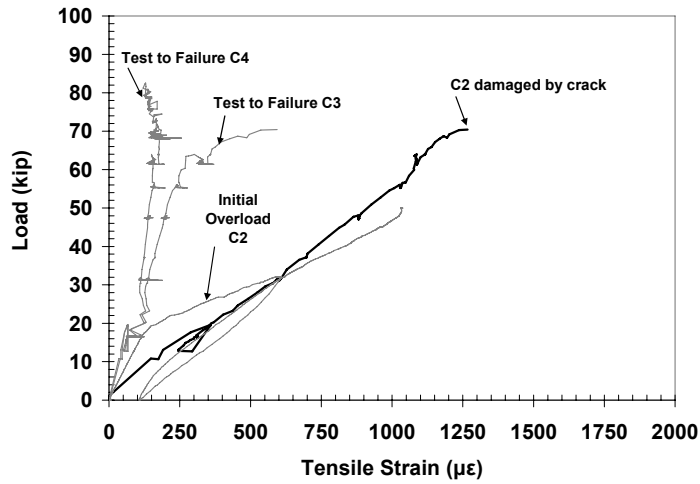
The overall load-displacement response was essentially linear for applied loads less than 65 kip. Above this load, the displacement increased rapidly with increasing load. This behavior might be the result of the yielding or buckling of the SEJ, because the measured compressive strain of the SEJ was also essentially linear for applied loads less than 65 kip.

The tensile strain response of the PC panel was essentially linear for applied loads less than 72 kip. Above this level of applied load, the data from gage C2 were unreliable because the path of a crack crossed the strain gage.

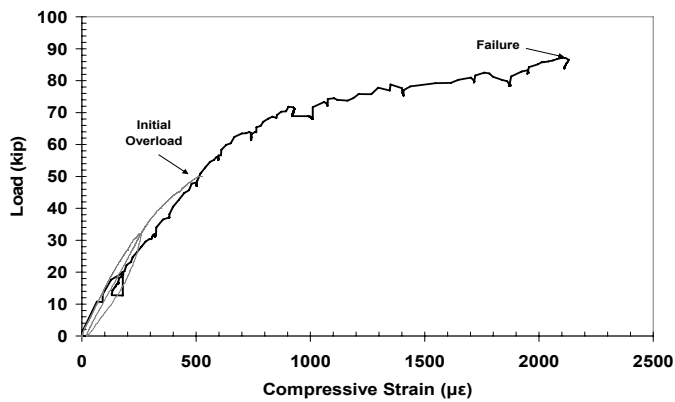
The crack patterns observed at failure are shown in Figure 5.9 and photographs of specimen POP1 are shown in Figure 5.10. At failure, the PC panel delaminated partially from the CIP deck near the support beams.



(a) Load-Deflection Response



(b) Tensile Strains on Surface of Concrete



(c) Compressive Strains on SEJ (Gage CT)

Figure 5.6: Measured Response of Specimen P0P1 during Static Test to Failure

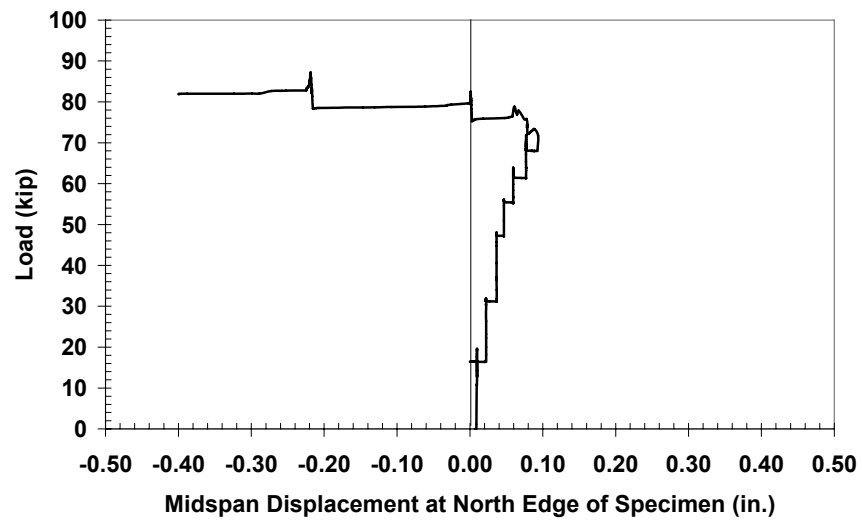


Figure 5.7: Upward Deflection of North End of Specimen P0P1 due to Delamination



Figure 5.8: Delamination from Support Beams at Northeast Corner of Specimen P0P1

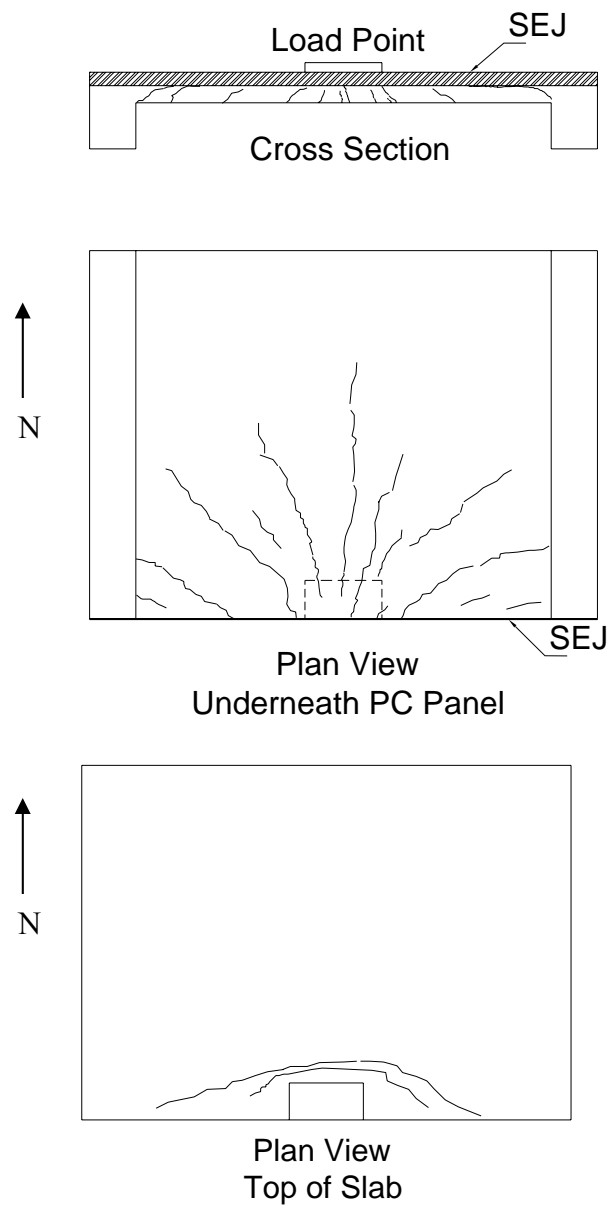


Figure 5.9: Crack Patterns for Specimen P0P1 after Punching Shear Failure



(a) Top of Specimen



(b) Southeast Corner of Specimen



(c) South End of Specimen

Figure 5.10: Photographs of Specimen P0P1 after Punching Shear Failure

5.2 SPECIMEN P0P2

Specimen P0P2 was subjected to a total of thirteen static tests before, during, and after the fatigue test (Table 5.2). During the fatigue test, the applied loads varied between 1 and 17 kip at a frequency of 3 Hz. The maximum applied load during the periodic static tests (16 kip) corresponded to the wheel load for the rear axle of the HL-93 Design Truck. During the overload test, a maximum load of 50 kip was applied.

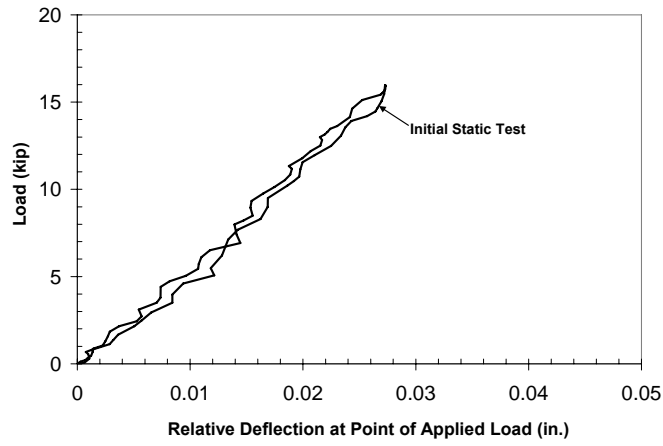
Table 5.2: Static Loading History for Specimen P0P2

Type of Static Test	Accumulated Fatigue Cycles*	Maximum Applied Load (kip)	Condition at Conclusion of Test
Initial	0	16	Uncracked
Periodic	500,000	16	
Periodic	760,000	16	
Periodic	1,000,000	16	
Periodic	1,250,000	16	
Periodic	2,000,000	16	
Periodic	2,190,000	16	
Overload	2,500,000	50	Cracked
Periodic	2,750,000	16	
Periodic	3,000,000	16	
Periodic	3,250,000	16	
Periodic	4,000,000	16	
Periodic	6,000,000	16	
Failure	6,000,000	90	Punching Failure

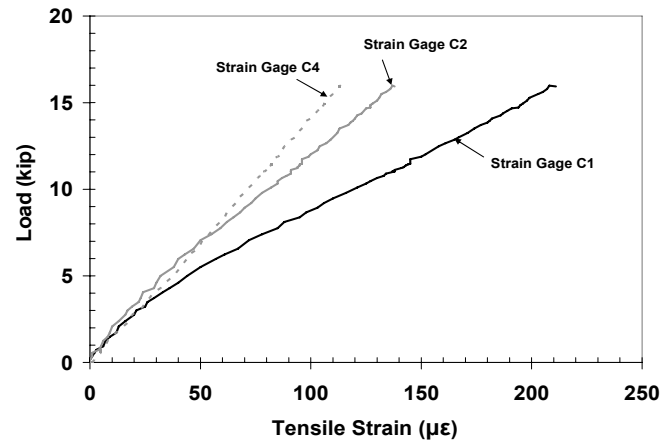
* Limiting fatigue loads: $P_{\min} = 1$ kip and $P_{\max} = 17$ kip

5.2.1 Initial Static Test

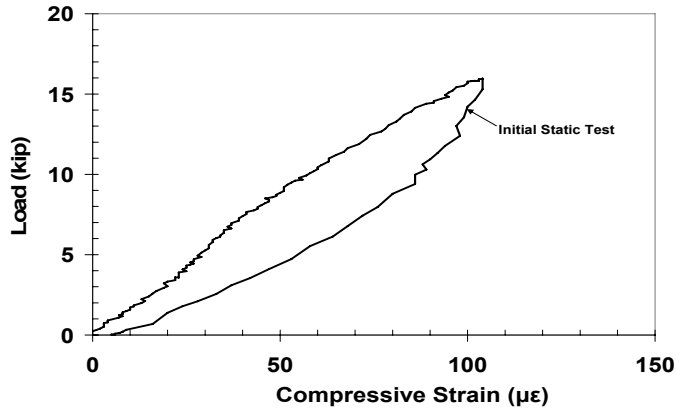
Key elements of the response of specimen P0P2 during the initial static test are presented in Figure 5.11, and the instrument nomenclature is presented in Chapter 4. The overall load-displacement response was linear, and all strains increased linearly with increasing load. On the precast concrete panel, the third strain gage, C3, was damaged during the initial static test and no strain data were obtained from this location.



(a) Load-Deflection Response



(b) Tensile Strains on Surface of Concrete



(c) Compressive Strains on SEJ (Gage CT)

Figure 5.11: Measured Response of Specimen P0P2 during Initial Static Test

5.2.2 Periodic Static Tests

As indicated in Table 5.2, the fatigue test was stopped six times during the first two million cycles. The measured response during these three tests is compared with the response during the initial static test in Figure 5.12. Similarly to specimen POP1, the load-deflection responses and measured strain responses were not sensitive to the number of fatigue cycles.

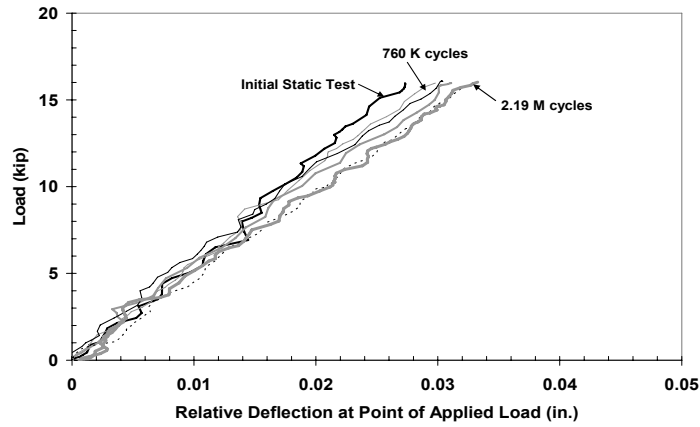
5.2.3 Static Overload Test

After 2.5 million fatigue cycles, a static overload test was conducted to crack the test specimen. Specimen POP2 was subjected to three loading cycles during this test. The maximum applied load was 16 kip in the first cycle and 50 kip in the second and third cycles. The measured responds during the static overload test is shown in Figure 5.12.

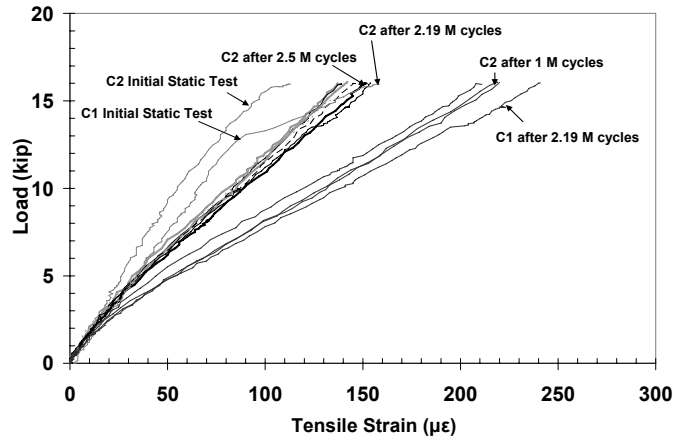
The overall load-deflection response was nearly linear for applied loads less than 30 kip. The stiffness decreased above this load level and residual displacements on the order of 0.2 in. were observed at the conclusion of the test. The compressive strain response in the SEJ was similar with a decrease in stiffness for applied loads exceeding 35 kip. The tensile strain response of the PC panel changed abruptly at an applied load of 30 kip.

During the static overload test, a crack formed through the strain gage (C1) located at the edge of the specimen directly below the point of applied load. The measured strain response of the both C1 and C2 are included for the periodic static tests conducted prior to the overload. Subsequent sections present the strain response measured at C2 instead of C1.

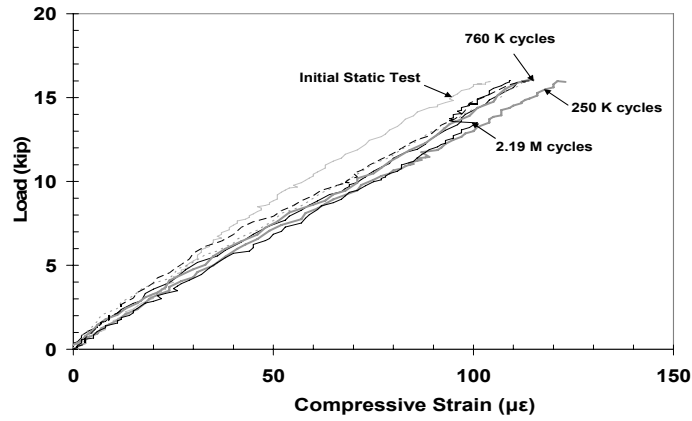
The crack patterns observed after the overload test are shown in Figure 5.14. No cracks were observed on the top of the slab, but several cracks were observed on the bottom of the PC panel.



(a) Load-Deflection Response

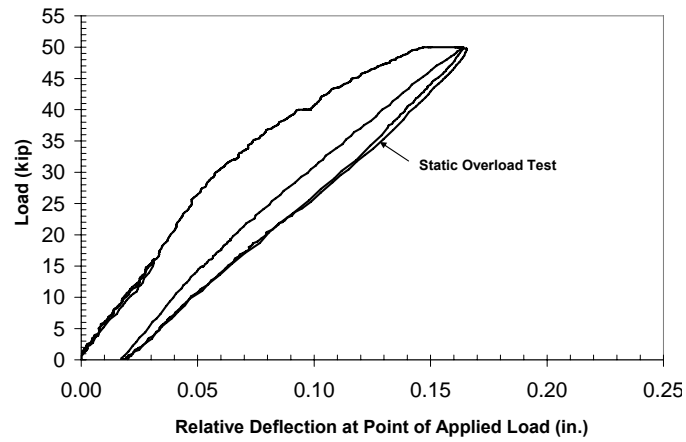


(b) Tensile Strains on Surface of Concrete (Gages C1 and C2)

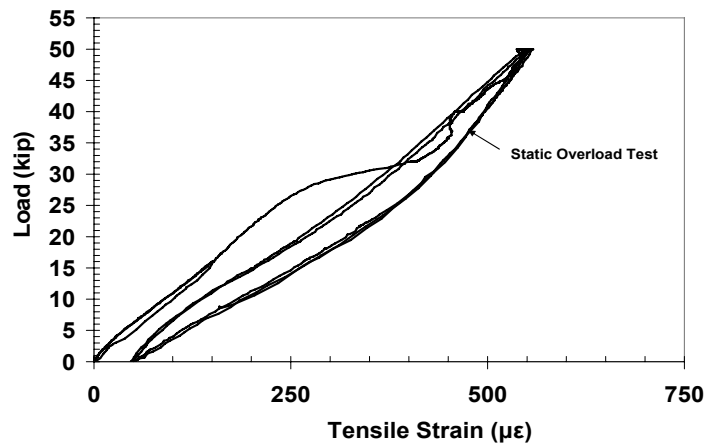


(c) Compressive Strains on SEJ (Gage CT)

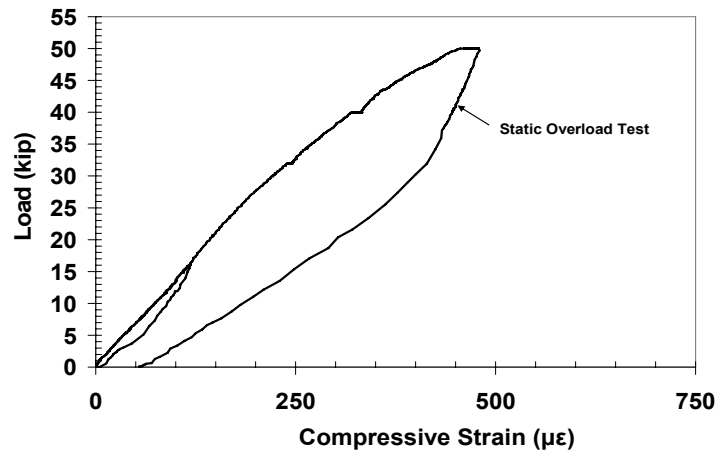
Figure 5.12: Measured Responses of Specimen P0P2 during Before Static Overload Tests



(a) Load-Deflection Response



(b) Tensile Strains on Surface of Concrete (Gage C2)



(c) Compressive Strains on SEJ (Gage CT)

Figure 5.13: Measured Response of Specimen P0P2 during Static Overload Test

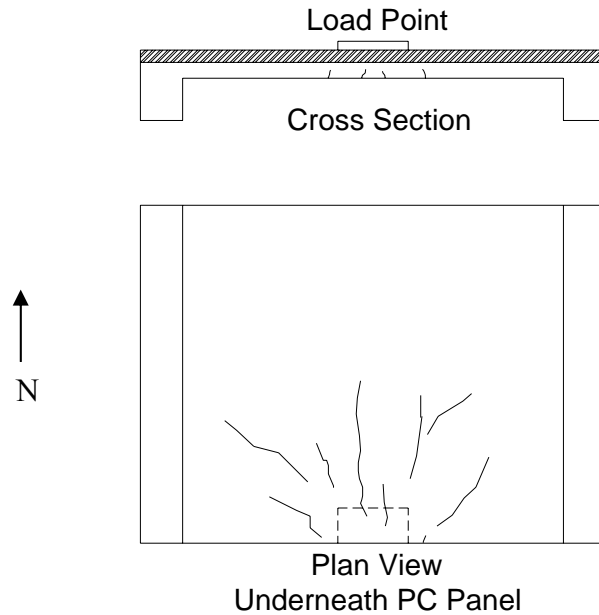
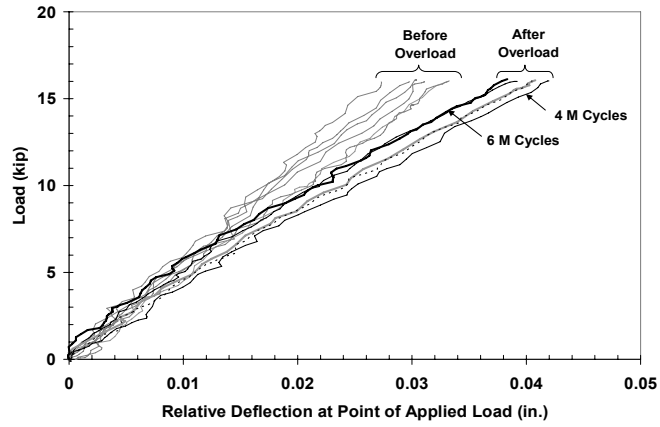


Figure 5.14: Cracks Observed during Static Overload Test for Specimen P0P2

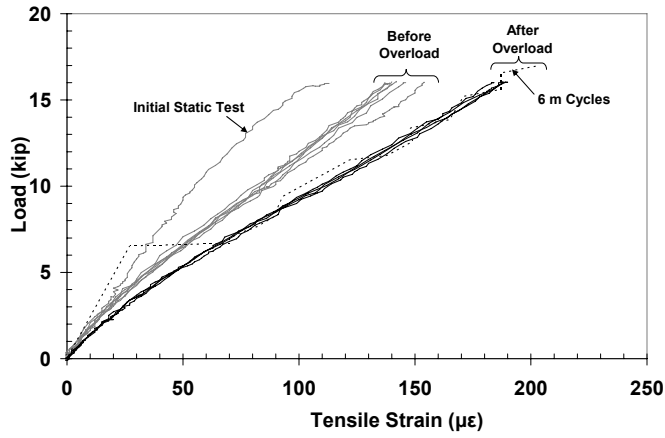
5.2.4 Additional Periodic Tests

After the overload test, the fatigue test was stopped five times between two million and six million cycles for additional static tests. The specimen was loaded statically to a maximum of 16 kip during each static test. The measured response during these static tests is shown in Figure 5.5.

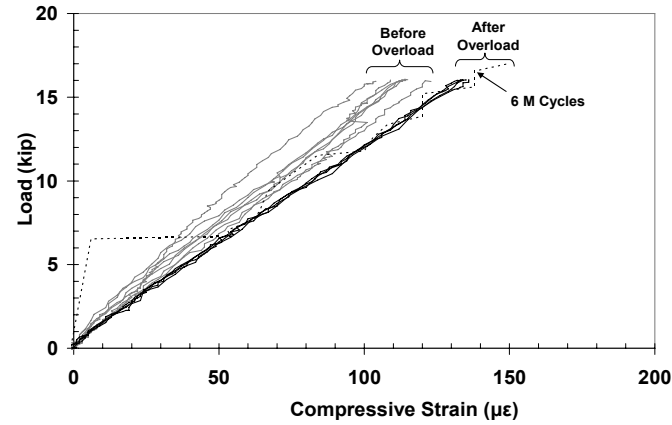
The stiffness of the specimen was less after cracks formed during the static overload test, but the nature of the response did not change appreciably as the number of loading cycles increased. The overall load-displacement response was linear and the compressive strains in the SEJ increased linearly with increasing load.



(a) Load-Deflection Response



(b) Tensile Strains on Surface of Concrete (Gage C2)



(c) Compressive Strains on SEJ (Gage CT)

Figure 5.15: Measured Response of Specimen P0P2 during Periodic Static Tests after Overload Test

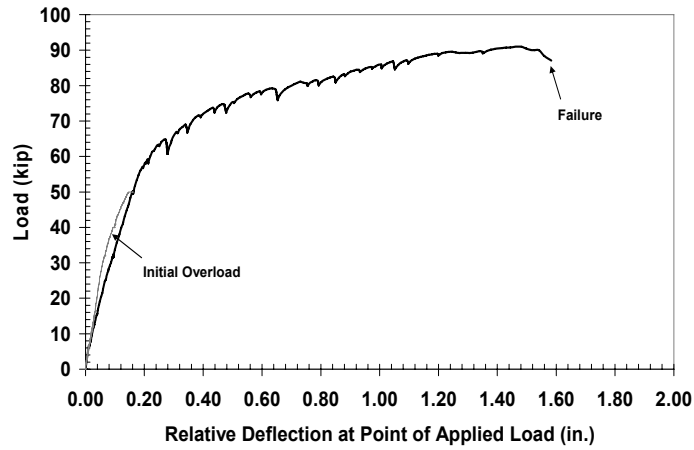
5.2.5 Test to Failure

After completion of the fatigue test, the specimen was tested to failure. The measured response is shown in Figure 5.16. The specimen failed abruptly in punching shear at an applied load of 90 kip, which corresponds to more than 5 times the wheel load for the rear axle of the HL-93 Design Truck. Similarly to specimen P0P1, the ductile response of the specimen was the result of delamination near the north corners of the specimen, where large cracks formed as the CIP slab pulled away from the support beams. The linear potentiometer (Figure 5.17) located at the north edge of specimen P0P1 indicated that the specimen was experiencing slight downward deflections until these cracks (Figure 5.18) formed at an applied load of 79 kip.

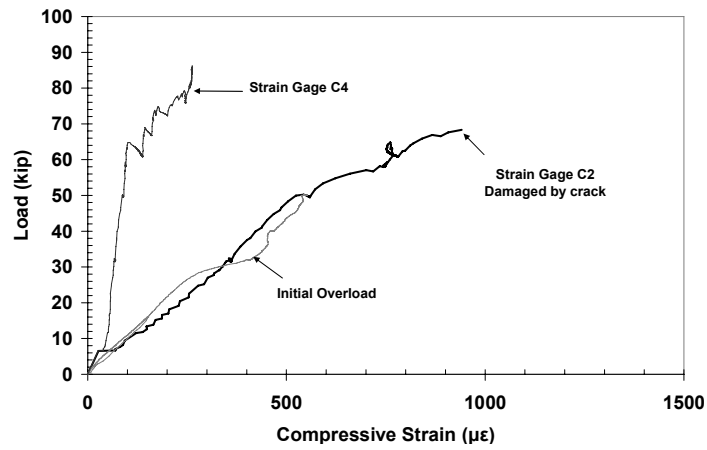
The stiffness of the overall load-displacement response decreased abruptly at an applied load of 60 kip. Above this load, the displacement increased rapidly with increasing load. The compressive response of the SEJ was also essentially linear for applied loads less than 60 kip (Figure 5.16c). The change in stiffness of the overall load-deflection response corresponds closely to the measured strain response of the SEJ.

The tensile strain response of the PC panel was essentially linear for applied loads less than 50 kip. Above this level of applied load, the data from gage C2 were unreliable because the path of a crack crossed the strain gage.

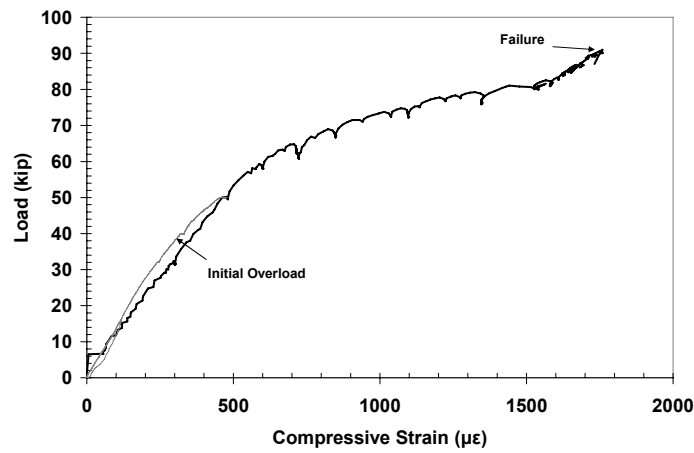
The crack patterns observed at failure are shown in Figure 5.19 and photographs of specimen P0P2 are shown in Figure 5.20. At failure, the PC panel delaminated partially from the CIP deck near the support beams.



(a) Load-Deflection Response



(b) Tensile Strains on Surface of Concrete (Gage C2 and C4)



(c) Compressive Strains on SEJ (Gage CT)

Figure 5.16: Measured Response of Specimen P0P2 during Static Test to Failure

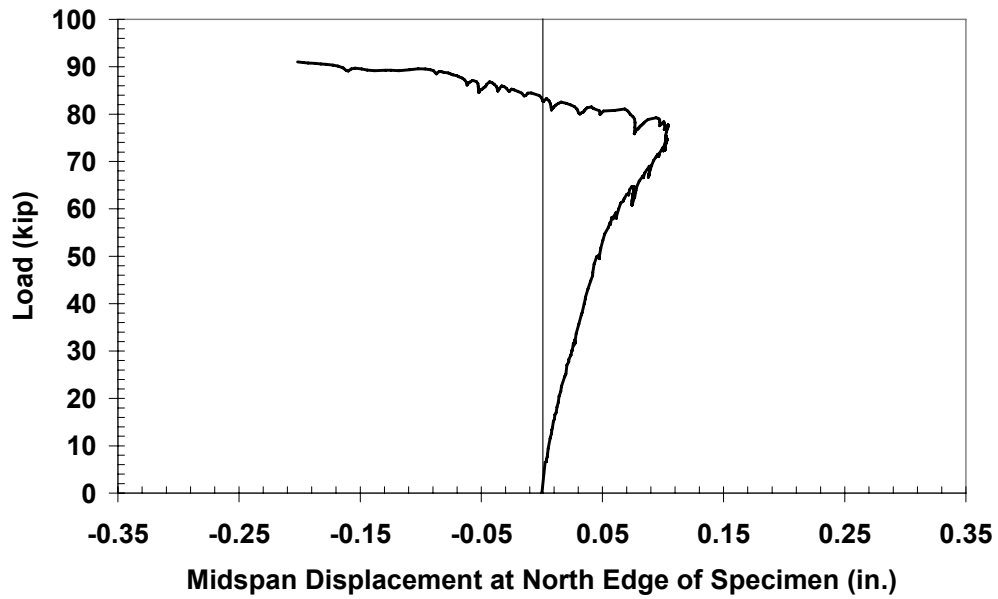


Figure 5.17: Upward Deflection of North End of Specimen P0P2 due to Delamination



Figure 5.18: Delamination from Support Beams at Northeast Corner of Specimen P0P2

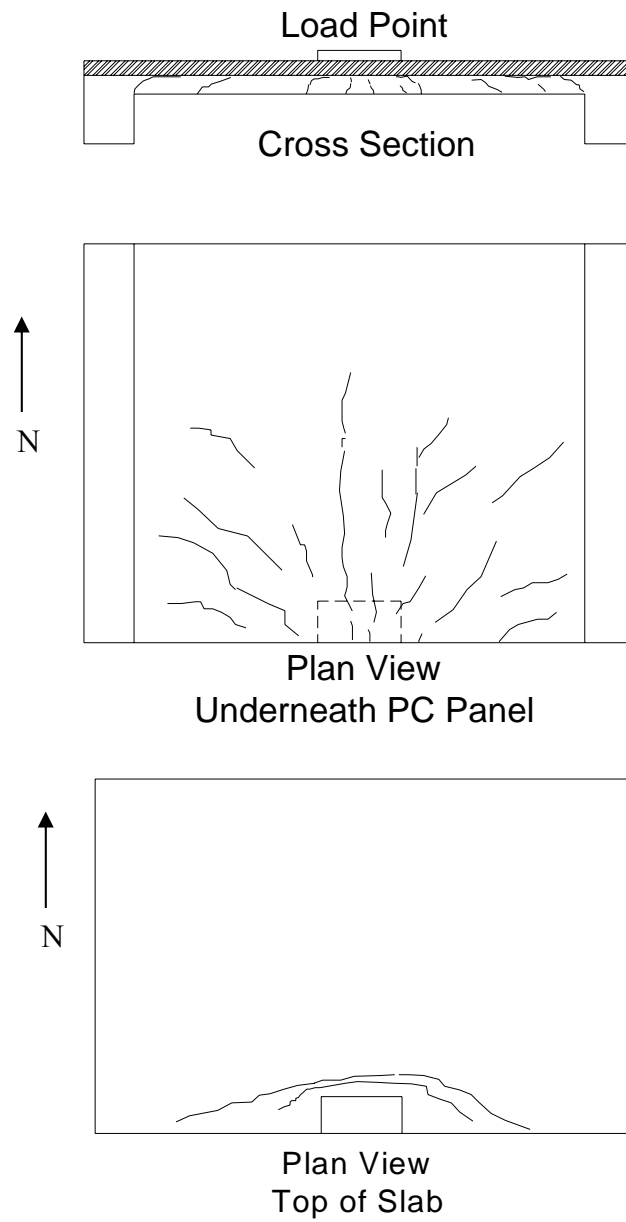


Figure 5.19: Crack Patterns for Specimen P0P2 after Punching Shear Failure



(a) Top of Specimen



(b) Southwest Corner of Specimen



(c) South End of Specimen

Figure 5.20: Photographs of Specimen P0P2 after Punching Shear Failure

5.3 SPECIMEN N0P1

Specimen N0P1 was subjected to a total of 16 static tests before, during, and after the fatigue test (Table 5.3). During the fatigue test, the applied loads varied between 2 and 34 kip at a frequency of 3 Hz. The maximum applied load during the periodic static tests (32 kip) corresponded to the rear axle of the HL-93 Design Truck.

Table 5.3: Static Loading History for Specimen N0P1

Type of Static Test	Accumulated Fatigue Cycles*	Maximum Applied Load (kip)	Condition at Conclusion of Test
Initial	0	32	Shrinkage Crack
Periodic	250,000	32	
Periodic	600,000	32	
Periodic	875,000	32	
Periodic	1,100,000	32	
Periodic	1,443,000	32	
Periodic	1,750,000	32	
Overload	2,000,000	50	
Periodic	2,250,000	32	
Periodic	3,000,000	32	
Periodic	3,290,000	32	
Periodic	3,680,000	32	
Periodic	4,000,000	32	
Periodic	4,425,000	32	
Periodic	5,000,000	32	
Failure	6,000,000	130	Punching Failure

* Limiting fatigue loads: $P_{\min} = 2$ kip and $P_{\max} = 34$ kip

During the overload static test to 50 kip (the maximum capacity of the MTS actuator), the negative moment specimens did not exhibit as many cracks as the positive moment specimens. The overload of 50 kip was only 1.5 times the rear axle of the HL-93 Design Truck, while for the positive moment specimens, the overload of 50 kip corresponded to 3 times the wheel load for the rear axle of the HL-93 Design Truck. However, before the initial static test, cracks were observed on the top of the slab directly above the edges of the center beam (Figure 5.21). These cracks corresponded closely to

the shrinkage cracks observed by Coselli (2004) in project 0-4418 (Figure 5.22). The “overload” for the negative moment specimens did not cause an appreciable change in the measured response. Therefore, the data are presented in three sections corresponding to the applied load histories from the initial static test, periodic static tests, and the test to failure.

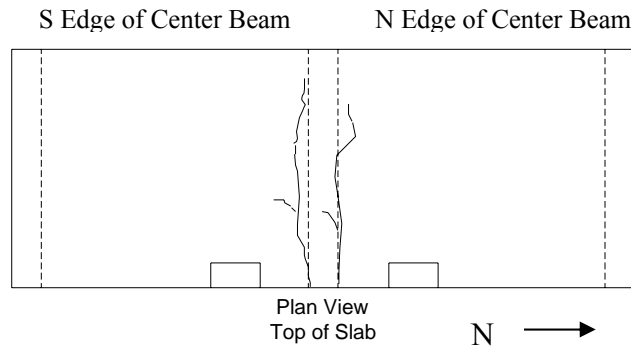


Figure 5.21: Cracks Observed in NOP1 before Initial Static Test

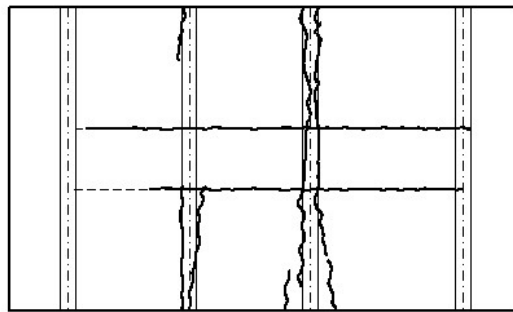
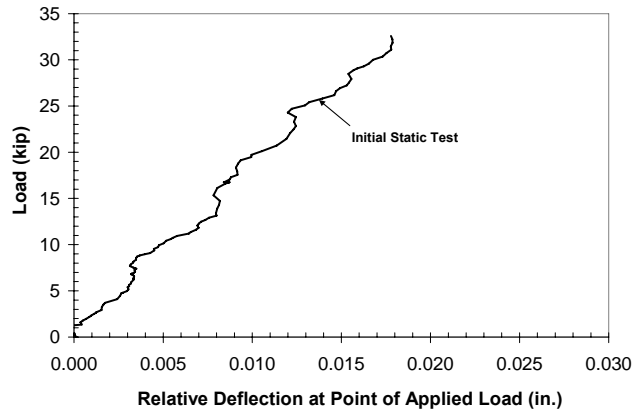


Figure 5.22: Shrinkage Cracks in Larger-Scale Specimen (Coselli 2004)

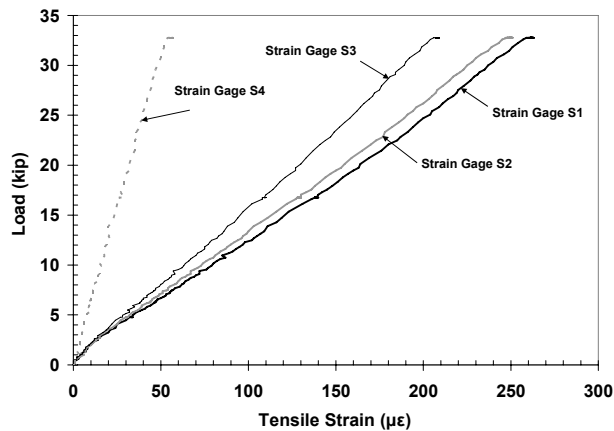
5.3.1 Initial Static Test

Key elements of the response of specimen NOP1 during the initial static test are presented in Figure 5.23. The rebar strain gages along the south edge (S1-S4), centerline (C1-C4), and north edge (N1-N4) of the center beam are included in Figure 5.23, and the instrument nomenclature is presented in Chapter 4. As shown in these figures, the highest strains were measured in the first bar above the north and south edges of the center beam. These strain gages were closely aligned with the cracks in the concrete; therefore, the stress was higher at these locations. The maximum tensile strain values

recorded at S1 and N1 were similar and were less than $300 \mu\epsilon$. In subsequent sections, only the strain data from the first bar located at the south edge (S1) are discussed. See Appendix A for strain data corresponding to the strain gages at other locations.

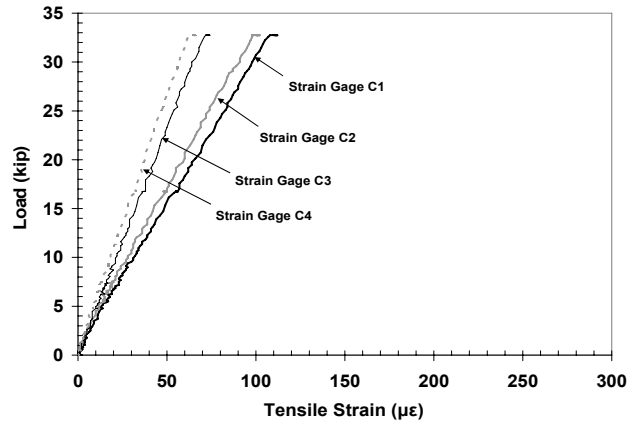


(a) Load-Deflection Response

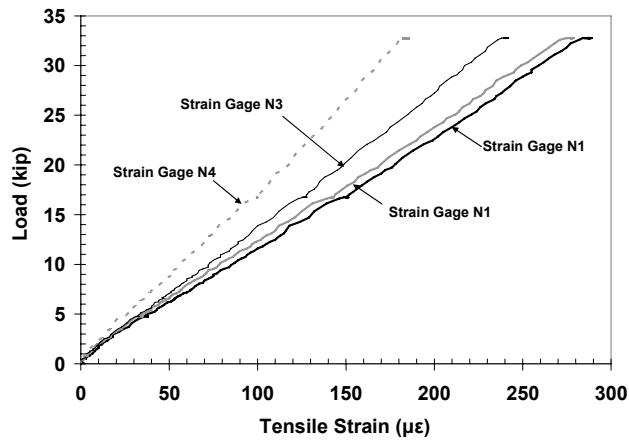


(b) Tensile Strains on #5 Bars along South Edge of Center Beam

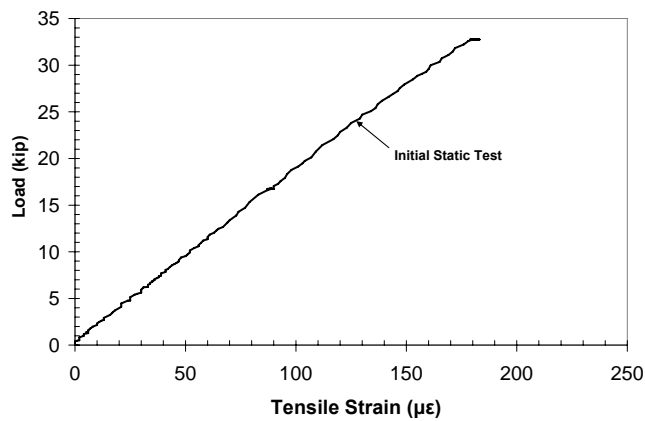
Figure 5.23: Measured Response of Specimen N0P1 during Initial Static Test



(c) Tensile Strains on #5 Bars along Centerline of Center Beam



(d) Tensile Strains on #5 Bars along North Edge of Center Beam



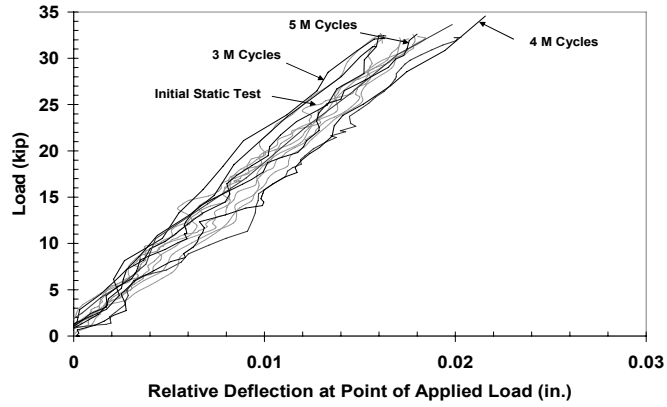
(e) Tensile Strains on SEJ (Gage CT)

Figure 5.23 (cont.): Measured Response of Specimen N0P1 during Initial Static Test

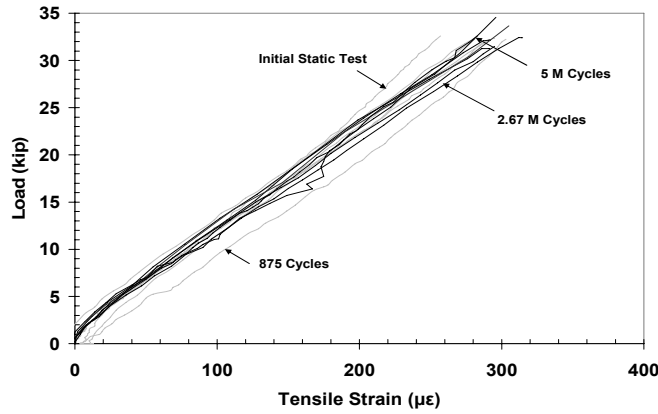
5.3.2 Periodic Static Tests

As indicated in Table 5.3, the fatigue test was stopped 14 times before testing to failure. The measured responses during each test are superimposed in Figure 5.24. Similarly to specimens POP1 and POP2, the load-deflection responses and measured strain responses were not sensitive to the number of fatigue cycles.

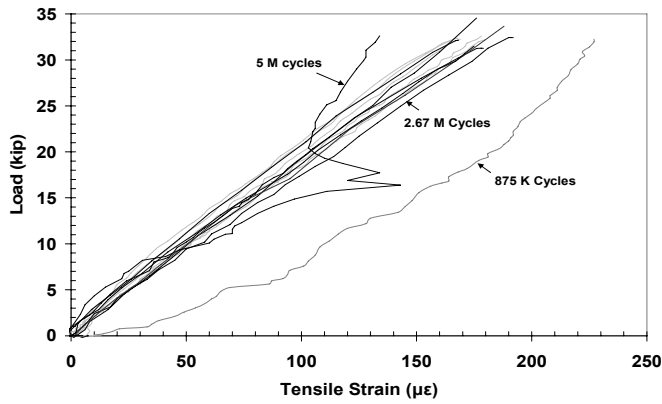
Except for the static test conducted at 875,000 cycles, the maximum tensile strain in the SEJ was approximately $180 \mu\epsilon$, and increased linearly with increasing load. The strain gage malfunctioned during the static test conducted after 5 million cycles, and the data after 875,000 cycles were inconsistent with other data and with expectations.



(a) Load-Deflection Response



(b) Tensile Strains on #5 Bar (S1)



(c) Tensile Strains on SEJ (Gage CT)

Figure 5.24: Measured Response of Specimen N0P1 during Periodic Static Tests

5.3.3 Test to Failure

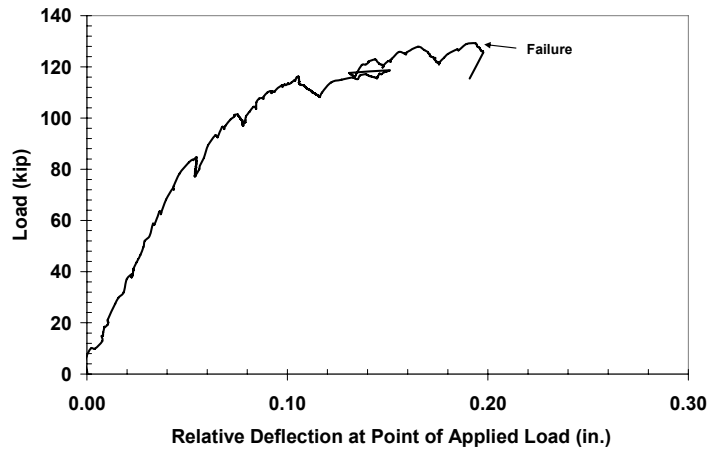
After completion of the fatigue test, the specimen was tested to failure. The measured response is shown in Figure 5.25. The specimen failed abruptly in punching shear at an applied load of 130 kip, which corresponds to approximately four times the rear axle load from the HL-93 Design Truck.

The overall load-displacement response was essentially linear for applied loads less than 85 kip. Above this load, the displacement increased rapidly with increasing load, indicating that the prestressed reinforcement in the PC panel had yielded.

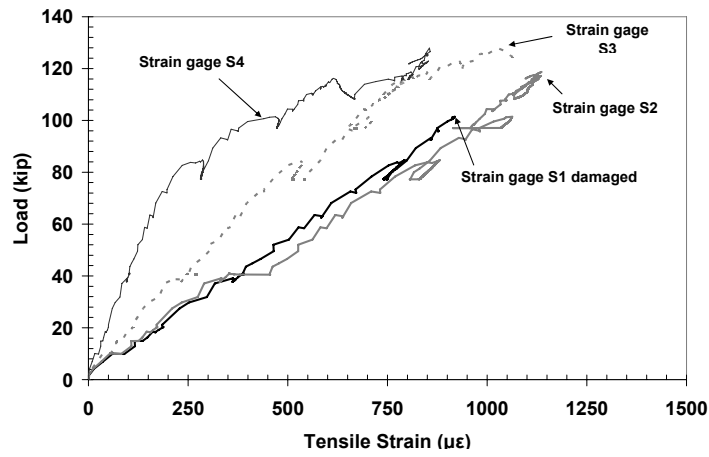
The tensile strain response of the strain gage located at S1 was essentially linear until the strain gage was damaged at an applied load of 100 kip. At 100 kip, the maximum tensile strain was less than $950 \mu\epsilon$ which is significantly less than yield strain ($2270 \mu\epsilon$ for $f_y = 66$ ksi). For comparison with S1, Figure 5.25b includes the measured strain response of the other three strain gages located along the south edge of the center beam. The strain values for S2 increased linearly until the strain gage failed at an applied load of 115 kip. The strain data from S4 and S3 were different than the data from S1 and S2. The measured strain response at S3 was linear until an applied load of 120 kip when the strain increased more rapidly with increasing load. Similarly, the strain response measured at S4 increased linearly until an applied load of 85 kip, when the strain increased more rapidly with increasing load. However, for both S3 and S4, the maximum strain values never reached the maximum strain values recorded at S2, and both values were significantly lower than the yield strain ($2270 \mu\epsilon$ for $f_y = 66$ ksi).

The tensile strain response of the SEJ was essentially linear for applied loads less than 110 kip, after which the response changed abruptly signifying initial yield of the cross section.

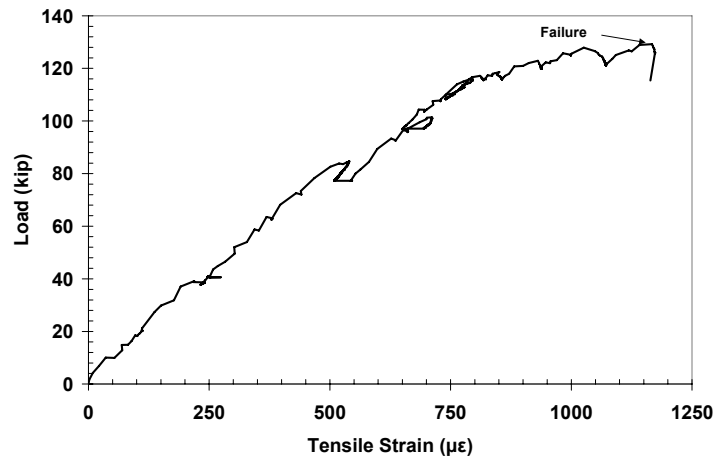
The crack patterns observed at failure are shown in Figure 5.26 and photographs of specimen NOP1 are shown in Figure 5.27.



(a) Load-Deflection Response



(b) Tensile Strains on #5 Bars (S1-S4)



(c) Tensile Strains on SEJ (Gage CT)

Figure 5.25: Measured Response of Specimen N0P1 during Static Test to Failure

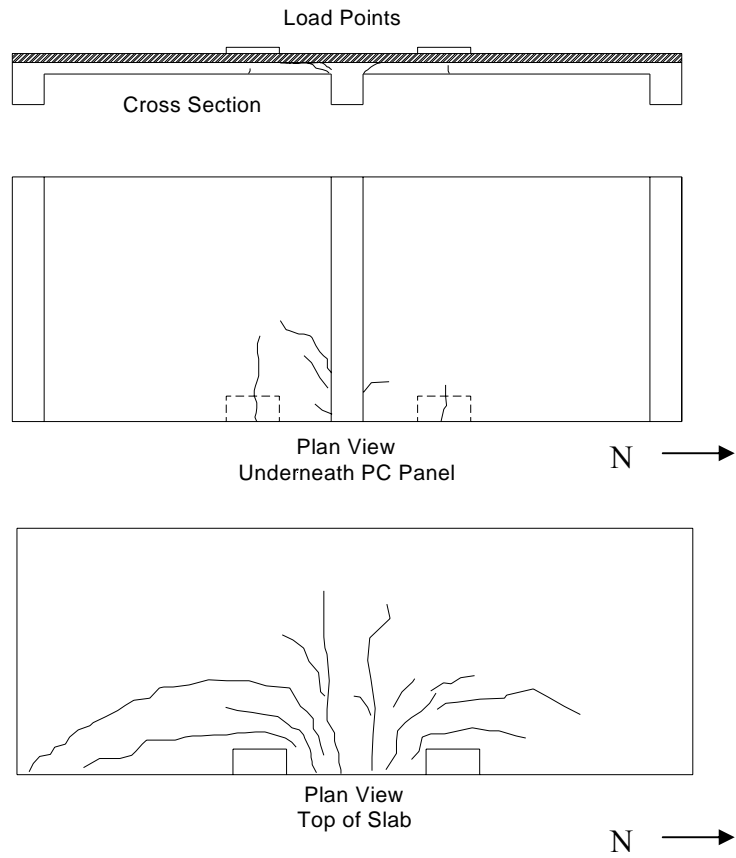


Figure 5.26: Crack Maps for Specimen N0P1 Test to Failure



(a) Top of Specimen

Figure 5.27: Photograph of Specimen N0P1 after Punching Shear Failure

5.4 SPECIMEN N0P2

The applied load history for specimen N0P2 differs from the previous three test specimens. Because the structural behavior of the specimens did not change significantly with increasing applied loads and number of cycles, it was decided to increase the fatigue load and static loads for all the tests of specimen N0P2. Also, because the previous static overload test did not appreciably change the behavior of the specimen, the maximum applied load was 50 kip for all periodic static tests.

Specimen N0P2 was subjected to a total of 12 static tests before, during, and after the fatigue test (Table 5.4). During the fatigue test, the applied loads varied between 2 and 48 kip at a frequency of 3.5 Hz. The periodic static tests (50 kip) corresponded to the rear axle of the HL-93 Design Truck multiplied by an overload factor (1.25) and by the AASHTO dynamic impact factor for fatigue design of bridge decks, (1+I) where I=0.15.

Table 5.4: Static Loading History for Specimen N0P2

Type of Static Test	Accumulated Fatigue Cycles*	Maximum Applied Load (kip)	Condition at Conclusion of Test
Initial	0	50	Shrinkage Cracks
Periodic	250,000	50	
Periodic	830,000	50	
Periodic	1,000,000	50	
Periodic	1,500,000	50	
Periodic	1,760,000	50	
Periodic	2,271,000	50	
Periodic	2,457,000	50	
Periodic	3,800,000	50	
Periodic	4,290,000	50	
Periodic	5,370,000	50	
Failure	5,370,000	140	Punching Failure

* Limiting fatigue loads: $P_{\min} = 2$ kip and $P_{\max} = 48$ kip

Before the initial static test, cracks were observed in the top of the slab directly above the edges of the center beam (Figure 5.28), which corresponded closely to the

cracks in specimen N0P1 and the shrinkage cracks observed by Coselli (2004) in project 0-4418 (Figure 5.22).

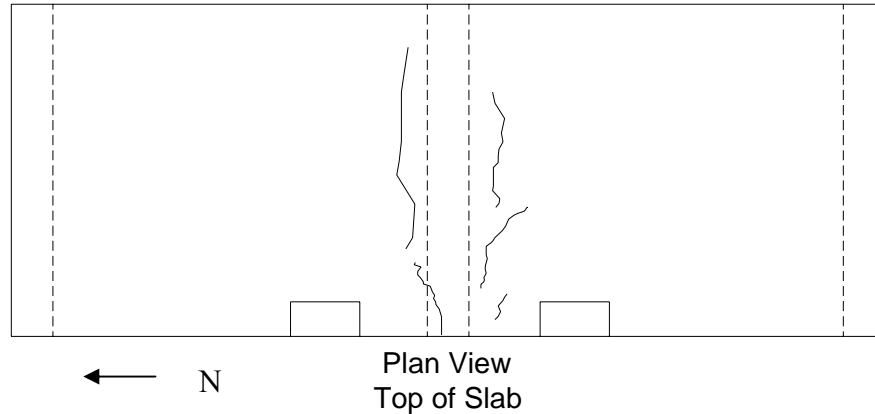


Figure 5.28: Cracks Observed in N0P2 before Initial Static Test

5.4.1 Initial Static Test

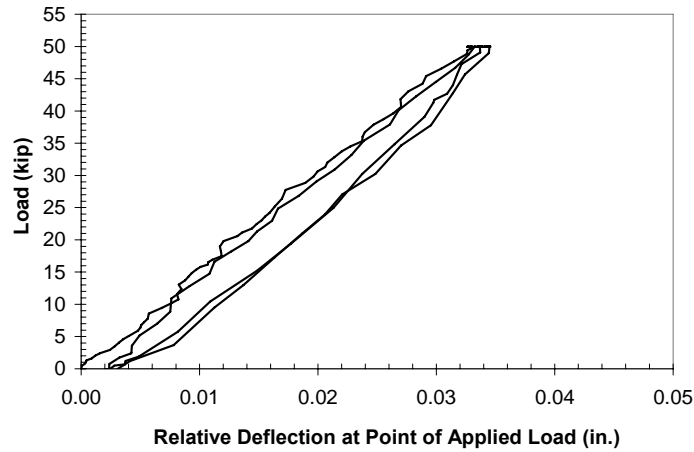
For specimen N0P2, tensile strains were measured on the #5 reinforcing bars and on the SEJ section, and the nomenclature used to identify these strain gages is described in Chapter 4. Three strain gages were attached to the transverse reinforcement immediately above the edges of the center beam. The measured response for the initial static test is presented in Figure 5.29.

As shown in these figures, the strain response of the reinforcing steel did not meet expectations. The locations of the strain gages were determined based on the crack pattern of the specimen N0P1, however, the cracks in specimen N0P2 did not occur as close to the locations of the strain gages, especially in the southern half of the test specimen. For example, the highest stress occurred in the bar that was the farthest away from the SEJ because the crack that formed was closer to strain gage S3 than gages S1 and S2. The maximum tensile strain values were less than $90 \mu\epsilon$ for S1 and S2, and the maximum strain at S3 was approximately $270 \mu\epsilon$.

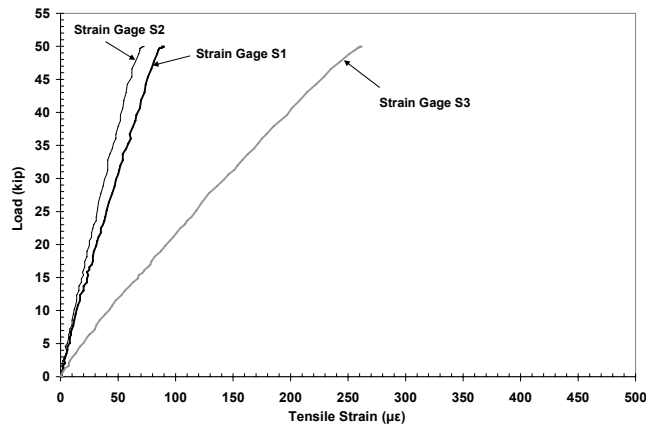
The strain response along the north edge of the center beam more closely represented the expected results based on specimen N0P1, because the cracks formed

closer to the locations of the strain gages. At a maximum applied load of 50 kip, the maximum tensile strain values were 422 $\mu\epsilon$ at N1, 404 at N2, and 395 at N3.

Because the amount of data from the periodic tests is limited, in subsequent sections, the strain data from S1 and N1 will both be presented. See Appendix A for strain data corresponding to the strain gages at other locations.

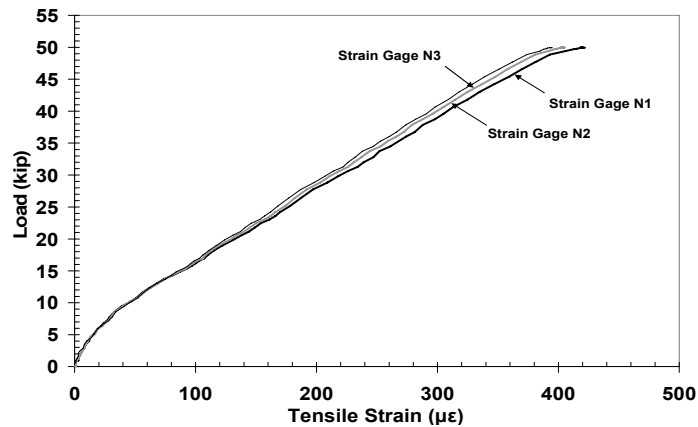


(a) Load-Deflection Response

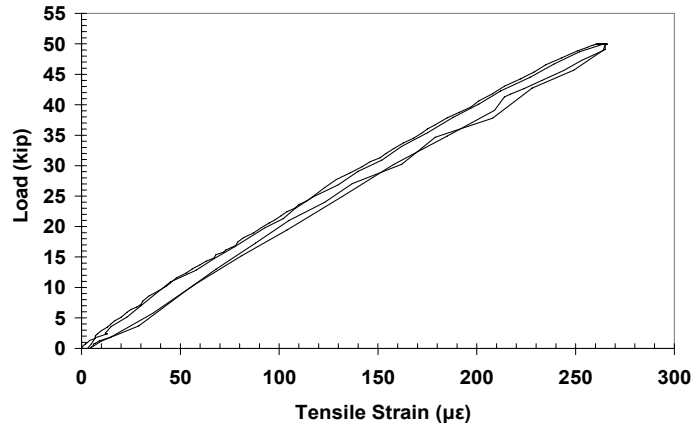


(b) Tensile Strains on #5 Bar along South Edge of Center Beam

Figure 5.29: Measured Response of Specimen N0P2 during Initial Static Test



(c) Tensile Strains on #5 Bars along North Edge of Center Beam



(d) Tensile Strains on SEJ (Gage CT)

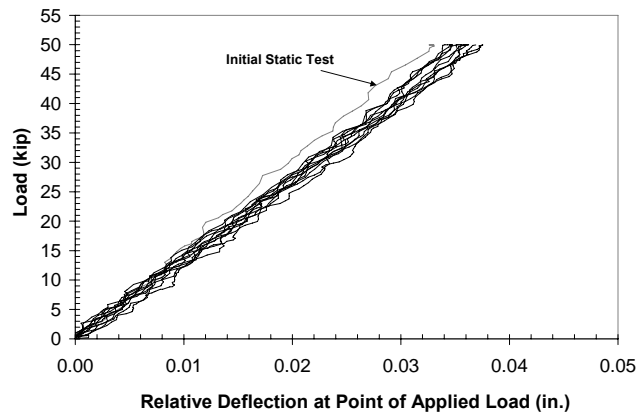
Figure 5.29(cont.): Measured Response of Specimen N0P2 during Initial Static Test

5.4.2 Periodic Static Tests

As indicated in Table 5.4, the fatigue test was stopped 10 times before testing to failure. Due to an error with the data acquisition system, the measured strain response for most of the static tests was not collected. However, data were collected from the initial static test, after 250,000 cycles, and the test to failure after 5.37 million fatigue cycles. The measured responses during each test are superimposed in Figure 5.30. Similarly to specimens P0P1, P0P2, and N0P1, the load-deflection responses were not sensitive to the number of fatigue cycles.

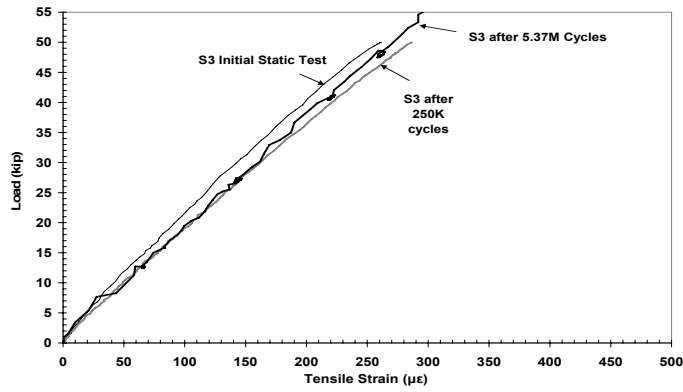
For the strain gages placed along the north edge of the center beam, there was a slight increase in measured strain after the initial static test, however, the response was essentially the same after 250,000 cycles as it was after 5.37 million cycles, and the maximum tensile strain was less than $500 \mu\epsilon$.

Similarly, for the initial static test and the test to failure, the strain responses measured at CT on the SEJ are superimposed in Figure 5.30d, and the initial measured strain response was considerably stiffer than the response at the conclusion of the fatigue test. However the response measured at the end of the fatigue test was essentially the same as that measured during the test to failure for specimen NOP1. The maximum strain was approximately $300 \mu\epsilon$ at an applied load of 50 kip.

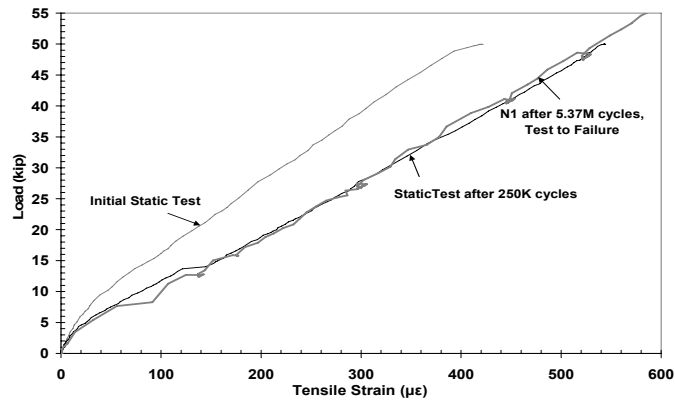


(a) Load-Deflection Response

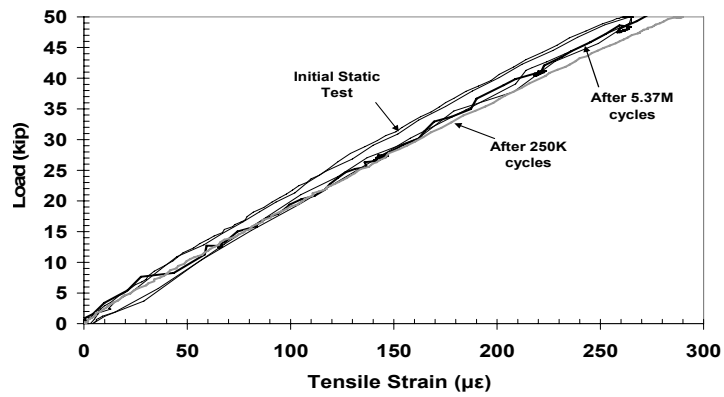
Figure 5.30: Measured Response of Specimen NOP2 during Periodic Static Tests



(b) Tensile Strains on #5 Bar along South Edge of Center Beam (S3)



(c) Tensile Strains on #5 Bar along North Edge of Center Beam (N1)



(d) Tensile Strains on SEJ (Gage CT)

Figure 5.30(cont.): Measured Response of Specimen N0P2 during Periodic Static Tests

5.4.3 Test to Failure

After completion of the fatigue test, the specimen was tested to failure. The measured response is shown in Figure 5.31. The specimen failed abruptly in punching shear at an applied load of 140 kip, which corresponds to more than four times the rear axle weight of the HL-93 Design Truck.

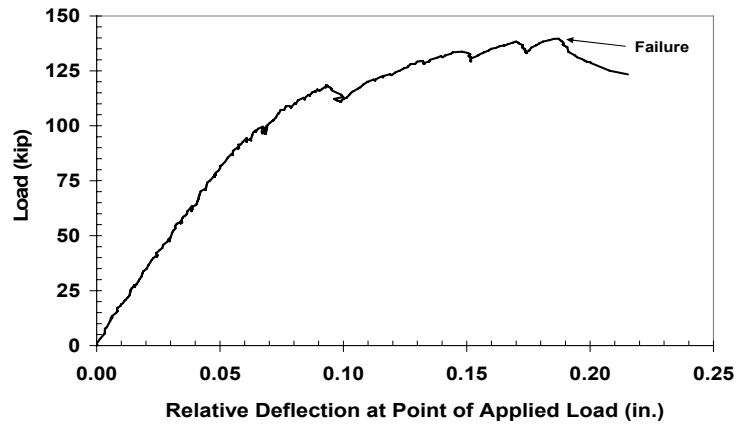
The overall load-displacement response was essentially linear for applied loads less than 100 kip. Above this load, the displacement increased rapidly with increasing load. The maximum relative structural deflection was less than 0.25 in. and was considered a brittle failure.

The measured tensile strain responses of strain gages S1, S2, and S3 were essentially linear up to an applied load of 90 kip, after which the response changed abruptly (Figure 5.31b). However, the maximum strain response was less than $900 \mu\epsilon$ at failure, which corresponds to less than 40% of yield strain ($2270 \mu\epsilon$ for $f_y = 66$ ksi). The abrupt change in measured response could be the result of crack formation near the strain gages which resulted in a lower stiffness that was linear until failure.

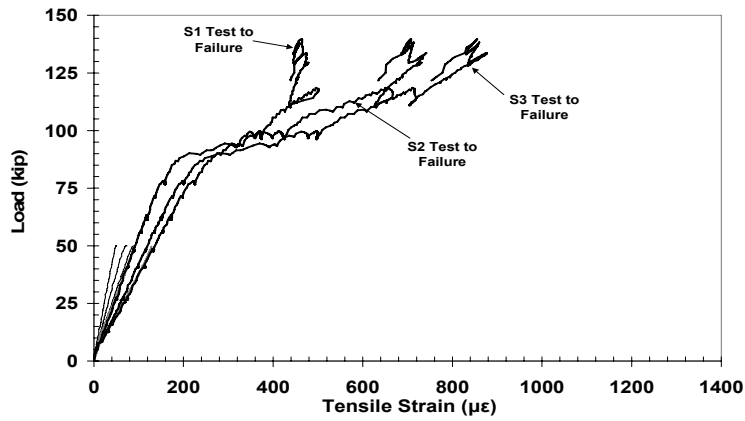
The measured strain response of strain gages N1, N2, and N3 was essentially linear until an applied load of 120 kip, at which the strain gages were damaged (Figure 5.31c). The maximum tensile strain (N1) was less than $1320 \mu\epsilon$ which is approximately 58% of the yield strain.

For the test to failure, the measured strain response of the SEJ is included Figure 5.31d. At an applied load of 100 kip, the slope of the load-strain response began to decrease, indicating initial yielding of the cross section. The yielding of the SEJ corresponded to the change in the load-deflection response shown in Figure 5.31a.

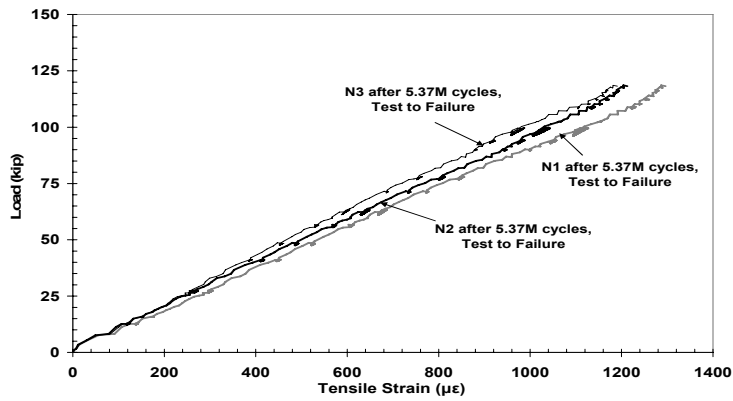
The crack patterns observed at failure are shown in Figure 5.32 and photographs of specimen N0P1 are shown in Figure 5.33.



(a) Load-Deflection Response

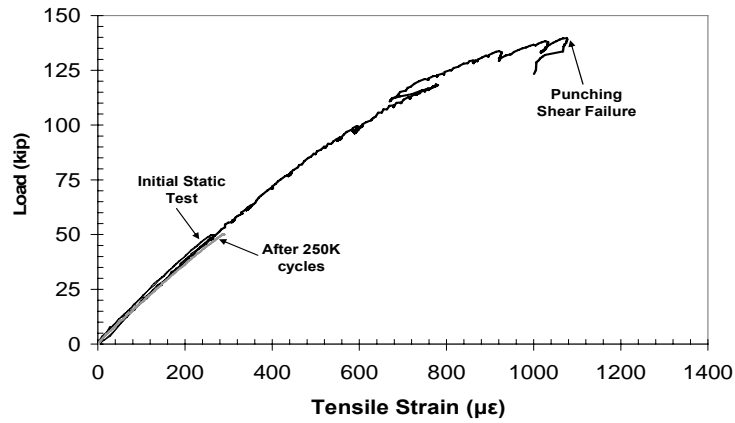


(b) Tensile Strains on #5 Bars along South Edge of Center Beam (S1-S3)



(c) Tensile Strains on #5 Bars along North Edge of Center Beam (N1-N3)

Figure 5.31: Measured Response of Specimen N0P2 during Static Test to Failure



(d) Tensile Strains on SEJ (Gage CT)

Figure 5.31(cont.): Measured Response of Specimen N0P2 during Static Test to Failure

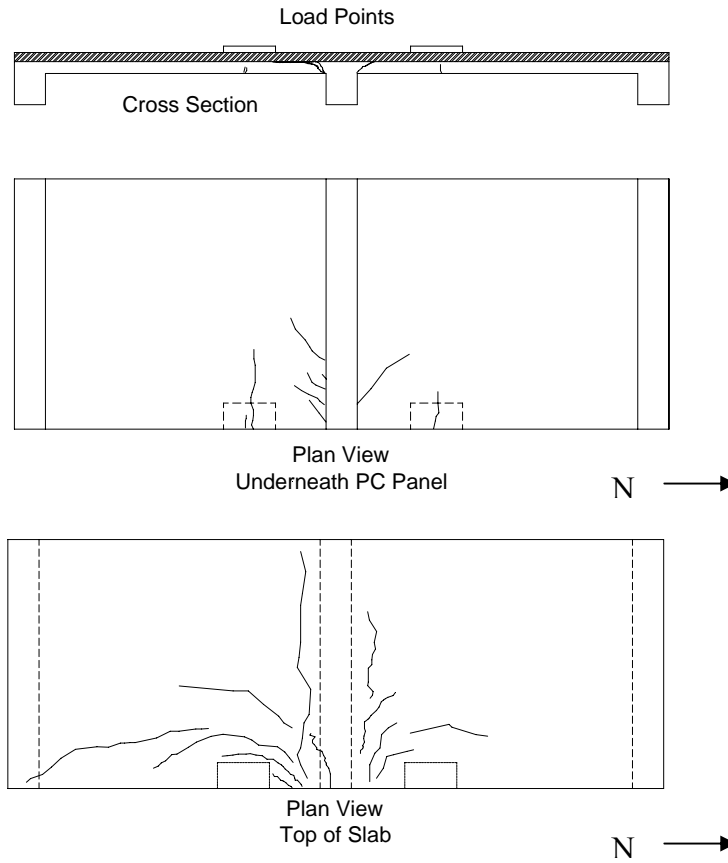


Figure 5.32: Crack Maps for Specimen N0P2 Test to Failure



(a) West Side of Specimen above Central Center Beam



(a) Top of Specimen Near Bearing Pad along NW side of Specimen

Figure 5.33: Photograph of Specimen N0P2 after Punching Shear Failure

Chapter 6: Discussion of Results

In this chapter, the results presented in Chapter 5 are compared and the measured response from each test specimen is discussed. The positive moment specimens are compared in Section 6.1, and the negative moment specimens are compared in Section 6.2. In Section 6.3, a discussion compares the results from the positive and negative test specimens.

6.1 COMPARISON OF POSITIVE MOMENT SPECIMENS

Because of the excellent fatigue response of specimen POP1, the service-level fatigue loads were increased to design-level fatigue loads for specimen POP2. The load ranges were 6 kip for specimen POP1 and 16 kip for POP2. The influence of these increased fatigue loads is addressed in this section.

After five million cycles, the maximum deflection for Specimen POP1 was 0.043 in. at an applied load of 16 kip. The response of specimen POP2 was quite similar, and the maximum deflection after six million cycles was 0.042 in. at an applied load of 16 kip. The deflection-to-span ratios were less than 1/2500 for both specimens. These very small deflections are significant because they indicate that the stiffness of the test specimens did not degrade appreciably during the fatigue tests. Also, the larger fatigue loads used for specimen POP2 did not influence the load-deflection behavior.

The overall responses of both specimens indicated linear behavior at the load corresponding to one wheel from the rear axle of the HL-93 Design Truck. A linear response indicates that structural elements did not yield at design-level loads. After the static overload test, changes in stiffness were observed due to cracking of the PC panels, but the overall response did not change appreciably during additional fatigue cycles. The larger fatigue loads used for specimen POP2 did not influence the measured strain response.

Visual inspections of both specimen POP1 and specimen POP2 further confirmed the satisfactory performance of the PC panel detail. No indications of crack propagation

were observed as the number of fatigue cycles was increased, and no evidence of delamination was observed at the interface of the PC panel and CIP slab.

During the tests to failure, there was no significant deterioration or delamination along the interface of the PC panel and CIP slab until the applied loads exceeded four times the design loads. When the applied loads approached the failure load, some delamination was observed at the interface near the support beams for both specimens. However, the capacities of both specimens were greater than 4.8 times the design loads, and delamination at such a high level of applied load was not considered significant. The larger fatigue loads used for specimen POP2 did not affect the capacity, and a summary of the failure loads is included in Table 6.1.

The overall load-displacement responses of the test specimens are compared with the measured responses of the larger-scale specimens tested by Coselli (2004) (Figure 6.1). However, four issues must be discussed regarding comparisons of the response of the two sets of specimens.

1. Coselli (2004) used two wheel loads, representing one half of each of the axles of the Design Tandem configuration, to test the two portions of the larger-scale specimen that were subjected to positive moment. A single wheel load, representing the rear axle of the Design Truck, was used to test specimens POP1 and POP2. Even though there were two wheel loads, the failure surface corresponded to the wheel load located at the edge of the expansion joint, and the crack patterns observed by Coselli (2004) were similar to the crack patterns observed in POP1 and POP2. The failure loads included in Figure 6.1 corresponds to the wheel load nearest the failure surface at the expansion joint, and are reported as “load per load point.”
2. The simply supported boundary conditions for the single panel in specimens POP1 and POP2 did not permit load redistribution, which was possible in the multiple-girder, larger-scale specimen. There was no evidence of yielding or redistribution in the positive moment specimens,

but the finite element analyses indicated higher moments in the simply-supported specimens.

3. Coselli (2004) used a deeper expansion joint rail in one portion of the test specimen than was used in specimens POP1 and POP2, and did not measure strains in the expansion joint rails. In another portion of the larger-scale test specimen, no rail was used. The sealed expansion joint used by Coselli (2004) required modifications to be used in construction. In Table 6.1 and Figure 6.1, these two tests are referred to as “Coselli without SEJ” and “Coselli with SEJ.”
4. Also, the measured compressive strengths of the concrete was higher for specimens POP1 and POP2 (5200 psi and 5700 psi) compared with the larger-scale specimen (4100-4400 psi). The deck reinforcement was the same in all three specimens, and the reinforcement in all of the PC panels was nominally identical.

Even though the test specimens were not equivalent, Figure 6.1 illustrates that the larger-scale specimen and the smaller specimens both performed in a similar manner. For the three tests including expansion joints, the maximum applied loads were within 10%, and all specimens exhibited capacities that significantly exceeded the design loads.

Table 6.1: Summary of Failure Response of Positive Moment Specimens

Specimen	Type of Load	Design Wheel Load (kip)	Applied Load at First Observed Crack (kip)	Applied Load at Failure (kip)	Failure Load / Design Wheel Load (kip)
POP1	Design Truck	16	32	77	4.8
POP2	Design Truck	16	32	79	4.9
Coselli without SEJ	Design Tandem	12.5	28	67	5.3
Coselli with SEJ	Design Tandem	12.5	28	84	6.7

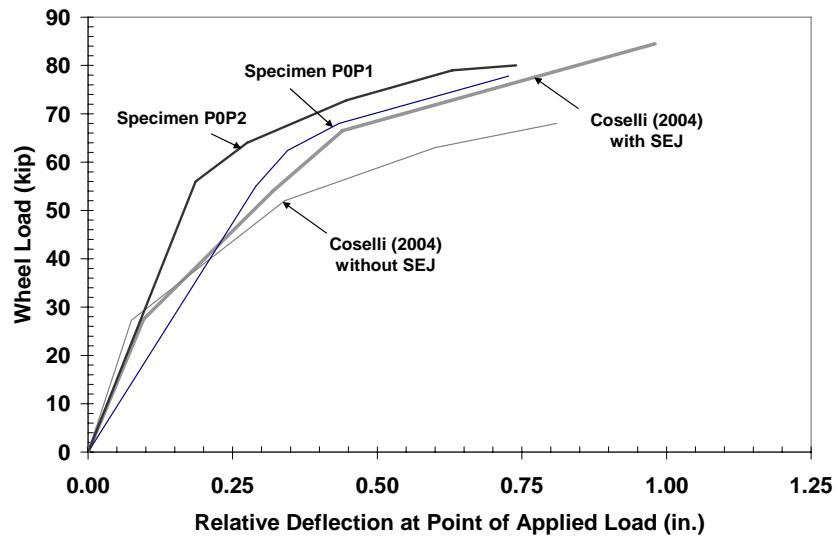


Figure 6.1: Comparison of Capacities of Specimens P0P1 and P0P2 with Larger-Scale Specimen

6.2 COMPARISON OF NEGATIVE MOMENT SPECIMENS

Because of the excellent fatigue response of specimen POP2, the fatigue loads for specimen NOP1 were design-level loads that corresponded to the rear axle of the HL-93 Design Truck (32 kip). Furthermore, based on the excellent fatigue response of specimen NOP1, the design-level fatigue loads were amplified for specimen NOP2. The overload-level fatigue loads for specimen NOP2 were 46 kip. The influence of the increased fatigue loads are addressed in this section.

For both specimens, the static overload tests did not crack the specimen; therefore, the responses of the specimens did not reflect a change in stiffness. After five million cycles, the maximum deflection for specimen NOP1 was 0.021 in. at an applied load of 32 kip. The response of specimen NOP2 was quite similar, even though the fatigue load was significantly increased, and the maximum deflection after 6 million cycles was 0.038 in. at an applied load of 50 kip. The deflection-to-span ratios were less than 1/2800 for both specimens. These small deflections are significant because they indicate that the stiffness of the test specimens did not appreciably degrade during the fatigue tests. Also, the

overload-level fatigue loads used for specimen N0P2 did not influence the load-deflection behavior.

Overall, the measured responses indicated linear behavior for applied loads less than 70 kip. For both specimens, the periodic static tests indicated essentially the same responses throughout the fatigue tests.

Visual inspections of specimen N0P1 and specimen N0P2 further confirmed satisfactory performance of the PC panel detail. There was no crack propagation as the number of fatigue cycles was increased, and no visible change in the appearance of the PC panel detail.

At failure, the measured strains indicated that the reinforcement did not yield, and visible inspection of the failure crack patterns also gave no indication of yielding. However, when the applied load approached the failure load, the failure of the specimen corresponded to the yielding of the SEJ. During the test to failure, there was no significant deterioration or delamination along the interface of the PC panel and the CIP slab until the loads exceeded three times the design loads. Because the capacity of both specimens significantly exceeded four times the design loads, the delamination near the support beams was not considered a significant problem. The overload-level fatigue loads used for specimen N0P2 did not affect the capacity, and a summary of the failure loads is included in Table 6.2.

The overall load-displacement response tested of the test specimens are compared with the response measure of the larger-scale specimens tested by Coselli (2004) (Figure 6.2). Similarly to specimens P0P1 and P0P2, a few issues must be addressed regarding comparisons of the response of the two sets of specimens.

1. Coselli (2004) used the Design Tandem configuration, and for specimens N0P1 and N0P2, the Design Truck configuration was used. Even though there were four wheel loads, each punching shear failure surface occurred at a wheel load at the edge of the expansion joint, and the crack patterns observed by Coselli (2004) were similar to the crack patterns observed in N0P1 and N0P2. The failure loads included in Figure 6.2 corresponds to

the wheel load nearest the failure surface at the expansion joint, and are reported as “load per load point.”

2. The girder spacing in specimens NOP1 and NOP2 was 10 ft in the negative moment specimens, and was 8 ft in the larger-scale specimen. The boundary conditions were more extreme for the negative moment specimens, but there was no evidence of yielding or redistribution in the positive moment specimens. The finite element analyses indicated higher moments in specimens NOP1 and NOP2.
3. Coselli (2004) used an armor joint rail in one test, and at another test location, no rail was used. Coselli (2004) did not measure the strain response of the armor joint rail. In Figure 6.2, these two tests are indicated “Coselli without Armor Joint” and Coselli with Armor Joint.”
4. Also, the measured compressive strengths of the concrete was higher for specimens NOP1 and NOP2 (5500 psi and 5900 psi) compared with the larger-scale specimen (4100-4400 psi). The deck reinforcement was the same in all three specimens, and the reinforcement in all of the PC panels was the same.

Table 6.2: Summary of Failure Response of Negative Moment Specimens

Specimen	Type of Load	Design Wheel Load (kip)	Applied Load at Failure (kip)	Failure Load / Design Wheel Load (kip)
N0P1	Design Truck	16	65	4.1
N0P2	Design Truck	16	70	4.4
Coselli without AJ	Design Tandem	12.5	70	5.6
Coselli with AJ	Design Tandem	12.5	90	7.2

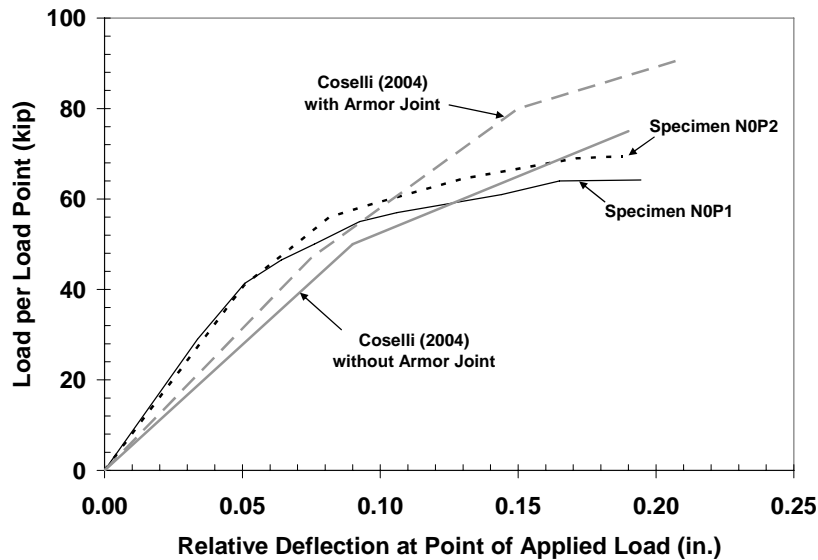


Figure 6.2: Comparison of Capacities of Specimens N0P1 and N0P2 with Larger-Scale Specimen

Even though the test specimens are not equivalent, Figure 6.2 generally illustrates that the larger-scale specimen and the smaller specimens both performed in a similar manner, and all specimens exhibited capacities that significantly exceeded the design-level loads.

6.3 COMPARISON BETWEEN POSITIVE AND NEGATIVE MOMENT SPECIMENS

Generally, a comparison of the positive and negative moment specimens shows that all the specimens performed similarly. Under the design loads, all specimens exhibited linear behavior, no yielding, and very small deflections. Once the fatigue cycling was initiated, the structural responses of the specimens did not change with increasing numbers of fatigue cycles. Furthermore, the overload fatigue loads used for specimen N0P2 did not appreciably change the structural response after five million fatigue cycles. The capacities of all test specimens greatly exceeded the required design strength.

Chapter 7: Summary, Conclusions, and Recommendations

A summary of the research project is provided in Section 7.1, and the conclusions are presented in Section 7.2. Recommendations for implementation and future research are made in Section 7.3.

7.1 SUMMARY

Through the Texas Department of Transportation (TxDOT) research project 0-4418, a new construction detail was developed for expansion joints of 0° skew bridge decks. This new detail uses precast, prestressed concrete (PC) panels as stay-in-place formwork and a 4-in. thick topping slab to form an 8-in. composite slab. The primary advantage of the new detail at the expansion joint is the elimination of the I-Beam Thickened Slab (IBTS) detail which requires temporary formwork which is difficult to place. The new detail represents a safer, faster, and more economical construction solution than the IBTS detail.

The primary objective of this research project was evaluate the fatigue performance of the proposed PC panel detail. The full-scale test specimens were designed to reproduce as-built conditions of typical TxDOT bridges. One research goal was to collect information to facilitate incorporation of the new PC panel detail into the future construction of bridge decks with 0° skew. Another long range goal was to understand the fatigue behavior of the proposed PC panel detail to assist in the development of new PC panel details for bridge decks with skewed angles.

Four full-scale specimens were designed, constructed, and subjected to a combination of static and fatigue loads. Specimens POP1 and POP2 were designed to evaluate the performance of the PC panel detail under positive moments, and specimens NOP1 and NOP2 were designed to evaluate the performance of the PC panel detail under negative moments. All specimens were subjected to at least five million fatigue cycles. Specimens POP1 and POP2 were subjected to a static overload after two million fatigue

cycles to induce cracks in the PC panels. All specimens were tested to failure at the conclusion of the fatigue tests.

Specimen POP1 was subjected to service-level fatigue loads. Because the fatigue response of specimen POP1 was excellent, the fatigue loads were increased to design-level loads for specimen POP2 and specimen NOP1. The fatigue loads were increased for specimen NOP2 to represent an overload truck.

7.2 CONCLUSIONS

It was concluded that the new PC panel for 0° skew bridge decks exhibited excellent fatigue response. The specific responses of each specimen are summarized below.

- Service-Level Fatigue Behavior (Specimen POP1)
 - The overall system response (load vs. deflection) and the measured strain response of specimen POP1 remained linear throughout the fatigue test, and did not change appreciably with increasing fatigue cycles.
 - The stiffness of specimen POP1 was reduced after the static overload test, but the fatigue response did not change appreciably with increasing fatigue cycles.
 - No delamination or deterioration was observed along the interface of the PC panel and the CIP slab during the fatigue tests.
- Design-Level Fatigue Behavior (Specimens POP2 and NOP1)
 - The overall system response (load vs. deflection) and the measured strain responses of specimen POP2 and NOP1 remained linear throughout the fatigue tests, and did not change appreciably with increasing fatigue cycles.
 - The stiffness of specimen POP2 was reduced after the static overload test (three times the design wheel load), but the fatigue response did not change appreciably with increasing fatigue cycles.

- The stiffness of specimen NOP1 was not reduced after the static overload test (1.5 times the design axle load), and the fatigue response did not change appreciably with increasing fatigue cycles.
- There was no indication of yielding of the deck reinforcement in specimen NOP1.
- No delamination or deterioration was observed along the interface of the PC panel and the CIP slab during the fatigue tests.
- Overload Fatigue Behavior (Specimen NOP2)
 - The overall system response (load vs. deflection) and the measured strain responses of specimen NOP2 remained linear throughout the fatigue test, and did not change appreciably with increasing fatigue cycles.
 - There was no indication of yielding of the deck reinforcement in specimen NOP2.
 - No delamination or deterioration was observed along the interface of the PC panel and the CIP slab during the fatigue tests.
- Failure Behavior
 - All four specimens failed by punching shear, but the maximum applied loads greatly exceeded the practical service-level loads.
 - The stiffness of all four specimens changed when the sealed expansion joint (SEJ-A) yielded. In all cases yielding of the SEJ occurred at more than 3.5 times the design wheel loads.
 - No yielding was observed in the CIP deck or the PC panels in any of the test specimens.
 - All four test specimens had capacities that corresponded to the capacities measured by Coselli (2004) for a larger-scale specimen. Therefore, it was concluded that the behavior of the smaller, full-scale specimens adequately represent the behavior of full-width bridge decks.

7.3 RECOMMENDATIONS FOR FUTURE RESEARCH

The results of this research project suggest that no further investigation is required for the fatigue behavior of the PC panel detail at expansion joints for bridges with 0° skew. Other types of expansion joint rails are available for use in bridge decks, but the use of the SEJ-A section works well for the new PC panel detail and requires no additional preparation to be used in construction.

Currently, construction details are being developed to use PC panels at expansion joints in bridges with skewed angle orientations. Additional large-scale tests are planned to determine the static and fatigue response of the skewed angle PC panel detail. The results of that phase of the project will further determine the feasibility of using PC panel construction in bridge decks at expansion joints.

The conclusions from this phase of the research project indicated that TxDOT should also consider using the PC panel detail over bent caps in multi-span bridges. Currently, the PC panels are discontinued before the ends of each span. A full-depth, 8-in. CIP slab is used in this region and provides the only continuity between adjacent spans. Faster, safer, and more economical construction practice can be achieved if the PC panel details are used in lieu of the CIP detail at these locations. However, additional research is required to develop new details for instances of skewed orientations, uneven span lengths, and unequal girder spacing.

Appendix A

The data that were not presented in Chapter 5 are presented in this appendix. These data were collected at locations away from the load point, and were mostly small values not relevant to the results and discussion included in Chapter 5 and Chapter 6.

Based on the measured response of specimen P0P1, the instrumentation was changed for subsequent specimens. For example, the strain data collected at the quarter points of the SEJ experienced much lower stress than the strain gage located at the top of midspan. Therefore, in specimens P0P2, N0P1, N0P2, only one strain gage was placed at the top of the SEJ at midspan.

For specimen P0P1, Figure A.1 and Figure A.2 include the displacements measured during the initial static test and the test to failure, respectively. Each figure presents two plots. First, the load vs. displacement measured at midspan of the north edge of the specimen is included to show that the back of the specimen (north end away from the point of applied load) did not deflect upwards until the PC panel delaminated from the support beams during the test to failure. Secondly, the load vs. displacement was measured adjacent to the front supports. The values at the front supports were used to determine the relative structural deflection at the point of applied load. Large cracks near the support beams resulted in large displacements measured by the linear potentiometers placed adjacent to the support beams.

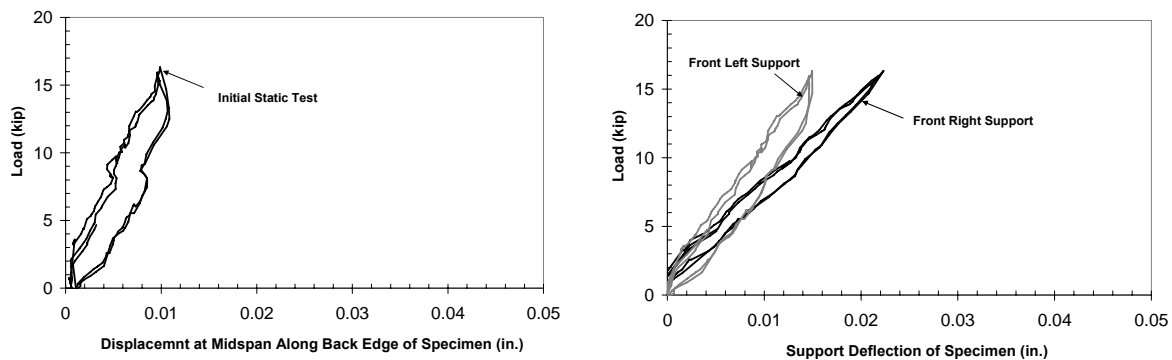


Figure A.1: Load vs. Deflection Response during Initial Static Test (P0P1)

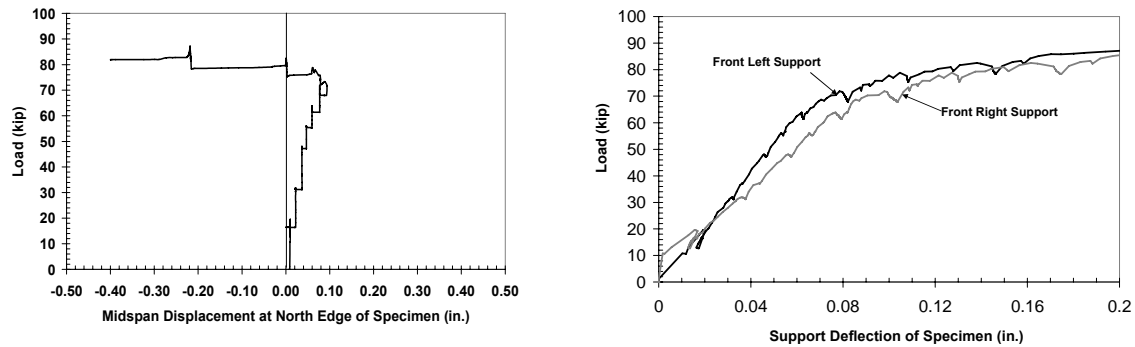
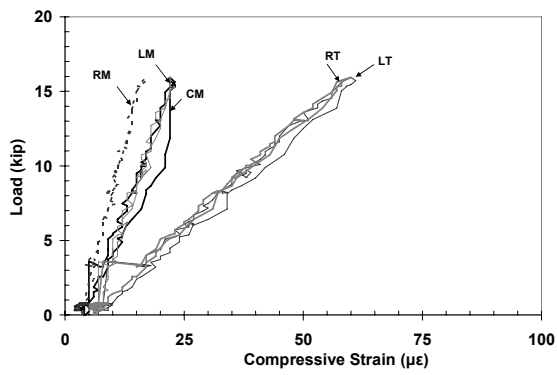
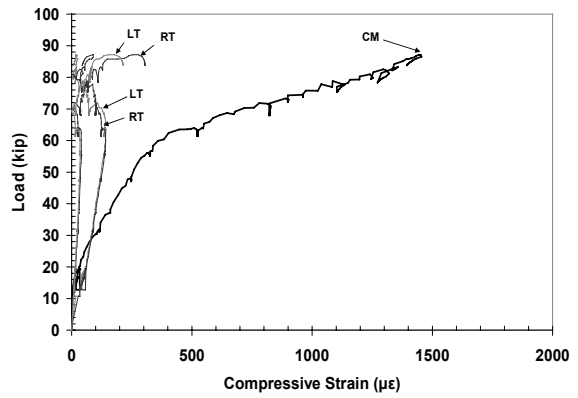


Figure A.2: Load vs. Deflection Response during Static Test to Failure (P0P1)

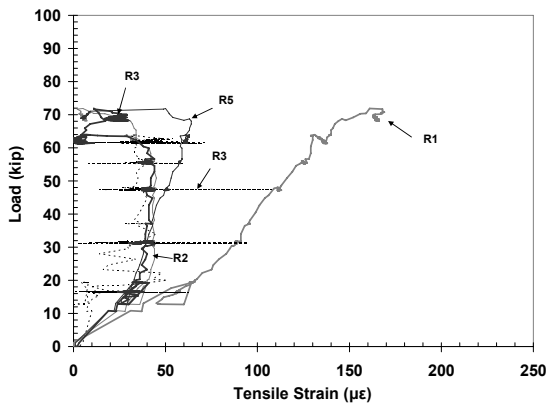
Strains were measured at mid-depth and at the top of the SEJ at the quarter points of the span, and strains were also measured on the bottom surface of the PC panel along the quarter points. The nomenclature used for the strain gages was presented in Chapter 4. These measured strain responses are included in Figure A.3. These figures show that the strain data collected at mid-depth of the SEJ were extremely small, except for the gage located at the point of the applied load. This strain gage experienced higher strains than the gages at other locations when the SEJ yielded at an applied load of 60 kip. Similarly, the strains measured on the bottom surface of the PC panel were much lower than the strains measured along the centerline of the panel. Several cracks were located near the strains located at L2 and L3, and resulted in larger than expected strain values.



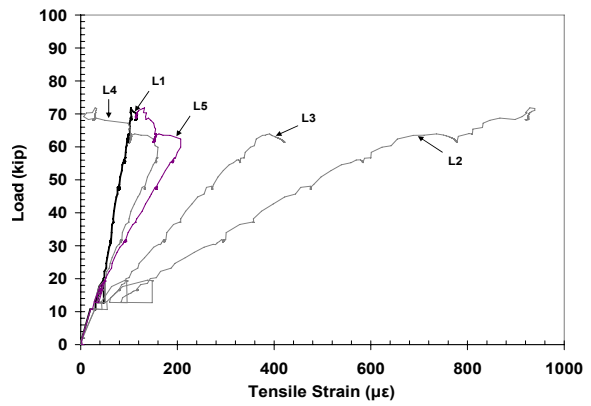
a) SEJ Initial Static Test



b) SEJ Test to Failure



c) PC Strains East Quarter Point Test to Failure



c) PC Strains West Quarter Point Test to Failure

Figure A.3: Measured Strain Responses during Initial Static Test and Static Test to Failure (P0P1)

For specimen P0P2, Figure A.4 and Figure A.5 include the displacements measured during the initial static test and the test to failure, respectively. Each figure presents the load vs. relative deflection measured at midspan of the north edge (back edge) of the specimen, and then also includes the load vs. displacement measured adjacent to the front supports. Fewer strain gages were used for specimen P0P2, and all of the strain data were included in Chapter 5.

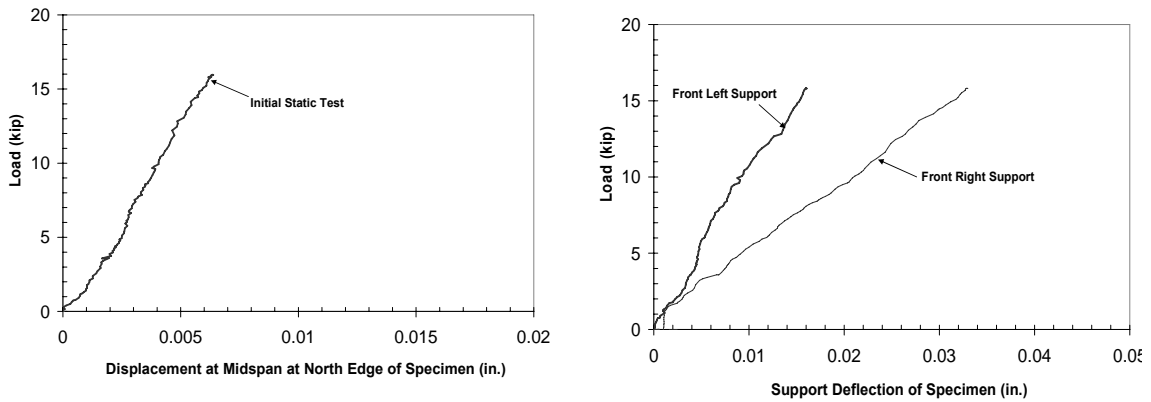


Figure A.4: Load vs. Deflection Response during Initial Static Test

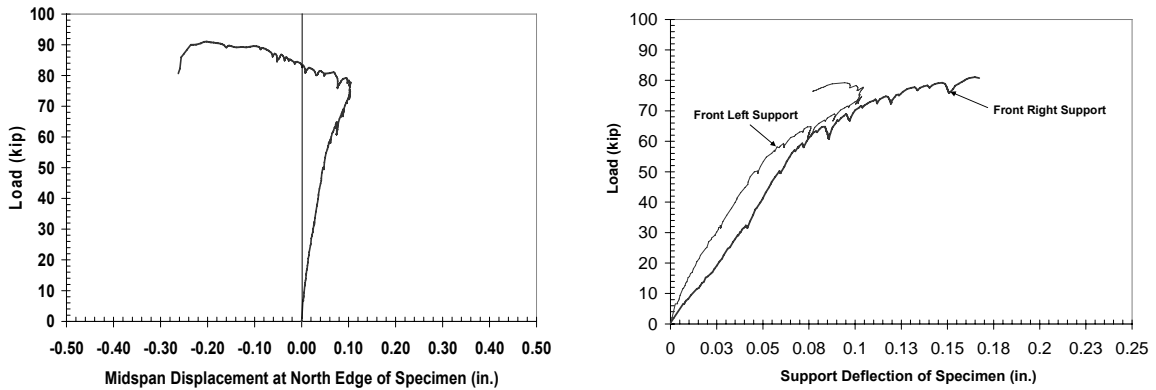
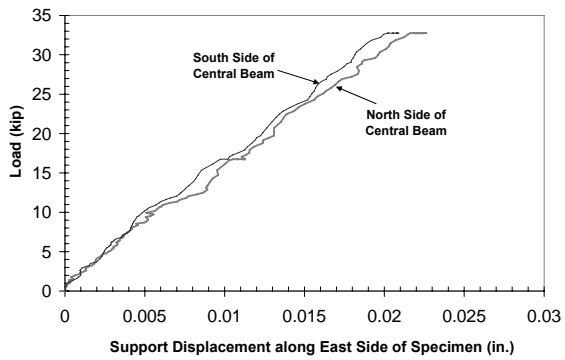
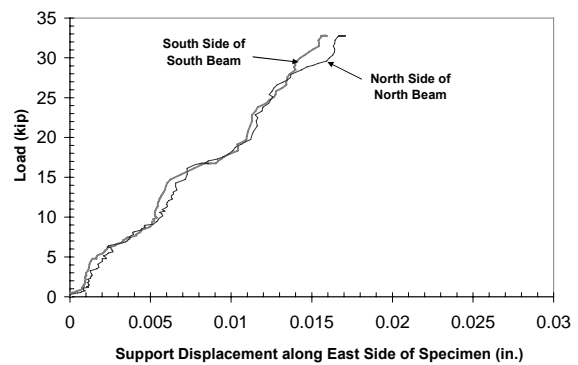


Figure A.5: Load vs. Deflection Response during Static Test to Failure

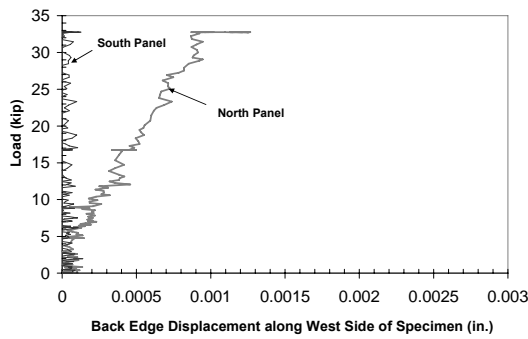
For specimen N0P1, Figure A.6 includes the displacements measured during the initial static test along the east edge (front edge) of the specimen. These displacements were recorded 1 in. from the support beams, and were used to determine the relative structural deflection in Chapter 5. Also, the displacements measured at midspan along the west edge (back edge) of the specimen are included. Then, for the test to failure, the displacement of the specimen at the central support beam is included in Figure A.6d. All of the strain data for specimen N0P1 were included in Chapter 5.



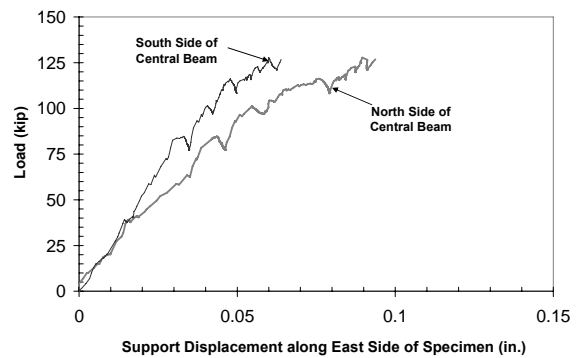
a) Central Support Beam Displacement during Initial Static Test



b) Outer Support Beam Displacement during Initial Static Test



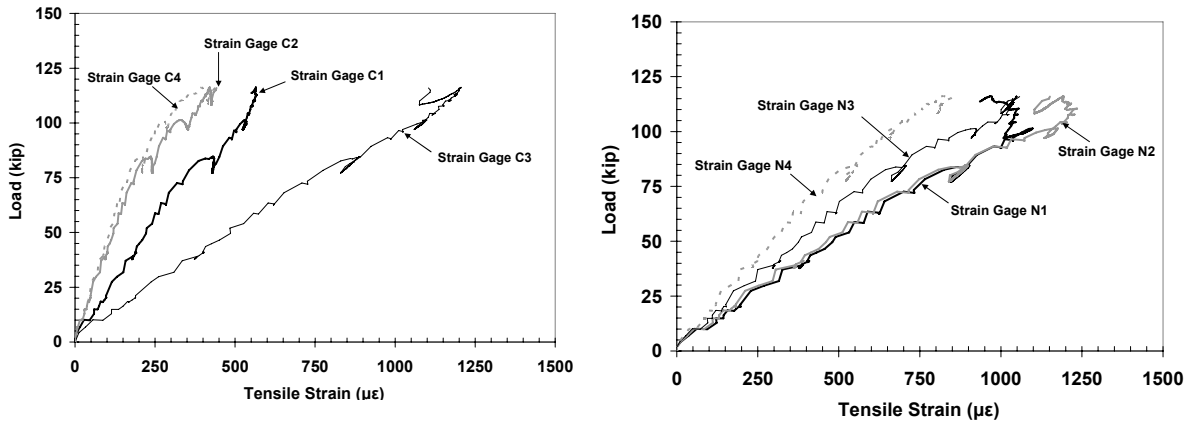
c) Displacement Measured at Midspan along North Edge during Initial Static Test



a) Central Support Beam Displacement during Static Test to Failure

Figure A.6: Load vs. Deflection Response Specimen N0P1

Most of the strain data were presented in Chapter 5, but Figure A.7 includes the strain data measured along the central support beam and above the north edge of the support beam.

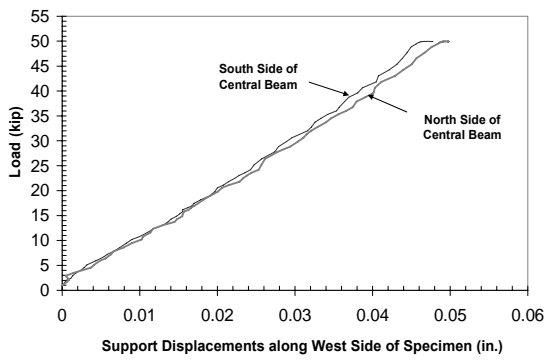


a) Strains along Centerline of Central Beam (C1-C4) during Test to Failure

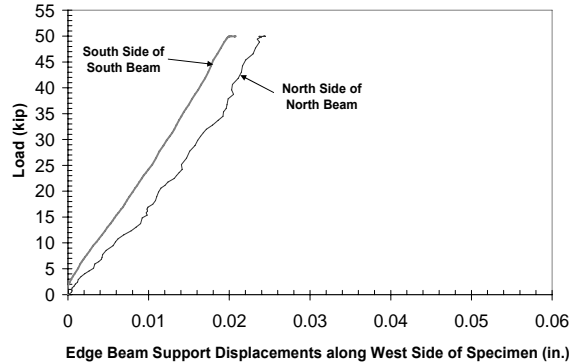
b) Strains along North Edge of Central Beam (N1-N4) during Test to Failure

Figure A.7: Measured Strain Response Specimen N0P1

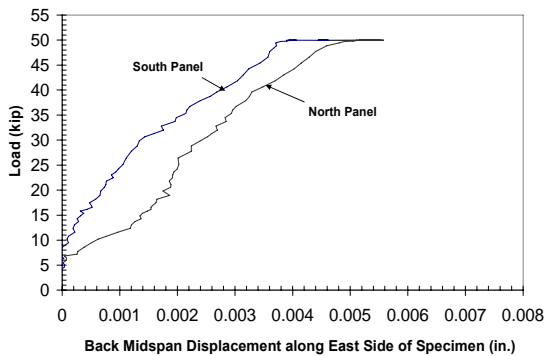
For specimen N0P2, Figure A.8 includes the displacements measured during the initial static test along the east edge (front edge) of the specimen. These displacements were recorded 1 in. from the support beams, and were used to determine the relative structural deflection in Chapter 5. Also, the displacements measured at midspan along the west edge (back edge) of the specimen are included. Then, for the test to failure, the displacement of the specimen at the central support beam is included in Figure A.6d. All of the available strain data for N0P2 were presented in Chapter 5.



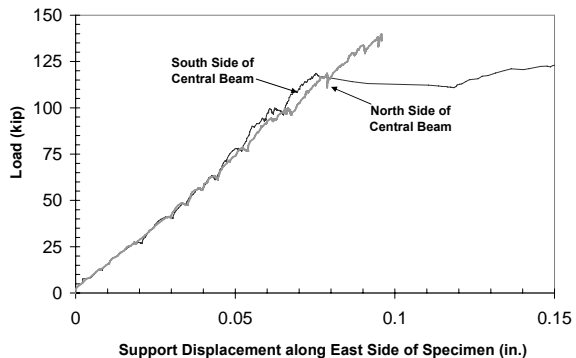
a) Central Support Beam Displacement during Initial Static Test



b) Outer Support Beam Displacement during Initial Static Test



c) Displacement Measured at Midspan along North Edge during Initial Static Test



a) Central Support Beam Displacement during Static Test to Failure

Figure A.8: Load vs. Deflection Response Specimen N0P1

References

1. American Association of State Highway and Transportation Officials (2004), *ASHTO LRFD Bridge Design Specifications, 3rd Edition*.
2. Bieschke, L.A. and Klingner, R.E. (1982), "The Effect of Transverse Strand Extensions on the Behavior of Precast Prestressed Panel Bridges," Research Report 303-1F, Center for Transportation Research, The University of Texas at Austin, June, 106 pp.
3. Buth, E., Furr, H.L., and Jones, H.L. (1972), "Evaluation of a Prestressed Panel, Cast-In-Place Concrete Bridge," Research Report 145-3, Texas Transportation Institute, Texas A&M University, College Station, Texas, Sept., 140 pp.
4. Coselli, C. (2004) "Behavior of Bridge Decks with Precast Panels at Expansion Joints," Master's Thesis, The University of Texas at Austin, May, 286 pp.
5. Dolan, V. and Frank, K. (1994), "Evaluation of Failure in Bridge Expansion Joint Rails," Research Report 1309-1F, Center for Transportation Research, The University of Texas at Austin, Oct., 38 pp.
6. Fagundo, F.E., Tabatabai, H., Soongswang, K., Richardson, M., and Callis, E.G. (1985), "Precast Panel Composite Bridge Decks," *Concrete International: Design and Construction*, Vol. 7, No. 5, May, pp. 59-65.
7. Fang, I., Tsui, C., Burns, N., and Klingner, R. (1990), "Fatigue Behavior of Cast-in-Place and Precast Panel Bridge Decks with Isotropic Reinforcement," *PCI Journal*, Vol. 35, No. 3, May-June, pp. 28-39.

8. Graddy, J, Burns, N, and Klingner, R. (1995), "Factors Affecting the Design Thickness of Bridge Slabs," Research Report 1305-3F, Center for Transportation Research, The University of Texas at Austin, March, 186 pp.
9. Graddy, J., Kim, J., Burns, N., Whitt, J., and Klingner, R. (2002), "Punching-Shear Behavior of Bridge Decks under Fatigue Loading," *ACI Structural Journal*, Vol. 99, No. 3, May-June, pp. 257-266.
10. Griffith, E. (2003), "Behavior of Bridge Slab ends at Expansion Joints," Master's Thesis, The University of Texas at Austin, December, 284 pp.
11. Kluge, R.W. and Sawyer, H.A. (1975), "Interacting Pretensioned Concrete Form Panels for Bridge Decks," *PCI Journal*, Vol. 20, No. 3, May-June, pp. 34-61.
12. Ryan, J. (2003), "Behavior of Bridge Slab Ends at Expansion Joints," Master's Thesis, The University of Texas at Austin, August, 253 pp.
13. Texas Department of Transportation, "Standard Detail Drawings" Retrieved April 15, 2007 from <http://www.dot.state.tx.us/insdtdot/orgchart/cmd/cserve/standard/bridge-e.htm>
14. Van Landuyt, Dean, "Survey of Skew Angles of TxDOT bridges," Results presented at research project meeting, Austin, Texas, September 2006.
15. Wood, S.L., Hagenberger, M.J, Heller, B.E, and Wagener, P.J (2007), Research Report 0-1895-1, Center for Transportation Research, The University of Texas at Austin, January.

Vita

Lewis Samuel Agnew, Jr., the son of Pat and Sam Agnew, was born in Phoenix, Arizona on September, 7, 1981. He was raised in Jackson, Mississippi and graduated from Jackson Preparatory School. After high school, he enrolled at Auburn University where he received a Bachelor of Civil Engineering in December 2004. In August 2005, he enrolled in graduate school at The University of Texas at Austin. Upon graduation from The University of Texas, he will be moving to Nashville, Tennessee to begin working for Stanley D. Lindsey, and Associates.

Permanent address: 97 N. Crownpointe Dr.
Jackson, MS 39211

This thesis was typed by the author.